SORPTION OF SELECTED HEAVY METAL IONS FROM AQUEOUS SOLUTIONS BY MANGO SEED SHELL DERIVED SORBENTS

by

Malvin Moyo

Dissertation submitted in fulfilment of the requirements for the degree
Magister Technologiae: Chemistry

in the

Faculty of Applied and Computer Sciences

Department of Chemistry

at

Vaal University of Technology

2017

Supervisor: Prof. Sekomeng J. Modise

Co-supervisor: Dr. Vusumzi E. Pakade

Declaration

I, Malvin Moyo (undersigned), declare that the contents of this dissertation represent my own unaided work, and that the dissertation has not previously been submitted in part, or in whole, to any university other that the Vaal University of Technology. Where use has been made of the work of others, it has been duly acknowledged in the text.

Signature: ……..

Date: ……..

Abstract

The use of biosorption to complement conventional water treatment techniques has gained widespread appeal partly due to the abundance of waste materials that can be used as low cost biosorbents. However, some materials have not yet been exploited in this regard. This research was aimed at evaluating the biosorption potential of *Mangifera indica* (mango) seed shells that are readily available in several farming areas of the Limpopo and Mpumalanga Provinces of South Africa.

In this work, powdered ethylenediaminetetraacetic acid (EDTA) functionalized biosorbent was prepared from alkali treated biomass of waste mango seed shells. The influence of alkali treatment and EDTA functionalization on the physicochemical properties of the biomass was characterized using Fourier transform infra-red spectroscopy, X-ray diffraction and thermogravimetric analysis. Results confirmed removal of hemicelluloses, conversion of crystalline to amorphous cellulose and the introduction of carboxyl, ester and tertiary amine groups from EDTA. Furthermore, the powdered biosorbent was immobilized using calcium alginate for adaptation to column sorption.

The powdered biosorbents were tested for sorption of lead(II) ions using batch sorption experiment. Through EDTA functionalization, improvement in sorption capacity for lead(II) ions from 59.25 $mg.g^{-1}$ to 306.33 $mg.g^{-1}$ was realized. The Langmuir and Pseudo-n^{th} order models most suitably simulated the equilibrium and kinetics of sorption by both functionalized and non-functionalized biomaterials. The calcium alginate immobilized biosorbent was evaluated for non-specific sorption of ionic species of copper, chromium, nickel and iron from electroplating wastewater through discontinuous column sorption experiments. Highest copper, chromium, nickel and iron removal was 12.3%, 14.8%, 4.4% and 13.8% from non-acidified samples at an initial pH of 3.4, and 15.5%, 18.7%, 13.7% and 17.3% from samples acidified to an initial pH of 1.8. Repeated sorption-desorption cycles involving acidified wastewater resulted in successive improvement in metal uptake against declining recovery indicating irreversible binding on –COOH groups formed from $–CH_2OH$ groups through a redox reaction involving reduction of chromium(VI) to chromium(III).

Keywords: *Mangifera indica*; biosorption; alkali treatment; carboxyl functionalization; calcium alginate

Acknowledgements

I wish to express my sincere gratitude to my Supervisors Prof. Sekomeng Johannes Modise and Dr. Vusumzi Emmanuel Pakade for their valuable advice, guidance and support throughout the research project.

This dissertation would be incomplete without the support of my wife, Bessie, and daughter, Lwandle. Thank you for believing in me and bearing with me during those times when I was absent and engrossed in my work.

I am indebted to staff and colleagues in the Department of Chemistry for their improvement suggestions and technical assistance. Special thanks to Mr. Patrick Ngoy for making the extra effort to get me familiarized with analytical equipment operation.

I am grateful for financial support provided by the Vaal University of Technology and National University of Science and Technology through the VUT Grant and Staff Development Fund, respectively.

Dedication

To Mirrie and Jeff.

Table of Contents

List of Figures

List of Abbreviations

AAS	Atomic absorption spectrophotometry
ARE	Average relative error
ATMS	Alkali treated mango seed shell biomass
CFMS	Carboxyl functionalized mango seed shell biomass
DMF	N,N-dimethylformamide
DTPA	Diethylenetriaminepentaacetic acid
DTG	Derivative thermogravimetry
EDTA	Ethylenediaminetetraacetic acid
FTIR	Fourier Transform Infrared spectroscopy
ICP-OES	Inductively coupled plasma optical emission spectrophotometry
MSSP	Mango seed shell powder
TGA	Thermogravimetric analysis
XRD	X-ray diffraction
XPS	X-ray photoelectron spectroscopy

CHAPTER 1

OVERVIEW OF RESEARCH PROJECT

1.1 Background

It is recognized globally that water has become scarce due, in part, to increased demand by a growing population as well as rising industrial and agricultural activities (United Nations Environment Programme 2012). Moreover, the situation is exacerbated by pollution of freshwater by industrial wastewater and agricultural run-off. Heavy metal pollutants, in comparison to some organic compounds, are non-degradable and thus tend to accumulate in living tissue and result in biomagnification (Peralta-Videa *et al.* 2009). Duruibe *et al*. (2007) documented that low to moderate concentrations of heavy metals have been shown to result in human disorders associated with lung and kidney function (cadmium), central and peripheral nervous system function (lead), cancer (arsenic) and congenital malformations (mercury).

Conventional methods for treatment of heavy metal laden water such as reverse osmosis, evaporation and condensation, precipitation and filtration, electrochemical treatment, ion exchange and adsorption onto activated carbon are often linked to high operational inputs, maintenance and/or waste (sludge) disposal costs that prohibit their application, especially in developing countries. The lack of financial resources for investment in conventional water treatment technologies may well be the primary reason for frequent use of contaminated freshwater with minimal or no treatment in isolated villages and communities in South Africa (Department of Water Affairs and Forestry 1996). Biosorption, which refers to the adsorptive removal of solutes by biomass-based materials, is a water treatment alternative worthy of research focus in developing nations.

Mango seed shells are typical lignocellulosic biomass that have lignin, cellulose and hemicelluloses as their major constituents (Henrique *et al*. 2013). These plant components possess hydroxyl, carbonyl and carboxyl functional groups capable of acting as metal ion binding sites. Therefore, mango seeds have the potential to provide an abundant resource for biosorbent preparation. Furthermore, the kernels obtained as a by-product following separation from the seeds can be used for extraction of fats and oils, which have been reported to possess medicinal properties (Kaur *et al*. 2010) and nutritive value (Jahurul *et al*. 2015).

In their natural state however, lignocellulosic biosorbents often exhibit low sorption capacities. Moreover, due to leaching of water soluble organics (Yang *et al*. 2011), they tend to increase the chemical oxygen demand and total organic content of the water being. Therefore, lignocellulosic biosorbents often require some physical and/or chemical treatment to remove extractable organic components and to improve their sorption properties.

1.2 Problem statement and significance of study

Marginalized areas of the South African society, which have not been spared of the challenges of scarce clean water, have been presented with the challenge of developing sustainable water treatment technologies using abundant low cost bioresources such as agricultural wastes. Mango seeds, while biodegradable, often create disposal problems owing mainly to their generation in large volumes and other environmental problems associated with attraction of flies and rodents, general unsightliness and generation of foul smelling by-products of biodegradation.

Since 1986, total mango (*Mangifera indica*) production in South Africa, situated principally in Limpopo and Mpumalanga Provinces, has realized a general increase in production from approximately 25000 tons in the 1987/88 season to 90000 tons in the 2004/05 cropping season. In 2008, production was 80000 tons, of which 73% of the mangoes were harvested for juicing as well as dried and pickled fruit production (Fivaz 2008). These production levels translated to generation of over 15000 tons of mango seed waste. Therefore, in the rural areas of mango producing regions in South Africa there exists a potential for sustainable use of such waste. The use of mango seed shells, as proposed in this research, will not only provide a means of sustainable waste management, but will also provide environmentally benign and complementary cost reducing alternatives to conventional water treatment techniques.

1.3 Research purpose, hypothesis and objectives

Based on the question of whether or not the shells of waste mango pips can be used for removal of metal ions from water, the aim of the research was to chemically modify powders obtained from the mango seed shells with the purpose of assessing their applicability in adsorptive water treatment technologies. Subsequently, the research hypothesis was that carboxyl functionalized mango seed shell sorbents will have higher sorption capacity than non-functionalized sorbents in the removal of metal ions from aqueous solutions. In order to provide answers to the research question and to test the hypothesis, the objectives of the research were:

- to prepare carboxyl functionalized biosorbent from *Mangifera indica* seed shells by chemical modification;
- to characterize the effects of chemical modification by comparison of physicochemical properties of both treated and untreated mango materials;
- to compare the performance of the modified mango seed shell biomass in the removal of Pb(II) ions from aqueous solutions;

- to immobilize the carboxyl functionalized seed shell biomass and examine the resultant granular biosorbent's performance in the removal of chromium, nickel and copper ions from electroplating wastewater.

1.4 Knowledge gap summary and statement of novelty

In the South African context, mango seed shells are readily available at low cost from farming and processing industries located chiefly in Limpopo and Mpumalanga. Though attention has been given to use of their kernels in the food and pharmaceutical industries (Arogba 1999; Solis-Fuentes & Duran-de-Bazua 2004; Abdalla *et al*. 2007; Kaur *et al*. 2010; Jahurul *et al*. 2015), the remainder of mango pips is considered waste. The use of mango seed shells as sorbents has, to a fair extent, been focused on the removal of dyes (Bhatnagar *et al*. 2009; Davila-Jimenez *et al*. 2009; Franca *et al*. 2010; Alencar *et al*. 2012; Malekbala *et al*. 2012).

Mohammad *et al*. (1997) demonstrated that mango seeds can be used for the removal of Cu(II) from aqueous solutions and remarked that the seed shells performed better than the kernels. Olu-Owolabi *et al*. (2012) found untreated mango stones to be a promising material for the development of low cost sorption technology for use in the removal of Cd^{2+} and Pb^{2+} from wastewater effluents. Ajaelu and Dawodu (2013) also noted the sequestration of Cd^{2+} using a whole mango seed sorbent. Using the alphonso variety, the work of Parekh *et al*. (2002) displayed mango seeds as an effective sorbent for copper, lead and cadmium ions in aqueous solution. Nadeem *et al*. (2015) revealed that autoclaving, boiling in water, and heating over a burner flame caused enhanced uptake of Cu^{2+} and Zn^{2+} by mango seed biomass. Recently, Nadeem *et al*. (2016) proceeded to immobilize the native mango seed biomass in calcium alginate and applied the granules in the treatment of Pb(II) ion bearing water.

A common feature of the aforementioned research is the use of the mango biomass in its natural or physically modified state thus leaving room for generation of data related to the use of chemically modified variants. To date, no literature is available on ligand grafted mango biosorbents for removal of metal ions from aqueous solutions. This work has presented, for the first time, modification of mango seed biomass by esterification with EDTA dianhydride thus synthesizing a novel biosorbent with significantly higher sorption capacity. Additionally, a calcium alginate immobilize form of the EDTA grafted biosorbent has been evaluated for removal of metal ions from electroplating wastewater.

References

Abdalla, A.E.M., Darwish, S.M., Ayad, E.H.E. & El-Hamahmy, R.M., 2007. Egyptian mango by-product 2: Antioxidant and antimicrobial activities of extract and oil from mango seed kernel. *Food Chem.*, 103(4), pp. 1141–1152.

Ajaelu, C.J. & Dawodu, M.O., 2013. Sequestration of cadmium ions onto mango (*Mangifera indica*) seed biomass: Kinetics and equilibrium studies. *J. Chem. Pharm. Res.*, 5(8), pp. 174–180.

Alencar, W.S., Acayanka, E., Lima, E.C., Royer, B., De Souza, F.E., Lameira, J. & Alves, C.N., 2012. Application of *Mangifera indica* (mango) seeds as a biosorbent for removal of Victazol Orange 3R dye from aqueous solution and study of the biosorption mechanism. *Chem. Eng. J.*, 209, pp. 577–588.

Arogba, S.S., 1999. The performance of processed mango (*Mangifera indica*) kernel flour in a model food system. *Bioresour. Technol.*, 70(3), pp. 277–281.

Bhatnagar, A., Minocha, A.K., Kumar, E., Sillanpaa, M. & Feon, B.-H., 2009. Removal of phenolic pollutants from water utilizing *Mangifera indica* (mango) seed waste and cement fixation. *Sep. Sci. Technol.*, 44(13), pp. 3150–3169.

Davila-Jimenez, M.M., Elizalde-Gonzalez, M.P. & Hernandez-Montoya, V., 2009. Performance of mango seed adsorbents in the adsorption of anthraquinone and azo acid dyes in single and binary aqueous solutions. *Bioresour. Technol.*, 100(24), pp. 6199–6206.

Department of Water Affairs and Forestry, 1996. *South African Water Quality Guidelines (second edition) Volume 1: Domestic Use*, Pretoria.

Duruibe, J.O., Ogwuegbu, M.O.C. & Egwurugwu, J.N., 2007. Heavy metal pollution and human biotoxic effects. *Int. J. Phys. Sci.*, 2(5), pp. 112–118.

Fivaz, J., 2008. South African Mango Growers Association Chairman's Report 2007/08. *S. Af. Mango Grow. Assoc. Res. J.*, 28, pp. 6–7.

Franca, A.S., Oliveira, L.S., Saldanha, S.A., Santos, P.I.A. & Salum, S.S., 2010. Malachite green adsorption by mango (*Mangifera indica L*.) seed husks: Kinetic, equilibrium and thermodynamic studies. *Desalin. Water Treat.*, 19(1-3), pp. 241–248.

Henrique, M.A., Silverio, H.A., Neto, W.P.F. & Pasquini, D., 2013. Valorization of an agro-

industrial waste, mango seed, by the extraction and characterization of its cellulose nanocrystals. *J. Environ. Manage.*, 121, pp. 202–209.

Jahurul, M.H.A., Zaidul, I.S.M., Ghafoor, K., Al-Juhaimi, F.Y., Nyam, K.-L., Norulaini, N.A.N., Sahena, F. & Omar, A.K.M., 2015. Mango (*Mangifera indica L.*) by-products and their valuable components: A review. *Food Chem.*, 183, pp. 173–180.

Kaur, J., Rathinam, X., Kasi, M., Leng, K.M., Ayyalu, R., Kathiresan, S. & Subramaniam, S., 2010. Preliminary investigation on the antibacterial activity of mango (*Mangifera indica L: Anacardiaceae*) seed kernel. *Asian Pac. J. Trop. Med.*, 3(9), pp. 707–710.

Malekbala, M.R., Soltani, S.M., Yazdi, S.K. & Hosseini, S., 2012. Equilibrium and kinetic studies of Safranine adsorption on alkali-treated mango seed integuments. *Int. J. Chem. Eng. Appl.*, 3(3), pp. 160–166.

Mohammad, A., Ajmal, M., Yousuf, R. & Ahmed, A., 1997. Adsorption of Cu(II) from water on the seed and seed shell of *Mangifera indica* (Mango). *Indian J. Chem. Technol.*, 4(5), pp. 223–227.

Nadeem, R., Manzoor, Q., Iqbal, M. & Nisar, J., 2016. Biosorption of Pb(II) onto immobilized and native *Mangifera indica* waste biomass. *J. Ind. Eng. Chem.*, 35, pp. 185–194.

Nadeem, R., Naqvi, M.A., Nasir, M.H., Saeed, R., Iqbal, T., Ashraf, M. & Ansri, T.M., 2015. Efficacy of physically pretreated *Mangifera indica* biomass for Cu^{2+} and Zn^{2+} sequestration. *J. Saudi Chem. Soc.*, 19(1), pp. 23–25.

Olu-Owolabi, B.I., Oputu, O.U., Adebowale, K.O., Ogonsolu, O. & Olujimi, O.O., 2012. Biosorption of Cd^{2+} and Pb^{2+} ions onto mango stone and cocoa pod waste: Kinetic and equilibrium studies. *Sci. Res. Essays*, 7(15), pp. 1614–1629.

Parekh, D.C., Patel, J.B., Sudhakar, P. & Kos, V.J., 2002. Removal of trace metals with mango seed powder. *Indian J. Chem. Technol.*, 9(6), pp. 540–542.

Peralta-Videa, J.R., Lopez, M.L., Narayan, M., Saupe, G. & Gardea-Torresdey, J., 2009. The biochemistry of environmental heavy metal uptake by plants: implications for the food chain. *Int. J. Biochem. Cell Biol.*, 41(8-9), pp. 1665–1677.

Solis-Fuentes, J.A. & Duran-de-Bazua, M.C., 2004. Mango seed uses: Thermal behaviour of mango seed almond fat and its mixtures with cocoa butter. *Bioresour. Technol.*, 92(1), pp. 71–78.

United Nations Environment Programme, 2012. *Status Report on The Application of Integrated Approaches to Water Resources Management*, Available at: http://www.un.org/waterforlifedecade/pdf/un_water_status_report_2012.pdf [Accessed: April 19, 2016].

Yang, F., Liu, H., Qu, J. & Chen, J.P., 2011. Preparation and characterization of chitosan encapsulated *Sargassum sp*. biosorbent for nickel ions sorption. *Bioresour. Technol.*, 102(3), pp. 2821–2828.

CHAPTER 2

LITERATURE REVIEW OF BIOSORPTION

2.1 Basic theory and concepts of sorption

Adsorption is the mass transfer process in which solutes, referred to as adsorbates, are transferred from the aqueous phase to, and accumulate on, the surface of a solid, designated as the adsorbent, upon which adsorbates are bound through chemical and/or physical interactions. Figure 2.1 illustrates the basic principles of adsorption. Initial contact of the adsorbent and adsorbate is dominated by occurrence the binding reaction. Thereafter, some of the bound sorbate may be simultaneously released through desorption. Eventually, equilibrium is established when the rate of binding is equivalent to the rate of desorption with neither solid nor fluid phase concentration changing. Alteration of the adsorbate concentration gradient between the aqueous and solid (adsorbed) phases as well as other properties of the former such as pH and temperature may result in the release of the adsorbates from the surface thus re-entering the aqueous phase.

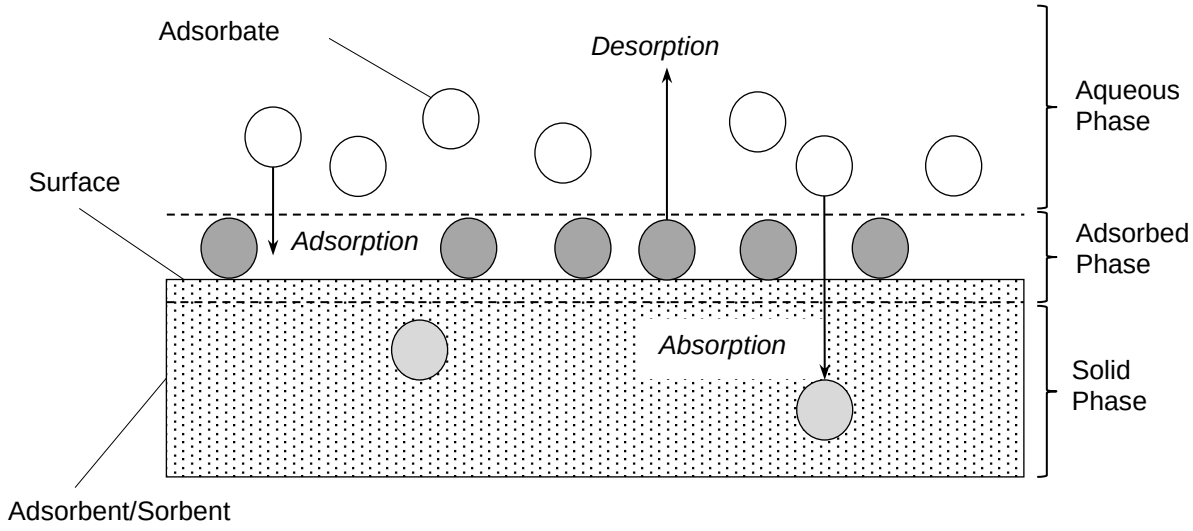

Figure 2.1: Basic terms associated with sorption (Worch 2012).

Adsorbent-adsorbate interaction at the surface can be considered as a reversible process represented thus:

$$\underset{(\textit{solid phase})}{\text{vacant binding site}} + \underset{(\textit{fluid phase})}{\text{adsorbate}} \underset{\text{desorption}}{\overset{\text{binding}}{\rightleftharpoons}} \underset{(\textit{adsorbed phase})}{\text{occupied binding site}} \qquad (1)$$

Apart from accumulating at the surface, the solutes may penetrate the surface thereby entering the solid phase. This dissolution process is referred to as absorption. The interaction of solids and fluids in nature is often associated with both adsorption and absorption. Accordingly, the term sorption is used to denote simultaneous and indistinguishable occurrence of both adsorption and absorption.

Biosorption and binding onto biosorbent surfaces is the subject of Section 2.1 whilst Section 2.2 deals with factors affecting the biosorption process. The focus of Section 2.3 is biosorbent preparation and Section 2.4 completes the chapter, focusing on the characterization of biosorption processes with respect to the application of various equilibrium and kinetic models.

2.2 Biosorption and biosorption mechanisms

Biosorption has been described by Volesky (2007) as the property of biomass to selectively bind and concentrate certain ionic and molecular species from aqueous solutions. Biosorption by living biomass features both adsorption on the external cell wall surface and absorption through metabolic transport across cell membranes followed by complex bioaccumulation processes. Conversely, biosorption processes involving non-living biomass are passive and only occur on the external surfaces.

Biosorbent surfaces comprise several types of functional groups with metal ion binding capabilities as revealed on numerous occasions by Fourier transform infra-red (FTIR) and X-ray photoelectron spectroscopic (XPS) analyses (Sun *et al*. 2008; Xu & Liu 2008; Zheng *et al*. 2009; Cruz-Olivares *et al*. 2011; Yang *et al*. 2011; Liu *et al*. 2015). Davis *et al*. (2003) categorized binding mechanisms as either physical or chemical. The former corresponds to physisorption in which the metal ions are attached onto the surface functional groups by van der Waals forces in the form of ion-permanent dipole and ion-transient dipole forces. Chemical binding mechanisms, which are associated with chemisorption, involve ionic (electrovalent) or dative covalent bonding between the metal ions and the binding groups. From this simplistic aspect it can be noted, in accordance with the recent attempt by Robalds *et al*. (2016) to highlight inconsistencies regarding metal biosorption, that:

(i) complexation fundamentally retains its status as a chemisorption process owing to formation of primary bonds between the metal ions and binding sites;
(ii) micro-precipitation or surface precipitation can be considered as a chemisorptive binding process since precipitation essentially involves crystallization; and
(iii) ion exchange can be viewed as a phenomenon that accompanies substitution of physically and/or chemically bound ions with the desired target ions.

Nonetheless, the existence of a wide variety of surface functional groups in conjunction with their dynamic response to environmental conditions means that these mechanisms can operate simultaneously, albeit to varying extents.

2.2.1 Complexation

Complexation of cationic species of the form M^{n+} typically involves coordination by at least two electron donating ligand atoms. An inner-sphere complex is the result of association of the surface ligands with the metal ion. Outer-sphere complexes are formed when the cation approaches the electron donating atom at a critical distance, but, the ligand atom and the cation are separated by at least one water molecule of its hydration sphere. Sheng *et al*. (2004) analyzed the deconvoluted XPS peaks assigned to Cu^{2+} species to distinguish between inner- and outer-sphere complexation. They reported that the first of two peaks appearing at lower binding energy indicated inner-sphere complexation thus the acceptance of electrons from the ligands to form a dative bond formation. A peak appearing at higher binding energy indicated outer-sphere complexation and represented an ionic environment with minimal negative density. In the same work, it was also noted that, owing to the possession of full *d* orbitals and a lack of unoccupied orbitals in the highest energy level, Zn^{2+} and Cd^{2+} complexation was only through outer-sphere coordination involving carboxylates.

Failure of Cd^{2+} to form inner-sphere complexes together with simultaneous binding of Cu^{2+} through both inner- and outer-sphere complexation was also highlighted by Xu and Liu (2008). Vinod *et al*. (2009) reported lead peak deconvolution and made reference to the existence of lead on the surface of *Cochlospermum gossypium* biomass in both the $(–COO)_2Pb$ and Pb^{2+} forms conforming to inner- and outer-sphere complexation, respectively. Following application of XPS on pristine and Pb^{2+} loaded *Pimenta dioica* biosorbent, Cruz-Olivares *et al*. (2010) suggested the formation of two types of complexes. The first was formed using oxygen atoms from hydroxyl and ether groups, and the second resulted from interaction with two hydroxyl ligands.

2.2.2 Physisorption and surface precipitation

Binding can occur on the basis of non-specific ion-dipole attractive forces existing between metal ions and polar functional groups or polarizable moieties such as lignin aromatic rings. Zhou *et al*. (2005) speculated that lead-oxygen interactions involved in the sorption of Pb^{2+} onto a cellulose-chitin composite were largely physical. This followed a revelation by XPS that only nitrogen atoms formed dative bonds with the metal ions. The same work documented precipitation of the hydrolysis products of complexation, which acted as the nucleation sites of micro-precipitation. Martinez *et al*. (2006) reported the binding of Cd^{2+} on lignin aromatic rings having noted significant attenuation of an FTIR band at 1610 cm^{-1} attributed to C=C stretch vibrations. This may have been a result of physical interaction of the π-electrons with the metal

ions. Interestingly, sorption of Pb^{2+} exhibited dissimilar behavior indicating existence of a different binding mechanism.

2.2.3 Ion-exchange

In ion exchange, ionized surface groups such as carboxylates, phenolates, and alkoxides experience replacement of their counter ions with the target pollutant ions. A vivid illustration of ion exchange involving acidic functional groups on coconut copra meal is surmised in the work of Ofomaja and Ho (2007) in which initial cadmium solution pH was fixed at 5.53 whilst initial cadmium concentration was varied within the 30–140 $mg.L^{-1}$ range where sorption was allowed to proceed under stirring for 2 h periods. They noted, with increasing initial concentration, decreases in pH to values within the 3.55–2.61 range together with increases in sorbent loading in the 0.461–1.70 $mg.g^{-1}$ range. This signified the exchange of H^+ ions for Cd^{2+} ions during sorption. Xu and Liu (2008) also reported release of Ca^{2+}, Mg^{2+} and K^+ into solution concurrently with the sorption of Cd^{2+}, Cu^{2+} and Ni^{2+} onto aerobic biomass granules.

Di Caprio *et al*. (2014) developed a mechanistic sorption equilibrium model describing the influence of pH and metal ion concentration on copper uptake by *Saccharomyces cerevisiae* biomass accounting for the exchange of Cu^{2+} for H^+ of hydroxyl, carboxylic, phosphoric, and protonated amine groups. The model was remarked to have satisfactorily reproduced sorption experimental data. Yakkala *et al*. (2013) explored the possibility of ion exchange in the sorption of cadmium (II) and lead (II) on buffalo weed biochar using energy-dispersive X-ray (EDX) spectroscopy to analyze the sorbent before and after sorption. They noted a significant reduction in the peaks assigned to Ca^{2+} with slight amplification of several peaks attributed to Cd^{2+} and Pb^{2+}. The exchange of Ca^{2+} for Cd^{2+} and Pb^{2+} suggested thus was corroborated by the reduction in calcium ion weight percentage from 76.7% to 11.5% accompanied by increases in Cd^{2+} and Pb^{2+} removal from 0 to 12.4% and 72.7%, respectively.

2.3 Factors affecting biosorption

Quantity, accessibility, type and form of surface functional groups have a significant role in the performance of a biosorbent. It is easily conceivable that the greater the proportion of binding groups, then the better will be the performance of the sorbent, a notion that has formed the basis of many biosorbent modification efforts (Karnitz *et al*. 2009; Zhang *et al*. 2010; Wu *et al*. 2012; Kaya *et al*. 2014; Madrid *et al*. 2014). Although FTIR analysis of raw biosorbents may indicate presence of numerous functional groups, inaccessibility resulting from poor porosity and hydrogen bonding frequently renders them poor performers. Ofomaja and Naidoo (2011)

revealed the usefulness of improving porosity, through alkali treatment of pine cone biomass, in enhancing Cu^{2+} sorption capacity especially in a backdrop of diminished surface negative charge. In this work, it was also recognized that some of the ordered crystalline cellulose fractions of the biosorbent were slightly disorientated by modification through breakage of hydrogen bonds. Hu *et al*. (2015) noted improved accessibility of hydroxyl groups following the disruption of cellulose hydrogen bonded structures highlighting it as an important factor in the enhancement of Cu^{2+} sorption onto *Acidosasa edulis* shoot shell biomass.

Surface functional group type relates to affinity for the sorbate and the primary binding mechanism. The value of electron donating oxygen and nitrogen bearing functional groups as cation binding sites has been widely established in the literature, with the key types being carbonyl, carboxyl, hydroxyl, ether and amine groups (Sun *et al*. 2008; Xu & Liu 2008; Zheng *et al*. 2009; Cruz-Olivares *et al*. 2011; Yang *et al*. 2011; Liu *et al*. 2015). Other groups, such as esters, have been shown to be rather passive. Subsequent to deactivation of carboxyl functional groups by esterification, Chubar *et al*. (2004) recorded significant reduction in the uptake of zinc, copper and nickel ions by cork oak tree biomass. Later, Iqbal *et al*. (2009) separately deactivated hydroxyl and carboxyl groups of mango peel waste biosorbents using formaldehyde and methanol, respectively. They observed that 23.7% and 26.7% removal of Pb^{2+} and Cd^{2+} was due to action of hydroxyl groups whilst 76.3% and 72.5% removal was attributable to binding on carboxyl moieties, respectively. Torab-Mostaedi *et al*. (2013) noted similar results for Cd^{2+} and Ni^{2+} removal by grapefruit peel having blocked the activity of hydroxyl and carboxyl groups in a similar manner. Therefore, replacement or conversion of low affinity functional groups through, for example, phosphorylation, amination, saponification and carboxylation has become common practice in biosorption research (Park *et al*. 2010).

Given that biosorption is primarily a surface process, surface area, which increases with decreasing particle size, greatly influences the performance of biosorbents. Generally, the greater the surface area that is exposed to the aqueous phase, then the better will be the performance of the adsorbent. The surface area of an adsorbent can be separated into an external and internal surface area. A precondition for raised internal surface area is high porosity. Normally, the more porous the adsorbent and the finer the pores, the higher will be the internal surface area. However, it is desirable for adsorbents to possess a certain fraction of large pores, which enable rapid transfer of sorbates to the active sites. Therefore, pore size distribution is an additional key parameter. The high adsorption capacities of activated carbons and other engineered adsorbents have been largely attributed to their high internal surface area, pore volume and pore size distribution (Mohan *et al*. 2006; Worch 2012).

Apart from sorbent related factors, several process factors have also been quoted as having an influence on the performance of a biosorbent. These include solution pH, initial sorbate

concentration, sorbent dose, sorbent particle size, temperature, agitation and ionic strength (Fomina & Gadd 2014). Amongst these, solution pH can be viewed as the most influential principally due to the effect that H^+ and OH^- ions have on the forms of the sorbates and binding sites in addition to competition with the target pollutant for binding (Basu *et al*. 2015; Guo *et al*. 2015; Guyo *et al*. 2015). At low pH, competition for and subsequent extensive occupation of binding sites by H^+ renders the surface functional groups positively charged. Therefore, in acidic solutions cationic sorbates experience repulsion by protonated sites. Gradual pH increase leads to de-protonation and thus increased attraction of cationic sorbates. Extensive de-protonation may even result in a net negative charge of the biosorbent surface. High sorbate uptake can be reached beyond which an increase in pH results in lowered uptake due to chemical precipitation and complexation by hydroxide ions. In cases whereby the latter results in negatively charged species such as $[Cu(OH)_4]^-$, repulsion with deprotonated functional groups arises.

2.4 Biosorbent preparation

The previous subsection highlighted the importance of small sorbent particle sizes. Typical biosorbent preparation processes, therefore, feature a particle size reduction step that is usually preceded by washing and drying for removal of debris from the raw biomass. Application of fine biosorbent powders in sorption columns, however, presents problems of clogging and the development of a high pressure drop, sorbent swelling and poor regeneration for reuse. Therefore, to adapt biosorbents for column sorption, sorbent preparation may include a granulation step.

In order to increase the sorption capacity of the biosorbent and/or to alter its function, the preparation process may include one or more physical or chemical modification steps. Physical modification includes boiling in water (Nadeem *et al*. 2015), plasma treatment (Prola *et al*. 2013) and freeze drying (Sar *et al*. 1999). Chemical modification includes chemical washing, reactions to enhance, eliminate or deactivate certain functional groups, and graft polymerization. However, it is important to note that modification and granulation increase biosorbent costs and nullify the low-cost advantage that is often recognized amongst the major advantages of biosorbents.

2.4.1 Chemical pre-treatment

Chemical pre-treatment usually involves washing with acid or alkali solutions, organic solvents and other reagent mixtures that remove certain components of the parent biomass and often

react with certain surface functional groups to improve functionality and performance of the biosorbent. Typical effects of acid and alkali washing on key physicochemical characteristics of biosorbents are highlighted in the work of Ronda *et al*. (2013) who used 1 M solutions of sulfuric acid, nitric acid and sodium hydroxide solutions for the pre-treatment of olive tree biomass for sorption of Pb^{2+}. They noted increases in the proportion of acidic titratable sites coupled with a drastic decrease in basic sites, which translated to a lowered point zero charge, owing to acid treatment; an indication of protonation of surface functional groups. Conversely, sodium hydroxide washing eradicated acidic sites from an estimated 0.491 $mmol.g^{-1}$ thus portraying all titratable groups as basic with point zero charge being noted to increase from 5.24 to 6.77. The most significant changes in specific surface area and total pore volume corresponded to sodium hydroxide treatment and were reflected by increases from 0.63 to 3.53 $m^2.g^{-1}$ and 1.54 x 10^{-3} to 5.85 x 10^{-3} $cm^3.g^{-1}$, respectively.

These could be ascribed to delignification and hemicellulose extraction, which were indicated by 46.7% loss in mass due to alkali treatment in comparison to 35.1% and 27.5% relating to nitric acid and sulfuric acid washing, respectively. In all instances, pre-treatment resulted in enhanced biosorption capacity as reflected by increases in equilibrium sorbent loading from 12.97 $mg.g^{-1}$ to 14.15, 15.36 and 16.04 $mg.g^{-1}$ corresponding to nitric acid, sulfuric acid and sodium hydroxide pre-treatment, respectively. Alkali treatment has also been noted to enhance the metal ion sorption capacity of biosorbents prepared from cork oak (Chubar *et al*. 2004), juniper fiber (Min *et al*. 2004), rice husk (Kumar & Bandyopadhyay 2006), orange peel (Feng *et al*. 2010), pine cone (Ofomaja *et al*. 2010), coir fiber (Shukla & Shukla 2013), banana peel (Massocatto *et al*. 2013) and rice bran (Zafar et al. 2015).

Several authors have also reported the use of formaldehyde as a pre-treatment agent chosen primarily for stabilization, through crosslinking and polymerization of water soluble organic components of the biomass thus mitigating their release into water that underwent treatment (Taty-Costodes *et al*. 2003; Chen & Yang 2005; Baral *et al*. 2006; Li *et al*. 2007; Lugo-Lugo *et al*. 2010; Karaoglu *et al*. 2011). Ethanol, pure or blended with other chemicals, has also been used as a pre-treatment agent for preparation of metal ion biosorbents (Goksungur *et al*. 2005; Y. Zhang *et al*. 2010; Ofomaja *et al*. 2013). However, formaldehyde and ethanol may inhibit binding by hydroxyl and carboxyl groups through esterification and etherification, respectively (Torab-Mostaedi *et al*. 2013).

2.4.2 Surface site modification

Surface modification to enhance the proportion and/or quality of binding functional groups or to eliminate inhibiting groups has become a common feature of biosorbent preparation (Wan

Ngah & Hanafiah 2008; Gautam *et al*. 2014). A vast majority of surface modification processes involve reactions that target abundant hydroxyl groups using them to attach desired functional groups through formation of ester (El-Gendy *et al*. 2013; Gusmao *et al*. 2013; Guo *et al*. 2015; Zhou *et al*. 2015) and ether (Yu *et al*. 2007; Deng *et al*. 2013; Singha & Guleria 2014; Guo *et al*. 2014; Xu *et al*. 2015) linkages. The use of anhydrides for modification of peanut shells (Li *et al*. 2012), babassu coconut (Vieira *et al*. 2010), olive stone (Aziz *et al*. 2009), sugarcane bagasse (Gurgel *et al*. 2008) and soya bean straw (Zhu *et al*. 2008) has been reported in the literature reviewed. The basic principle of the process is the reaction of nucleophilic alcoholic and phenolic –OH groups with the anhydride groups of the modifying agent (formed *in situ* when citric acid is used) thus forming an ester bond and a terminal carboxylic acid group on the grafted chain. The use of ethylenediaminetetraacetic (EDTA) bisanhydride as a modifying agent is particularly preferred for introduction of chelating properties owing to the presence of five binding sites on each grafted group.

Inoue *et al*. (1999) accomplished ligand immobilization by reacting EDTA bisanhydride and diethylenetriaminepentaacetic acid (DTPA) bisanhydride with chitosan and polyallylamine resulting in successful use of the material for chromatographic separation and concentration of Co^{2+} and Ni^{2+} in the presence of a large excess of Al^{3+}. Using baker's yeast and EDTA bisanhydride as a modification agent, Yu *et al*. (2008) revealed sorption capacity enhancement from 4.5 to 65.0 $mg.g^{-1}$ for Cu^{2+} as well as 20.0 to 192.3 $mg.g^{-1}$ for Pb^{2+} can be achieved. EDTA bisanhydride has also been used to modify cellulose (Karnitz *et al*. 2009), *Manilkara sp*. wood sawdust and sugarcane bagasse (Pereira *et al*. 2010) with subsequent application in the removal of Zn^{2+}, Cu^{2+}, Cd^{2+} and Pb^{2+} from aqueous solutions.

Grafting by etherification has extensively been achieved by using epoxidated intermediates formed by a reaction of the biosorbent with epichlorohydrin. However, Yu *et al*. (2007) exploited the reaction of aldehyde groups with hydroxyls and amines to graft polymeric chains of a cystine and glutaraldehyde polymer to baker's yeast. Guo *et al*. (2014) modified bamboo powder with epichlorohydrin prior to treatment with diethylenetriamine and noted that the preliminary treatment with sodium hydroxide solution was necessary to convert the alcoholic and phenolic –OH groups into more nucleophilic alkoxide and phenoxide ions that better suited the reaction with the epichlorohydrin. For the purpose of grafting tannin onto the surface of jute fiber, Roy *et al*. (2013) used a similar pre-treatment step in which, after separating the activated material from the spent sodium hydroxide solution, the jute fiber was placed in fresh alkali solution prior to epichlorohydrin addition. The presence of the alkali solution promoted epoxidation of the halohydrin bearing product of the reaction with epichlorohydrin.

Zhu *et al*. (2015) prepared a bagasse pulp cellulose sorbent through initial epoxidation with epichlorohydrin followed by primary and secondary grafting with diethylenetriamine and

carbon disulfide, noting a significant introduction of both nitrogen and sulfur onto the material. Liu *et al*. (2010) developed aminated peanut shell sorbent by modification with epichlorohydrin and ethylenediamine realizing over two- and fifteen-fold increase in the sorption capacity for Cd^{2+} and Hg^{2+}, respectively. Several hydrocarbon substituents have been grafted onto various lignocelluloses in organic media often using N,N-dimethylformamide as a solvent and pyridine as a wetting agent for epoxidation (Orlando *et al*. 2002; Abdel-Halim *et al*. 2007; Anirudhan & Unnithan 2007; Wang *et al*. 2010; Chen *et al*. 2011; Keranen *et al*. 2013; Xu *et al*. 2015). However, high procurement costs associated with the organic chemicals together with the need for proper waste disposal necessitated by the chemicals' hazardous nature tend to increase the biosorbent processing costs.

2.4.3 Granulation

Depending on the nature of the biosorbent, granulation can be achieved through reacting the biosorbent with chemical cross-linkers such as formaldehyde and epichlorohydrin, immobilization on solid supports such as zeolite (Quintelas *et al*. 2013) and activated carbon (Mahmoud *et al*. 2015), or encapsulation within a porous polymeric matrix such as polyurethane (Alhakawati & Banks 2004; Zhang & Banks 2006), polysulfone (Beolchini *et al*. 2003; Vijayaraghavan & Jegan 2015) or alginate (Sag *et al*. 1995; Fiol *et al*. 2004; Jeon *et al*. 2015). Alginate encapsulation provides opportunities for the control of granule size and achievement of high sorbent loading through simple and rapid procedures that essentially involve dropping a suspension of the biosorbent and alginate solution into a fixing solution containing divalent metal ions usually Ca^{2+}. The droplets immediately form hydrogel beads upon contact with the fixing solution and harden when left in the solution.

Alginates are the salts of alginic acid, a polysaccharide containing 1,4-linked β-D-mannuronic acid (M) and guluronic acid (G) residues forming irregularly ordered long chains comprising heteropolymeric $(–MG–)_n$ together with homopolymeric $(–M–)_n$ and $(–G–)_n$ blocks (Haug *et al*. 1966). Alignment of two G-blocks, which have higher affinity for divalent metal ions (Davis *et al*. 2003), creates coordination sites that can accommodate the ions. Therefore, when alginate solution is introduced into a calcium ion solution, binding of Ca^{2+} on G-block dimers formed by separate chains results in interconnection or cross-linkage. These regions of dimerization are largely terminated by M-blocks in accordance with the recognized egg-box model (Ibanez & Umetsu 2002). Increasing cross-linkage yields increased viscosity and thus gelation as illustrated in Figure 2.2.

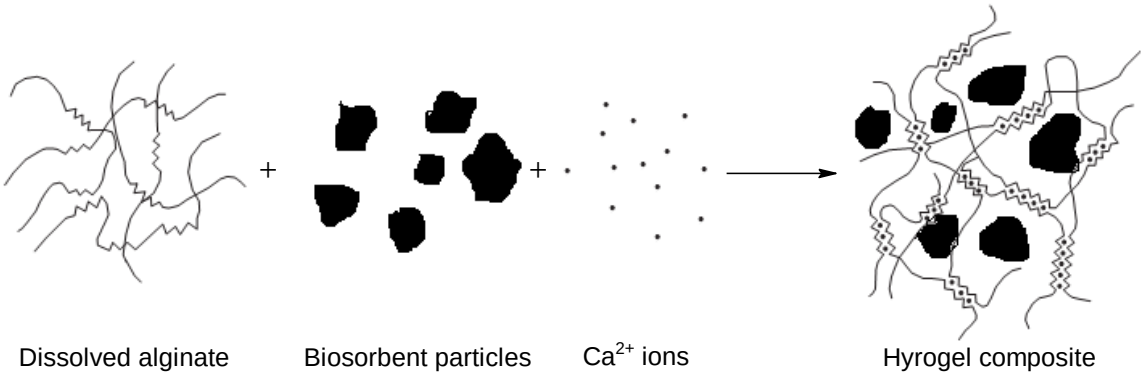

Figure 2.2: Schematic depiction of alginate encapsulation (Davis *et al*. 2003).

Recently, An *et al*. (2015) prepared alginate immobilized jujube biosorbent and compared the characteristics of oven dried (90°C and 20°C) and freeze dried forms of the beads. Freeze dried bead exhibited the greatest surface area and pore volume followed by 20°C dried beads and, lastly, the beads dried at 90°C. In spite of these observations, however, insignificant differences in removal of lead and copper were noted. This highlighted the importance of the role of immobilized jujube biomass within the composite. This was confirmed by the outcome of experiments using similarly prepared beads of different biomass content, which showed increasing lead adsorption capacity with increasing jujube content. Fiol *et al*. (2005) drew attention to the activity of grape stalk waste immobilized in calcium alginate by noting a Langmuir maximum sorption capacity of 71.98 mg per bead for grape stalk biosorbent loaded beads compared to 19.93 mg per neat alginate bead. They also asserted that encapsulation in calcium alginate, which allowed the employment of sorbent powders with a finer texture than those used in conventional batch sorption tests, resulted in an apparent increase in the sorption capacity of the biomass.

2.5 Characterization of sorption processes

Sorbent uptake can be expressed in terms of the quantity of bound sorbent, given by the difference in solution content before and after sorption, and mass of sorbent as follows:

$$.q = \frac{(C_i - C_f)\ V}{m} \qquad (2)$$

where q (mg.g^{-1}) is referred to as sorbent loading. V (L) and m (g) represent solution volume and sorbent mass, respectively. C_i (mg.L^{-1}) and C_f (mg.L^{-1}) are the initial and final concentration of sorbate the aqueous phase, respectively.

Two important elements of the sorption theory are sorption equilibrium and sorption kinetics, which describe the dependence of q on equilibrium sorbate concentration and time, respectively. Accordingly, two fundamental types of data can be obtained from batch sorption experiments: kinetic data, which is collected at periodically during the progress of sorption, and equilibrium data relating to the state of the sorption process characterized by insignificant change in the concentration of sorbent in the solid and aqueous phases. For this reason, common practice has been to denote q and C_f at any time t prior to attainment of equilibrium as q_t and C_t, respectively, whereas after attainment of equilibrium $q = q_e$ and $C_f = C_e$. When q_e is plotted against C_e for data obtained at constant temperature and fixed initial operating conditions, the outcome is referred to as an isotherm.

The dependence of sorbent loading on equilibrium sorbate concentration and time can be analyzed by the application of various equilibrium and kinetic models, respectively. Furthermore, these models enable the prediction of different characteristics of the sorption process including sorption capacity and binding mechanisms.

2.5.1 Kinetic models

From a mechanistic point of view, biosorption can be split into the following five stages involving transport and surface reaction: (i) sorbate transportation from the bulk of the aqueous solution to the external surface of the boundary layer surrounding the sorbent particle – bulk diffusion; (ii) transport across the boundary layer to its inner surface in contact with the sorbent – film diffusion; (iii) reaction with binding sites on the external sorbent surface – external physisorption or chemisorption; (iv) transportation through the liquid contained in the pores of the sorbent toward the internal sorbent surface – pore or intra-particle diffusion; and (v) binding reactions on the internal sorbent surface. The slowest of these five steps is considered to be rate-determining. However, it is generally acceptable to ignore bulk diffusion under sufficient agitation owing to relative rapidity of this first step. The binding reactions of steps (iii) and (v) are also considered to be so rapid that they negligibly contribute to sorption rate control.

For the purpose of investigating biosorption rate control, several kinetic models including the pseudo-first order, pseudo-second order, Elovich, double exponential, Bangham's and intra-particle diffusion models have been used (Liu & Liu 2008; Febrianto *et al*. 2009). Ho *et al*. (2000) and Qiu *et al*. (2009) have categorized these as either reaction models or diffusion models (Figure 2.3). Sorption reaction models do not distinguish any particular step as rate determining as they consider the overall sorption process. Sorption diffusion models regard one or more of the sorbate transport steps to be rate-controlling.

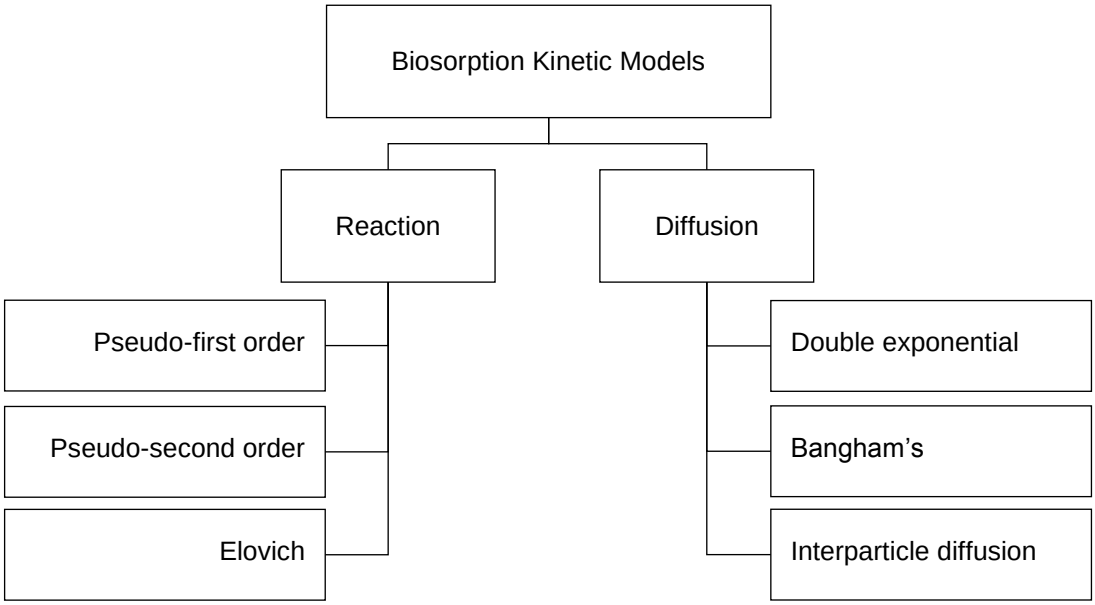

Figure 2.3: Classification of biosorption kinetic models.

2.5.1.1 Sorption Reaction models

Sorption rate according to the pseudo-first order model of Lagergren (1898) is given by the following expression:

$$\frac{dq_t}{dt} = k_1(q_e - q_t) \tag{3}$$

where k_1 (min^{-1}) represents the pseudo-first order and q_e ($mg.g^{-1}$) is the model's prediction of equilibrium sorbent loading. After integration and consideration of the boundary conditions $q_t = 0$ at $t = 0$ and $q_t = 0$ q_t at $t = t$, Equation (3) takes up the following form:

$$q_t = q_e(1 - e^{-k_1 t}) \tag{4}$$

Since its development, Boyd *et al*. (1947), Liu *et al*. (2003) and Azizian (2004) have used different theoretical approaches to derive Equation (4) based on stoichiometric reactions between sorbate species and sorbent binding sites. All three approaches revealed a direct proportionality relationship between sorption rate and the number of available binding sites.

Ho and Mckay (1999) documented the development of a pseudo-second order kinetic model with a rate equation that can be expressed as follows:

$$\frac{dq_t}{dt} = k_2(q_e - q_t)^2 \tag{5}$$

where k_2 (g.mg^{-1}.min^{-1}) is the pseudo-second order rate constant and q_e (mg.g^{-1}) represents the model's prediction of equilibrium sorbent loading. After integration and consideration of the boundary conditions $q_t = 0$ at $t = 0$ and $q_t = 0$ q_t at $t = t$, Equation (5) becomes:

$$q_t = \frac{k_2 q_e^{\,2} t}{1 + q_e k_2 t} \tag{6}$$

The pseudo-second order model assumes sharing of valence electrons between binding functional groups and bound metal ions. Using a more general approach that does not specify the nature of both sorbent binding site, Azizian (2004) also arrived at Equation (6) thus corroborating the proposed binding reaction. Instead of assuming the sorption reaction order to be 1 or 2 as implied by the pseudo-first and pseudo second order models, Ozer (2007) proposed calculation of the rate constant together with the reaction order, designated *n*. Accordingly, the rate equation of the pseudo-nth order model can be represented as:

$$\frac{dq_t}{dt} = k_{nth}(q_e - q_t)^n \tag{7}$$

where k_{nth} [min^{-1} (mg.g^{-1})$^{1-n}$] is the pseudo-nth order rate constant and q_e (mg.g^{-1}) represents the model's prediction of equilibrium sorbent loading. After integration with application of the boundary conditions, $q_t = 0$ at $t = 0$ and $q_t = 0$ q_t at $t = t$, Equation (7) assumes the following form:

$$q_t = q_e - \left[(n - 1)k_{nth}t + q_e^{\,(1-n)}\right]^{1/(1-n)} \tag{8}$$

The equation of the Elovich kinetic model (Zeldowitsch 1934) can be expressed as follows:

$$\frac{dq_t}{dt} = \alpha \exp(-\beta q_t) \tag{9}$$

where α (mg.g^{-1}.min^{-1}) is the initial sorption rate and β (g.mg^{-1}) is the desorption constant. Integration with application of the boundary conditions $q_t = 0$ at $t = 0$ and $q_t = 0$ q_t at $t = t$, yields:

$$q_t = \frac{1}{\beta}\ln(1 + \alpha\beta t) \tag{10}$$

The Elovich kinetic model is applicable to chemisorption onto heterogeneous sorbents (Rudzinski & Panczyk 2000; Cheung *et al*. 2001; Cruz-Olivares *et al*. 2011; Pezoti *et al*. 2016).

2.5.1.2 Diffusion models

Intra-particle diffusion is presumably the slowest of the steps involved in the biosorption process. However, the extent of its occurrence is largely dependent on key textural properties of the sorbent including pore volume and pore size distribution. The application of Bangham's pore diffusion model (Aharoni *et al*. 1979) and the Weber-Morris intra-particle diffusion model (Weber & Morris 1963) facilitates the determination of the contribution of intra-particle diffusion to sorption rate control. The Bangham's model equation can be expressed as follows:

$$\log\left[\log\left(\frac{C_i}{C_i - q_t m_s}\right)\right] = \log\left(\frac{K_B m_s}{2.303V}\right) + \alpha_B \log t \qquad (11)$$

where m_s (g.L^{-1}) represents sorbent dosage, V (L) is solution volume, and K_B (L.g^{-1}) and α (dimensionless; $\alpha < 1$) are model constants. The nonlinear form of the equation that has q_t as the subject is given by:

$$q_t = \frac{C_i}{m_s}\left[1 - 10^{-\frac{K_B m_s t^{\alpha_B}}{2.303V}}\right] \qquad (12)$$

The model describes experimental data to distinguish intra-particle diffusion as the sole rate determining step. Failure of the model to fit experimental data may mean that intra-particle diffusion is partly responsible for sorption rate-control. The Weber-Morris model equation can be expressed as follows:

$$q_t = k_{id} t^{0.5} + c \qquad (13)$$

where k_{id} (mg.g^{-1}.min$^{-0.5}$) represents the intra-particle diffusion rate constant and c (mg.g^{-1}) is a constant related to the thickness of the boundary layer surrounding the sorbent particles. If Equation (13) fits the experimental data well, implying linearity, such that c = 0, then the kinetics of sorption are deemed to be controlled by intra-particle diffusion, that is, values of the intercept that deviate from the origin are considered to imply significant contribution of film diffusion to sorption rate-control. In several studies the plots of q_t versus $t^{0.5}$ have been separated into two or three successive linear portions to illustrate distinctly the occurrence of film diffusion prior to intra-particle diffusion (Ronda *et al*. 2013; Blazquez *et al*. 2014; Hu *et al*. 2015).

The occurrence of film and intra-particle diffusion can also be illustrated by the application of a model suggested by Wilczak and Keinath (1993) used empirically to describe sorption of Cu(II) and Pb(II) onto activated carbon. Observations from the study were that the uptake processes featured an initial rapid step that was followed by a slower, prolonged step, as

sorption equilibrium was approached. The equation of this two-step sorption model can be expressed as follows:

$$q_t = q_e - \frac{D_1}{m_s}\exp(-K_{D1}t) - \frac{D_2}{m_s}\exp(-K_{D2}t) \quad (14)$$

where D_1 and D_2 ($mg.L^{-1}$) are sorption rate parameters of the rapid and slow step, respectively, with K_{D1} and K_{D2} (min^{-1}) being the rapid and slow step rate constants while m_s ($g.L^{-1}$) represents sorbent dosage. Chiron *et al*. (2003) highlighted that although the two steps involve both film and intra-particle diffusion, film diffusion is predominant in the rapid step whereas intra-particle diffusion is predominant in the slow step.

2.5.2 Equilibrium/Isotherm models

Models that have been developed to represent biosorption isotherms can be categorized as empirical or mechanistic. Empirical models only simulate observed isotherms and no inference regarding the sorbate binding mechanisms can be made from their application. In addition to simulating experimental data, mechanistic models reveal and account for certain aspects of, the mechanisms involved in sorbate binding (Fomina & Gadd 2014). Di Caprio *et al*. (2014) developed a model for the sorption of divalent copper ions using yeast to describe binding by ion exchange involving carboxylic, amino and phosphoric groups. Pagnanelli *et al*. (2005) validated two mechanistic models that accounted for the sorption of Cu^{2+}, Cd^{2+}, Pb^{2+} and their respective hydroxo-complexes onto olive pomace through surface complexation involving carboxylate and phenoxide ions. Such development of mechanistic models essentially involves close monitoring of sorbent and sorbate properties in order to hypothesize binding reactions.

Although inferences regarding mechanisms cannot be made application of empirical models, they often provide good simulation of biosorption isotherms. The need for sophisticated algorithms for data manipulation coupled with the complexity of biosorbents possessing different functional groups thus varied binding capabilities results in complications when applying mechanistic models. This possibly accounts for their infrequent use relative to that of empirical isotherm models. Additionally, empirical models are easy to interpret and have some physical meaning. Common empirical isotherm models employed in biosorption include the two-parameter Langmuir, Freundlich and Dubinin-Radushkevich as well as three-parameter Sips, Redlich Peterson and Toth models.

The Langmuir model (Langmuir 1916) essentially assumes (i) energetic equivalence of binding sites, (ii) accommodation of one sorbate particle per binding site, (iii) independence of

adsorption of one sorbate particle from occupancy of neighboring sites, and (iv) the formation of a sorbate monolayer. The model equation can be represented as:

$$q_e = \frac{q_{maxL} K_L C_e}{1 + K_L C_e} \tag{15}$$

where q_{maxL} is the maximum monolayer sorbent loading ($mg.g^{-1}$) corresponding to binding site saturation and K_L is the Langmuir isotherm constant ($L.mg^{-1}$), which is related to the affinity of the sorbent for the sorbate. The former is often quoted as the sorption capacity of a particular sorbent under specified experimental conditions.

The Freundlich model (Freundlich 1906) assumes heterogeneity of binding sites and that those with greater affinity for the sorbate are occupied initially. The model equation can be expressed as:

$$q_e = K_F C_e^{1/n_F} \tag{16}$$

where K_F is the Freundlich isotherm constant [$(mg.g^{-1})$ $(L.mg^{-1})^{1/n}$] considered to be indicative of sorption capacity and strength of the binding force. n_F is the Freundlich exponent (dimensionless), which is a measure of sorption intensity.

The Dubinin-Radushkevich model (Dubinin & Radushkevich 1947) was originally formulated for the adsorption of gases onto heteroporous solids following a pore filling mechanism. However, in biosorption it is widely used in facilitating the distinction between physisorption and chemisorption (Vijayaraghavan *et al*. 2006; Sari & Tuzen 2009; Rubio *et al*. 2013; Khan *et al*. 2015). The Dubinin-Radushkevich model equation can be expressed as follows:

$$q_e = q_{maxDR} \exp\left\{ - K_{DR} \left[RT \ln\left(1 + \frac{1}{C_e}\right)\right]^2 \right\} \tag{17}$$

where q_{maxDR} and K_{DR} represent the Dubinin-Radushkevich maximum monolayer sorbent loading capacity ($mg.g^{-1}$) and Dubinin-Radushkevich isotherm constant ($mol^2.kJ^{-2}$), respectively. R is the universal gas constant (8.314×10^{-3} $kJ.mol^{-1}.K^{-1}$) and T represents absolute temperature (K). The change in free energy of the system due to the transfer of one mole ions from solution to the biosorbent surface, E_{DR}, in $kJ.mol^{-1}$, can be computed from the value of K_{DR} using the following relationship:

$$E_{DR} = \frac{1}{\sqrt{2K_{DR}}} \tag{18}$$

Small values of E_{DR}, typically below 8 kJ.mol^{-1} reflect physisorption while values in between 8 and 16 kJ mol^{-1} indicate chemisorption.

The Sips (1948), Redlich-Peterson (1959) and Toth (1971) isotherm models incorporate features of both the Langmuir and Freundlich models. The Sips model equation can be expressed as follows:

$$q_e = \frac{q_{maxS} K_S C_e^{\,1/n_s}}{1 + K_S C_e^{\,1/n_s}} \tag{19}$$

where q_{maxS} is the Sips model maximum sorbent loading (mg.g^{-1}) corresponding to binding site saturation, K_S is the Sips isotherm constant [(L.mg^{-1})$^{1/n}$] and $1/n_S$ is the Sips exponent (dimensionless). The Redlich-Peterson isotherm model has the following form:

$$q_e = \frac{q_{maxRP} K_{RP} C_e}{1 + (K_{RP} C_e)^{\beta_{RP}}} \tag{20}$$

where q_{maxRP} is the Redlich-Peterson model maximum sorbent loading (mg.g^{-1}). K_{RP} (L.mg^{-1}) is the Redlich-Peterson model constants and β_{RP} (dimensionless) is the Redlich-Peterson exponent. The Toth model equation can be represented as:

$$q_e = \frac{q_{maxT} K_T C_e}{[1 + (K_L C_e)^{1/n_T}]^{n_T}} \tag{21}$$

where q_{maxT} is the Toth model maximum sorbent loading (mg.g^{-1}), K_T is the Toth model constant (L.mg^{-1}) and n_T is the Toth model exponent (dimensionless).

2.5.3 Determination of model parameters

Isotherm and kinetic model parameters are determined by fitting model equations into experimental data with adjustment of the equation parameter values so that the least regression error is achieved. For two-parameter model equations, the parameters can be determined with ease by transformation of the equation into a linear form followed by application of linear regression. Values of the slope and intercept of each transformed equation are expressed in terms of one or both of the model parameters to allow their computation using simple methods of solving simultaneous equations. Though simple, the linear regression method has inherent bias associated with calculation of the plots' axis values, and, to some extent, the linear form used.

A study by Kumar and Sivanesan (2005) revealed vastly divergent values of both the parameters and coefficient of determination values obtained from plots of the four linear forms of the Langmuir model. In fact, linear forms 1, 2, 3, and 4 resulted in q_{maxL} values of 84.84 $mg.g^{-1}$, 97.72 $mg.g^{-1}$, 90.76 $mg.g^{-1}$ and 94.71 $mg.g^{-1}$, respectively. In contrast, determination by nonlinear regression yielded a value of 88.44 $mg.g^{-1}$. Nonlinear regression not only circumvents inherent bias introduced by linearization, but also applies to models with three or more parameters. The procedure of parameter determination begins with using reasonable estimates of the parameters to calculate the model's set of predicted values for sorbent loading, denoted $q_{e,calc}$ and $q_{t,calc}$, corresponding to the studied range of C_e and t for isotherm and kinetic modelling, respectively. Thereafter, an error function or statistic that compares the model predictions to the experimental values, denoted $q_{e,expt}$ and $q_{t,expt}$, is selected for evaluating the model's fit to the experimental data. Using a trial and error iterative method, the parameter estimates are adjusted to statistically minimize errors (Schiewer & Balaria 2009; Keranen *et al*. 2013; Nadeem *et al*. 2015).

References

Abdel-Halim, E.S., Abou-Okeil, A. & Hashem, A., 2007. Adsorption of Cr(VI) oxyanions onto modified wood pulp. *Polym. Plast. Technol. Eng.*, 45(1), pp. 71–76.

Aharoni, C., Sideman, S. & Hoffer, E., 1979. Adsorption of phosphate ions by colloid ion-coated alumina. *J. Chem. Technol. Biotechnol.*, 29, pp. 404–412.

Alhakawati, M.S. & Banks, C.J., 2004. Removal of copper from aqueous solution by *Ascophyllum nodosum* immobilised in hydrophilic polyurethane foam. *J. Environ. Manage.*, 72(4), pp. 195–204.

An, B., Lee, C.-G., Song, M.-K., Ryu, J.-C., Lee, S., Park, S.-J., Zhao, D., Kim, S.-B., Park, C., Lee, S.-H., Hong, S.W. & Choi, J.-W., 2015. Applicability and toxicity evaluation of an adsorbent based on jujube for the removal of toxic heavy metals. *React. Funct. Polym.*, 93, pp. 138–147.

Anirudhan, T.S. & Unnithan, M.R., 2007. Arsenic(V) removal from aqueous solutions using an anion exchanger derived from coconut coir pith and its recovery. *Chemosphere*, 66(1), pp. 60–66.

Aziz, A., Elandaloussi, E.-H., Belhalfaoui, B., Ouali, M.S. & De Menorval, L.C., 2009. Efficiency of succinylated-olive stone biosorbent on the removal of cadmium ions from aqueous solutions. *Colloids Surf., B*, 73(2), pp. 192–198.

Azizian, S., 2004. Kinetic models of sorption: A theoretical analysis. *J. Colloid Interface Sci.*, 276(1), pp. 47–52.

Baral, S.S., Das, S.N. & Rath, P., 2006. Hexavalent chromium removal from aqueous solution by adsorption on treated sawdust. *Biochem. Eng. J.*, 31(3), pp. 216–222.

Basu, M., Guha, A.K. & Ray, L., 2015. Biosorptive removal of lead by lentil husk. *J. Environ. Chem. Eng.*, 3(2), pp. 1088–1095.

Beolchini, F., Pagnanelli, F., Toro, L. & Veglio, F., 2003. Biosorption of copper by *Sphaerotilus natans* immobilised in polysulfone matrix: equilibrium and kinetic analysis. *Hydrometallurgy*, 70(1-3), pp. 101–112.

Blazquez, G., Calero, M., Ronda, A., Tenorio, G. & Martin-Lara, M.A., 2014. Study of kinetics in the biosorption of lead onto native and chemically treated olive stone. *J. Ind. Eng. Chem.*, 20(5), pp. 2754–2760.

Boyd, G.E., Adamson, A.W. & Myers, L.S., 1947. The exchange adsorption of ions from aqueous solutions by organic zeolites. II. Kinetics. *J. Am. Chem. Soc.*, 69(11), pp. 2836–2848.

Di Caprio, F., Altimari, P., Uccelletti, D. & Pagnanelli, F., 2014. Mechanistic modelling of copper biosorption by wild type and engineered *Saccharomyces cerevisiae* biomasses. *Chem. Eng. J.*, 244, pp. 561–568.

Chen, J.P. & Yang, L., 2005. Chemical modification of *Sargassum sp*. for prevention of organic leaching and enhancement of uptake during metal biosorption. *Ind. Eng. Chem. Res.*, 44(26), pp. 9931–9942.

Chen, S., Yue, Q., Gao, B., Li, Q. & Xu, X., 2011. Preparation and characteristics of anion exchanger from corn stalks. *Desalination*, 274(1-3), pp. 113–119.

Cheung, C.W., Porter, J.F. & Mckay, G., 2001. Sorption kinetic analysis for the removal of cadmium ions from effluents using bone char. *Water Res.*, 35(3), pp. 605–612.

Chiron, N., Guilet, R. & Deydier, E., 2003. Adsorption of Cu(II) and Pb(II) onto a grafted silica: Isotherms and kinetic models. *Water Res.*, 37(13), pp. 3079–3086.

Chubar, N., Carvalho, J.R. & Correia, M.J.N., 2003. Cork biomass as biosorbent for Cu(II), Zn(II) and Ni(II). *Colloids Surf., A*, 230(1-3), pp. 57–65.

Chubar, N., Carvalho, J.R. & Correia, M.J.N., 2004. Heavy metals biosorption on cork biomass: Effect of the pre-treatment. *Colloids Surf., A*, 238(1-3), pp. 51–58.

Cruz-Olivares, J., Perez-Alonso, C., Barrera-Diaz, C., Lopez, G. & Balderas-Hernandez, P., 2010. Inside the removal of lead(II) from aqueous solutions by De-Oiled Allspice Husk in batch and continuous processes. *J. Hazard. Mater.*, 181(1-3), pp. 1095–1101.

Cruz-Olivares, J., Perez-Alonso, C., Barrera-Diaz, C., Natividad, R. & Chaparro-Mercado, M.C., 2011. Thermodynamical and analytical evidence of lead ions chemisorption onto *Pimenta dioica*. *Chem. Eng. J.*, 166(3), pp. 814–821.

Davis, T.A., Volesky, B. & Mucci, A., 2003. A review of the biochemistry of heavy metal biosorption by brown algae. *Water Res.*, 37(18), pp. 4311–4330.

Deng, Y., Gao, Z., Liu, B., Hu, X., Wei, Z. & Sun, C., 2013. Selective removal of lead from aqueous solutions by ethylenediamine- modified attapulgite. *Chem. Eng. J.*, 223, pp. 91–98.

Dubinin, M.M. & Radushkevich, L. V, 1947. Equation of the characteristic curve of activated charcoal. *Proc. Acad. Sci. USSR, Phys. Chem. Sect.*, 55, pp. 331–333.

El-Gendy, A.A., Mohamed, S.H. & Abd-Elkader, A.H., 2013. Ion exchanger from chemically modified banana leaves. *Carbohydr. Polym.*, 96(2), pp. 481–486.

Febrianto, J., Kosasih, A.N., Sunarso, J., Ju, Y.-H., Indraswati, N. & Ismadji, S., 2009. Equilibrium and kinetic studies in adsorption of heavy metals using biosorbent: A summary of recent studies. *J. Hazard. Mater.*, 162(2-3), pp. 616–645.

Feng, N.-C., Guo, X.-Y. & Liang, S., 2010. Enhanced Cu(II) adsorption by orange peel modified with sodium hydroxide. *Trans. Nonferrous Met. Soc. China*, 20, pp. s146–s152.

Fiol, N., Poch, J. & Villaescusa, I., 2004. Chromium (VI) uptake by grape stalks wastes encapsulated in calcium alginate beads: equilibrium and kinetics studies. *Chem. Speciat. Bioavailab.*, 16(1-2), pp. 25–33.

Fiol, N., Poch, J. & Villaescusa, I., 2005. Grape stalks wastes encapsulated in calcium alginate beads for Cr(VI) removal from aqueous solutions. *Sep. Sci. Technol.*, 40(5), pp. 1013–1028.

Fomina, M. & Gadd, G.M., 2014. Biosorption: current perspectives on concept, definition and application. *Bioresour. Technol.*, 160, pp. 3–14.

Freundlich, H.M.F., 1906. Over the adsorption in solution. *J. Phys. Chem.*, 57, pp. 385–470.

Gautam, R.K., Mudhoo, A., Lofrano, G. & Chattopadhyaya, M.C., 2014. Biomass-derived biosorbents for metal ions sequestration: Adsorbent modification and activation methods and adsorbent regeneration. *J. Environ. Chem. Eng.*, 2(1), pp. 239–259.

Goksungur, Y., Uren, S. & Guvenc, U., 2005. Biosorption of cadmium and lead ions by ethanol treated waste baker's yeast biomass. *Bioresour. Technol.*, 96(1), pp. 103–109.

Guo, H., Zhang, S., Kou, Z., Zhai, S., Ma, W. & Yang, Y., 2015. Removal of cadmium(II) from aqueous solutions by chemically modified maize straw. *Carbohydr. Polym.*, 115, pp. 177–185.

Guo, J.-Z., Li, B., Liu, L. & Lv, K., 2014. Removal of methylene blue from aqueous solutions by chemically modified bamboo. *Chemosphere*, 111, pp. 225–231.

Gurgel, L.V.A., De Freitas, R.P. & Gil, L.F., 2008. Adsorption of Cu(II), Cd(II), and Pb(II) from aqueous single metal solutions by sugarcane bagasse and mercerized sugarcane

bagasse chemically modified with succinic anhydride. *Carbohydr. Polym.*, 74(4), pp. 922–929.

Gusmao, K.A.G., Gurgel, L.V.A., Melo, T.M.S. & Gil, L.F., 2013. Adsorption studies of methylene blue and gentian violet on sugarcane bagasse modified with EDTA dianhydride (EDTAD) in aqueous solutions: Kinetic and equilibrium aspects. *J. Environ. Manage.*, 118, pp. 135–143.

Guyo, U., Mhonyera, J. & Moyo, M., 2015. Pb(II) adsorption from aqueous solutions by raw and treated biomass of maize stover - A comparative study. *Process Saf. Environ. Prot.*, 93, pp. 192–200.

Haug, A., Larsen, B. & Smidsrod, O., 1966. A study of the constitution of alginic acid by partial acid hydrolysis. *Acta Chem. Scand.*, 20, pp. 183–190.

Ho, Y.-S. & Mckay, G., 1999. Pseudo-second order model for sorption processes. *Process Biochem.*, 34(5), pp. 451–465.

Ho, Y.-S., Ng, J.C.Y. & McKay, G., 2000. Kinetics of pollutant sorption by biosorbents: Review. *Sep. Purif. Rev.*, 29(2), pp. 189–232.

Hu, H., Zhang, J., Lu, K. & Tian, Y., 2015. Characterization of *Acidosasa edulis* shoot shell and its biosorption of copper ions from aqueous solution. *J. Environ. Chem. Eng.*, 3(1), pp. 357–364.

Ibanez, J.P. & Umetsu, Y., 2002. Potential of protonated alginate beads for heavy metals uptake. *Hydrometallurgy*, 64(2), pp. 89–99.

Inoue, K., Yoshizuka, K. & Ohto, K., 1999. Adsorptive separation of some metal ions by complexing agent types of chemically modified chitosan. *Anal. Chim. Acta*, 388(1-2), pp. 209–218.

Iqbal, M., Saeed, A. & Iqbal, S., 2009. FTIR spectrophotometry, kinetics and adsorption isotherms modeling, ion exchange, and EDX analysis for understanding the mechanism of Cd^{2+} and Pb^{2+} removal by mango peel waste. *J. Hazard. Mater.*, 164(1), pp. 161–171.

Jeon, C., Cha, J.-H. & Choi, J.-Y., 2015. Adsorption and recovery characteristics of phosphorylated sawdust bead for indium(III) in industrial wastewater. *J. Ind. Eng. Chem.*, 27, pp. 201–206.

Karaoglu, M.H., Ugurlu, M. & Kula, I., 2011. Adsorption characterisation of Co(II) ions onto

chemically treated *Quercus coccifera* shell: Equilibrium, kinetic, and thermodynamic studies. *BioResources*, 6(2), pp. 1954–1971.

Karnitz, O., Gurgel, L.V.A., De Freitas, R.P. & Gil, L.F., 2009. Adsorption of Cu(II), Cd(II), and Pb(II) from aqueous single metal solutions by mercerized cellulose and mercerized sugarcane bagasse chemically modified with EDTA dianhydride (EDTAD). *Carbohydr. Polym.*, 77(3), pp. 643–650.

Kaya, K., Pehlivan, E., Schmidt, C. & Bahadir, M., 2014. Use of modified wheat bran for the removal of chromium(VI) from aqueous solutions. *Food Chem.*, 158, pp. 112–117.

Keranen, A., Leiviska, T., Gao, B.-Y., Hormi, O. & Tanskanen, J., 2013. Preparation of novel anion exchangers from pine sawdust and bark, spruce bark, birch bark and peat for the removal of nitrate. *Chem. Eng. Sci.*, 98, pp. 59–68.

Khan, T.A., Chaudhry, S.A. & Ali, I., 2015. Equilibrium uptake, isotherm and kinetic studies of Cd(II) adsorption onto iron oxide activated red mud from aqueous solution. *J. Mol. Liq.*, 202, pp. 165–175.

Kumar, K. V & Sivanesan, S., 2005. Prediction of optimum sorption isotherm: Comparison of linear and non-linear method. *J. Hazard. Mater.*, 126(1-3), pp. 198–201.

Kumar, U. & Bandyopadhyay, M., 2006. Sorption of cadmium from aqueous solution using pretreated rice husk. *Bioresour. Technol.*, 97(1), pp. 104–109.

Lagergren, S., 1898. Zur theorie der sogenannten adsorption geloster stoffen. *K. Sven. Vetenskapsakad. Handl.*, 24(4), pp. 1–39.

Lai, Y.-L., Annadurai, G., Huang, F.-C. & Lee, J.-F., 2008. Biosorption of heavy metals from aqueous solution using modified activated carbon: comparison of linear and nonlinear methods. *J. Chem. Technol. Biotechnol.*, 83(6), pp. 788–798.

Langmuir, I., 1916. The constitution and fundamental properties of solids and liquids. *J. Am. Chem. Soc.*, 38(11), pp. 2221–2295.

Li, L., Sun, X. & Li, B., 2012. Adsorption of cytochrome c by succinic anhydride-modified peanut shells. *Adv. Biosci. Biotechnol.*, 3(1), pp. 14–19.

Li, Q., Zhai, J., Zhang, W., Wang, M. & Zhou, J., 2007. Kinetic studies of adsorption of Pb(II), Cr(III) and Cu(II) from aqueous solution by sawdust and modified peanut husk. *J. Hazard. Mater.*, 141(1), pp. 163–167.

Liu, W., Zhang, J., Jin, Y., Zhao, X. & Cai, Z., 2015. Adsorption of Pb(II), Cd(II) and Zn(II) by extracellular polymeric substances extracted from aerobic granular sludge: Efficiency of protein. *J. Environ. Chem. Eng.*, 3(2), pp. 1223–1232.

Liu, Y. & Liu, Y.-J., 2008. Biosorption isotherms, kinetics and thermodynamics. *Sep. Purif. Technol.*, 61(3), pp. 229–242.

Liu, Y., Sun, X. & Li, B., 2010. Adsorption of Hg^{2+} and Cd^{2+} by ethylenediamine modified peanut shells. *Carbohydr. Polym.*, 81(2), pp. 335–339.

Liu, Y., Yang, S.-F., Xu, H., Woon, K.-H., Lin, Y.-M. & Tay, J.-H., 2003. Biosorption kinetics of cadmium(II) on aerobic granular sludge. *Process Biochem.*, 38(7), pp. 997–1001.

Lugo-Lugo, V., Barrera-Diaz, C., Urena-Nunez, F., Bilyeu, B. & Linares-Hernandez, I., 2010. Biosorption of Cr(III) and Fe(III) in single and binary systems onto pretreated orange peel. *J. Environ. Manage.*, 112, pp. 120–127.

Madrid, J.F., Nuesca, G.M. & Abad, L. V, 2014. Amine functionalized radiation-induced grafted water hyacinth fibers for Pb^{2+}, Cu^{2+} and Cr^{3+} uptake. *Radiat. Phys. Chem.*, 97, pp. 246–252.

Mahmoud, M.E., Ahmed, S.B., Osman, M.M. & Abdel-Fattah, T.M., 2015. A novel composite of nanomagnetite-immobilized-baker's yeast on the surface of activated carbon for magnetic solid phase extraction of Hg(II). *Fuel*, 139, pp. 614–621.

Martinez, M., Miralles, N., Hidalgo, S., Fiol, N., Villaescusa, I. & Poch, J., 2006. Removal of lead(II) and cadmium(II) from aqueous solutions using grape stalk waste. *J. Hazard. Mater.*, 133(1-3), pp. 203–211.

Massocatto, C.L., Paschoal, E.C., Buzinaro, N., Oliveria, T.F., Tarley, C.R.T., Caetano, J., Goncalves, A.C., Dragunski, D.C. & Diniz, K, M., 2013. Preparation and evaluation of kinetics and thermodynamics studies of lead adsorption onto chemically modified banana peels. *Desalin. Water Treat.*, 51(28-30), pp. 5682–5691.

Min, S.H., Han, J.S., Shin, E.W. & Park, J.K., 2004. Improvement of cadmium ion removal by base treatment of juniper fiber. *Water Res.*, 38(5), pp. 1289–1295.

Mohan, D., Singh, K.P. & Singh, V.K., 2006. Trivalent chromium removal from wastewater using low cost activated carbon derived from agricultural waste material and activated carbon fabric cloth. *J. Hazard. Mater.*, 135(1-3), pp. 280–295.

Nadeem, R., Naqvi, M.A., Nasir, M.H., Saeed, R., Iqbal, T., Ashraf, M. & Ansri, T.M., 2015. Efficacy of physically pretreated *Mangifera indica* biomass for Cu^{2+} and Zn^{2+} sequestration. *J. Saudi Chem. Soc.*, 19(1), pp. 23–25.

Ofomaja, A.E. & Ho, Y.-S., 2007. Effect of pH on cadmium biosorption by coconut copra meal. *J. Hazard. Mater.*, 139(2), pp. 356–362.

Ofomaja, A.E. & Naidoo, E.B., 2011. Biosorption of copper from aqueous solution by chemically activated pine cone: A kinetic study. *Chem. Eng. J.*, 175, pp. 260–270.

Ofomaja, A.E., Naidoo, E.B. & Modise, S.J., 2010. Kinetic and pseudo-second-order modeling of lead biosorption onto pine cone powder. *Ind. Eng. Chem. Res.*, 49(6), pp. 2562–2572.

Ofomaja, A.E., Pholosi, A. & Naidoo, E.B., 2013. Kinetics and competitive modeling of cesium biosortion onto chemically modified pine cone powder. *J. Taiwan Inst. Chem. Eng.*, 44(6), pp. 943–951.

Orlando, U.S., Baes, A.U., Nishijima, W. & Okada, M., 2002. A new procedure to produce lignocellulosic anion exchangers from agricultural waste materials. *Bioresour. Technol.*, 83(3), pp. 195–198.

Ozer, A., 2007. Removal of Pb(II) ions from aqueous solutions by sulphuric acid-treated wheat bran. *J. Hazard. Mater.*, 141(3), pp. 753–761.

Pagnanelli, F., Mainelli, S. & Toro, L., 2005. Optimisation and validation of mechanistic models for heavy metal bio-sorption onto a natural biomass. *Hydrometallurgy*, 80(1-5), pp. 107–125.

Park, D., Yun, Y.-S. & Park, J.M., 2010. The past, present, and future trends of biosorption. *Biotechnol. Bioprocess Eng.*, 15(1), pp. 86–102.

Pereira, F. V, Gurgel, L.V.A. & Gil, L.F., 2010. Removal of Zn^{2+} from aqueous single metal solutions and electroplating wastewater with wood sawdust and sugarcane bagasse modified with EDTA dianhydride (EDTAD). *J. Hazard. Mater.*, 176(1-3), pp. 856–863.

Pezoti, O., Cazetta, A.L., Bedin, K.C., Souza, L.S., Souza, R.P., Melo, S.R. & Almeida, V.C., 2016. Percolation as new method of preparation of modified biosorbents for pollutants removal. *Chem. Eng. J.*, 283, pp. 1305–1314.

Prola, L.D.T., Acayanka, E., Lima, E.C., Umpierres, C.S., Vaghetti, J.C.P., Santos, W.O., Laminsi, S. & Djifon, P.T., 2013. Comparison of Jatropha curcas shells in natural form

and treated by non-thermal plasma as biosorbents for removal of Reactive Red 120 textile dye from aqueous solution. *Ind. Crops Prod.*, 46, pp. 328–340.

Qiu, H., Lv, L., Pan, B.-C., Zhang, Q.-J., Zhang, W.-M. & Zhang, Q.-X., 2009. Critical review in adsorption kinetic models. *J. Zhejiang Univ., Sci., A*, 10(5), pp. 716–724.

Quintelas, C., Pereira, R., Kaplan, E. & Tavares, T., 2013. Removal of Ni(II) from aqueous solutions by an *Arthrobacter viscosus* biofilm supported on zeolite: From laboratory to pilot scale. *Bioresour. Technol.*, 142, pp. 368–374.

Redlich, O. & Peterson, D.L., 1959. A useful adsorption isotherm. *J. Phys. Chem.*, 63, pp. 1024–1026.

Robalds, A., Naja, G.M. & Klavins, M., 2016. Highlighting inconsistencies regarding metal biosorption. *J. Hazard. Mater.*, 304, pp. 553–556.

Ronda, A., Martin-Lara, M.A., Calero, M. & Blazquez, G., 2013. Analysis of the kinetics of lead biosorption using native and chemically treated olive tree pruning. *Ecol. Eng.*, 58, pp. 278–285.

Roy, A., Chakraborty, S., Kundu, S.P., Majumder, S.B. & Adhikari, B., 2013. Surface grafting of *Corchorus olitorius* fibre: A green approach for the development of activated bioadsorbent. *Carbohydr. Polym.*, 92(2), pp. 2118–2127.

Rubio, F., Goncalves, A.C.F., Dragunski, D.C., Tarley, C.R.T., Meneghel, A.P. & Schwantes, D., 2013. A *Crambe abyssinica* seed by-product as biosorbent for lead(II) removal from water. *Desalin. Water Treat.*, pp. 1–10.

Rudzinski, W. & Panczyk, T., 2000. Kinetics of isothermal adsorption on energetically heterogeneous solid surfaces: A new theoretical description based on the statistical rate theory of interfacial transport. *J. Phys. Chem. B*, 104(39), pp. 9149–9162.

Sag, Y., Nourbakhsh, M., Aksu, Z. & Kutsal, T., 1995. Comparison of Ca-alginate and immobilized *Z. ramigera* as sorbents for copper removal. *Process Biochem.*, 30(2), pp. 175–181.

Sar, P., Kazy, S.K., Asthana, R.K. & Singh, S.P., 1999. Metal adsorption and desorption by lyophilized *Pseudomonas aeruginosa*. *Int. Biodeterior. Biodegradation*, 44(2-3), pp. 101–110.

Sari, A. & Tuzen, M., 2009. Kinetic and equilibrium studies of biosorption of Pb(II) and Cd(II)

from aqueous solution by macrofungus (*Amanita rubescens*) biomass. *J. Hazard. Mater.*, 164(2-3), pp. 1004–11.

Schiewer, S. & Balaria, A., 2009. Biosorption of Pb^{2+} by original and protonated citrus peels: Equilibrium, kinetics, and mechanism. *Chem. Eng. J.*, 146(2), pp. 211–219.

Sheng, P.X., Ting, Y.-P., Chen, J.P. & Hong, L., 2004. Sorption of lead, copper, cadmium, zinc, and nickel by marine algal biomass: Characterization of biosorptive capacity and investigation of mechanisms. *J. Colloid Interface Sci.*, 275(1), pp. 131–141.

Shukla, P.M. & Shukla, S.R., 2013. Biosorption of Cu(II), Pb(II), Ni(II), and Fe(II) on alkali treated coir fibers. *Sep. Sci. Technol.*, 48(3), pp. 421–428.

Singha, A.S. & Guleria, A., 2014. Chemical modification of cellulosic biopolymer and its use in removal of heavy metal ions from wastewater. *Int. J. Biol. Macromol.*, 67, pp. 409–417.

Sips, R., 1948. Combined form of Langmuir and Freundlich equation. *J. Chem. Phys.*, 16, pp. 490–495.

Sun, X.-F., Wang, S.-G., Liu, X.-W., Gong, W.-X., Bao, N. & Gao, B.-Y., 2008. Competitive biosorption of zinc(II) and cobalt(II) in single- and binary-metal systems by aerobic granules. *J. Colloid Interface Sci.*, 324(1-2), pp. 1–8.

Taty-Costodes, V.C., Fauduet, H., Porte, C. & Delacroix, A., 2003. Removal of Cd(II) and Pb(II) ions, from aqueous solutions, by adsorption onto sawdust of *Pinus sylvestris*. *J. Hazard. Mater.*, 105(1-3), pp. 121–142.

Torab-Mostaedi, M., Asadollahzadeh, M., Hemmati, A. & Khosravi, A., 2013. Equilibrium, kinetic, and thermodynamic studies for biosorption of cadmium and nickel on grapefruit peel. *J. Taiwan Inst. Chem. Eng.*, 44(2), pp. 294–301.

Toth, J., 1971. State equations of the solid gas interface layer. *Acta Chim. Acad. Sci. Hungaricae*, 69, pp. 311–317.

Vieira, A.P., Santana, S.A.A., Bezerra, C.W.B., Silva, H.A.S., De Melo, J.C.P., Filho, E.C.D.-S. & Airoldi, C., 2010. Copper sorption from aqueous solutions and sugar cane spirits by chemically modified babassu coconut (*Orbignya speciosa*) mesocarp. *Chem. Eng. J.*, 161(1-2), pp. 99–105.

Vijayaraghavan, K. & Jegan, J., 2015. Entrapment of brown seaweeds (*Turbinaria conoides* and *Sargassum wightii*) in polysulfone matrices for the removal of praseodymium ions

from aqueous solutions. *J. Rare Earths*, 33(11), pp. 1196–1203.

Vijayaraghavan, K., Padmesh, T.V.N., Palanivelu, K. & Velan, M., 2006. Biosorption of nickel(II) ions onto *Sargassum wightii*: Application of two-parameter and three-parameter isotherm models. *J. Hazard. Mater.*, 133(1-3), pp. 304–308.

Vinod, V.T.P., Sashidhar, R.B., Sreedhar, B., Rao, B.R., Rao, T.N. & Abraham, J.T., 2009. Interaction of Pb^{2+} and Cd^{2+} with gum kondagogu (*Cochlospermum gossypium*): A natural carbohydrate polymer with biosorbent properties. *Carbohydr. Polym.*, 78(4), pp. 894–901.

Volesky, B., 2007. Biosorption and me. *Water Res.*, 41(18), pp. 4017–4029.

Wan Ngah, W.S. & Hanafiah, M.A.K.M., 2008. Removal of heavy metal ions from wastewater by chemically modified plant wastes as adsorbents: A review. *Bioresour. Technol.*, 99(10), pp. 3935–3948.

Wang, W.Y., Yue, Q.Y., Xu, X., Gao, B.Y., Zhang, J., Li, Q. & Xu, J.T., 2010. Optimized conditions in preparation of giant reed quaternary amino anion exchanger for phosphate removal. *Chem. Eng. J.*, 157, pp. 161–167.

Weber, W.J. & Morris, J.C., 1963. Kinetics of adsorption on carbon from solution. *J. Sanit. Eng. Div. Am. Soc. Civ. Eng.*, 89(2), pp. 31–60.

Wilczak, A. & Keinath, T.M., 1993. Kinetics of sorption and desorption of copper(II) and lead(II) on activated carbon. *Water Environ. Res.*, 65(3), pp. 238–244.

Worch, E., 2012. *Adsorption technology in water treatment: Fundamentals, processes, and modeling*, Berlin, Germany: de Gruyter.

Wu, Z., Cheng, Z. & Ma, W., 2012. Adsorption of Pb(II) from glucose solution on thiol-functionalized cellulosic biomass. *Bioresour. Technol.*, 104, pp. 807–809.

Xu, H. & Liu, Y., 2008. Mechanisms of Cd^{2+}, Cu^{2+} and Ni^{2+} biosorption by aerobic granules. *Sep. Purif. Technol.*, 58(3), pp. 400–411.

Xu, X., Gao, B., Huang, X., Ling, J., Song, W. & Yue, Q., 2015. Physicochemical characteristics of epichlorohydrin, pyridine and trimethylamine functionalized cotton stalk and its adsorption/desorption properties for perchlorate. *J. Colloid Interface Sci.*, 440, pp. 219–228.

Yakkala, K., Yu, M.-R., Roh, H., Yang, J.-K. & Chang, Y.-Y., 2013. Buffalo weed (*Ambrosia*

trifida L. var. trifida) biochar for cadmium(II) and lead(II) adsorption in single and mixed system. *Desalin. Water Treat.*, 51(40-42), pp. 7732–7745.

Yang, F., Liu, H., Qu, J. & Chen, J.P., 2011. Preparation and characterization of chitosan encapsulated *Sargassum sp*. biosorbent for nickel ions sorption. *Bioresour. Technol.*, 102(3), pp. 2821–2828.

Yu, J., Tong, M., Sun, X. & Li, B., 2007. Cystine-modified biomass for Cd(II) and Pb(II) biosorption. *J. Hazard. Mater.*, 143(1-2), pp. 277–284.

Yu, J., Tong, M., Sun, X. & Li, B., 2008. Enhanced and selective adsorption of Pb^{2+} and Cu^{2+} by EDTAD-modified biomass of baker's yeast. *Bioresour. Technol.*, 99(7), pp. 2588–2593.

Zafar, M.N., Aslam, I., Nadeem, R., Munir, S., Rana, U.A. & Khan, S.U.-D., 2015. Characterization of chemically modified biosorbents from rice bran for biosorption of Ni(II). *J. Taiwan Inst. Chem. Eng.*, 46, pp. 82–88.

Zeldowitsch, J., 1934. Uber denmechanismus der katalytischen oxydation von CO an MnO_2. *Acta Physicochim. URSS*, 1, pp. 364–449.

Zhang, W., Li, C., Liang, M., Geng, Y. & Lu, C., 2010. Preparation of carboxylate-functionalized cellulose via solvent-free mechanochemistry and its characterization as a biosorbent for removal of Pb^{2+} from aqueous solution. *J. Hazard. Mater.*, 181(1-3), pp. 468–473.

Zhang, Y. & Banks, C., 2006. A comparison of the properties of polyurethane immobilised Sphagnum moss, seaweed, sunflower waste and maize for the biosorption of Cu, Pb, Zn and Ni in continuous flow packed columns. *Water Res.*, 40(4), pp. 788–798.

Zhang, Y., Liu, W., Xu, M., Zheng, F. & Zhao, M., 2010. Study of the mechanisms of Cu^{2+} biosorption by ethanol/caustic-pretreated baker's yeast biomass. *J. Hazard. Mater.*, 178(1-3), pp. 1085–1093.

Zheng, J.-C., Feng, H.-M., Lam, M.H.-W., Lam, P.K.-S., Ding, Y.-W. & Yu, H.-Q., 2009. Removal of Cu(II) in aqueous media by biosorption using water hyacinth roots as a biosorbent material. *J. Hazard. Mater.*, 171(1-3), pp. 780–785.

Zhou, D., Zhang, L. & Guo, S., 2005. Mechanisms of lead biosorption on cellulose/chitin beads. *Water Res.*, 39(16), pp. 3755–3762.

Zhou, Y., Min, Y., Qiao, H., Huang, Q., Wang, E. & Ma, T., 2015. Improved removal of malachite green from aqueous solution using chemically modified cellulose by anhydride. *Int. J. Biol. Macromol.*, 74, pp. 271–277.

Zhu, B., Fan, T. & Zhang, D., 2008. Adsorption of copper ions from aqueous solution by citric acid modified soybean straw. *J. Hazard. Mater.*, 153(1-2), pp. 300–308.

Zhu, H.-X., Cao, X.-J., He, Y.-C., Kong, Q.-P., He, H. & Wang, J., 2015. Removal of Cu^{2+} from aqueous solutions by the novel modified bagasse pulp cellulose: Kinetics, isotherm and mechanism. *Carbohydr. Polym.*, 129, pp. 115–126.

CHAPTER 3

MATERIALS AND METHODS

3.1 Reagents and solutions

Lead (II) nitrate (99.99%), ethanol (99.8%), diethyl ether (99.0%) and N,N-dimethylformamide (99.8%) were purchased from Sigma Aldrich (Johannesburg, South Africa). Sodium hydroxide pellets (97.0%) EDTA disodium salt (99.0%), sodium alginate, sodium hydrogen carbonate (99.7%), calcium chloride hexahydrate (98.0%), acetic anhydride (98%), pyridine (99.0%), nitric acid (70%), acetic acid (99.7%), sulfuric acid (98%) and hydrochloric acid (37%) were purchased from Associated Chemical Enterprises (Johannesburg, South Africa). Fresh stock solution of lead(II) was prepared every two weeks from lead nitrate and working solutions of desired concentration were obtained by dilution with distilled water. Prior to every sorption experiment, the pH of each working lead(II) solutions was adjusted to 5.2 using droplets of nitric acid and sodium hydroxide solutions. Wastewater samples were collected from a spent electrolyte and spillages tank in a medium scale electroplating plant in Cape Town (South Africa). When necessary, pH of the wastewater was adjusted to 1.8 using sulfuric acid.

3.2 Sorbent preparation

Waste mango seed obtained from a farm in Tzaneen – Limpopo Province (South Africa) was washed under running tap water and sun dried for two days prior to shelling and removal of the kernels. The shells were washed in deionized water before drying in an oven maintained at 90°C for 24 h. The material was then milled and sieved to obtain mango seed shell powder (MSSP). Powder particles within the 90–425 µm diameter range were used for alkali treatment.

3.2.1 Alkali treatment

In this preliminary process, 10.0 g of MSSP was mixed with 100 mL of 5 M sodium hydroxide solution at room temperature under stirring for 3 h. The residue was filtered off and washed once with 1% (v/v) acetic acid solution and then repeatedly rinsed with distilled water until the pH of the rinse water was approximately 7. Thereafter, the alkali treated mango seed shell biomass (ATMS) was dried in an oven at 90°C for 24 h and left to cool in a desiccator before storage in a stoppered glass bottle.

3.2.2 EDTA bisanhydride synthesis and carboxyl functionalization

The surface functionalization agent, EDTA bisanhydride, was synthesized by EDTA dehydration using the procedure described by Gusmao *et al*. (2013) with slight modifications.

A mass of 35 g of EDTA disodium salt was dissolved in 300 mL of distilled water and concentrated hydrochloric acid was added dropwise with continuous stirring on a magnetic stirrer. The precipitate was filtered and washed with 95% ethanol then 99% diethyl ether. Afterwards it was dried in an oven at 90°C for 2 h and then left to cool in a desiccator. The EDTA tetra acid was then suspended in 40 mL of N,N-dimethylformamide (DMF). Thereafter, 15 mL of pyridine followed by 50 mL of acetic anhydride were added and the reaction mixture was stirred at 65°C under reflux for 4 h. The resultant EDTA bisanhydride was filtered off, washed thoroughly with acetic anhydride then diethyl ether. Thereafter, the washed powder was dried at 40°C under vacuum for 4 h and stored in a desiccator.

Carboxyl functionalized mango seed shell biomass (CFMS) was prepared by treating 10.0 g of ATMS with 30 g of EDTA bisanhydride in 400 mL DMF under stirring and reflux at 75°C for 20 h. The suspension was then filtered and washed sequentially with separate 200 mL aliquots of DMF, distilled water, saturated sodium hydrogen carbonate solution, distilled water and finally 95% ethanol. The CFMS was then dried in an oven at 90°C for 24 h, left to cool in a desiccator and stored in a stoppered glass bottle.

3.2.3 Granulation

A 2% (w/v) alginate solution was prepared by dissolving sodium alginate in distilled water previously heated to between 60 and 70°C. Thereafter, a 2% (w/v) suspension was prepared by adding CFMS to the alginate solution and stirring overnight to ensure homogeneity. The suspension was then pumped through a micropipette tip and dropped into a 0.1 M aqueous solution of calcium chloride. The beads formed on contact were left in the calcium chloride solution for 20 h to allow hardening. Afterwards the solution was filtered off and the hydrogel beads were thoroughly washed with distilled water. The beads were frozen at -4°C and then freeze dried for 48 h.

3.3 Physicochemical mango material characterization

Elemental, thermal degradation and functional group analysis of the sorbents was carried out using a CHNS-O analyzer (Flash 2000, Thermo Scientific, USA), a thermogravimetric analyzer (TGA 400, PerkinElmer, USA) and a Fourier transform infra-red (FTIR) spectrometer (Spectrum 400, PerkinElmer, USA), respectively. Powder X-ray diffraction (XRD) analysis was carried out using an X-ray diffractometer (D8 ADVANCE, Bruker, USA) and the crystallinity index, *CI* (%), of with each mango material was calculated in accordance with the Segal method (Segal *et al*. 1959) using the following expression:

$$CI = \frac{I_{002} - I_{am}}{I_{002}} \times 100\ \% \qquad (22)$$

where I_{002} is the maximum intensity between 2θ values of 22° and 23°, and I_{am} is the minimum intensity between 18° and 19° representing amorphous regions.

3.4 Sorption experiments

3.4.1 Batch experiments

Batch contact experiments were carried out in 1 L conical flasks in which a 750 mg portions of ATMS or 375 mg of CFMS were stirred on a magnetic stirrer in a series of 750 mL of working lead(II) solutions containing varied initial concentration. In each experiment, 1 mL samples were taken before commencement and after 24 h of contact, deemed sufficient for attainment of equilibrium. One mL were withdrawn using a micropipette after 5, 10, 15, 20, 30, 40, 60, 80, 100,120, 140, 160, 180 and 1440 min of contact. The samples were then diluted to 10 mL and then taken for determination of metal ion concentration on an atomic absorption spectrophotometric (AAS) analyzer (AA-7000, Shimadzu, Japan). Three replicate measurements were made and the quantity of lead(II) ions loaded was calculated using Equation (2) expressed as an average.

3.4.2 Column experiments

Column contact experiments were carried out in polythene columns of 100 mm length and 15.5 mm internal diameter packed with calcium alginate immobilized CFMS pellets and stoppered on either end using caps fitted with ceramic frits. One liter of electroplating wastewater was pumped from a reservoir and fed upward through the column at a constant flow rate of 30 $mL.min^{-1}$. The effluent was channeled back to the reservoir and the sorption cycle was run for 24 h (see Figure 3.1). For each sorption cycle carried out thus, samples of the initial and final electroplating wastewater were collected from the reservoir and quantified for total copper, chromium, nickel and iron content on an inductively coupled plasma optical emission spectrophotometric (ICP-OES) analyzer (iCAP 7000, Thermo Scientific, USA).

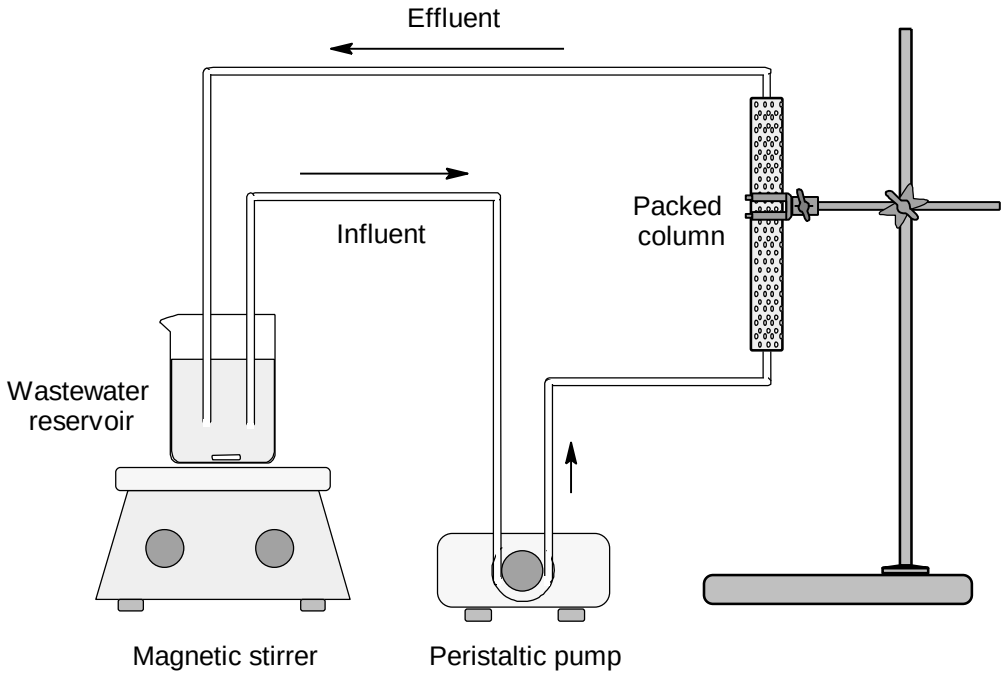

Figure 3.1: Schematic diagram of column sorption experimental set-up.

Prior to the commencement of desorption cycle, the column was rinsed by continuously pumping with distilled water through it. Desorption cycles were then carried out analogous to sorption with use of 500 mL of 0.2 M hydrochloric acid solution as an eluent in place of the electroplating wastewater. After desorption, a sample of the spent eluent was collected from the reservoir and quantified for total copper, chromium, nickel and iron content using ICP-OES. The column was flushed with 0.01 M sodium carbonate solution and then rinsed with distilled water prior to reuse in subsequent sorption and desorption cycles. Percentage metal removal was calculated using the following expression:

$$Removal = \frac{C_i - C_f}{C_i} \times 100\ \% \qquad (23)$$

where C_i (mg.L^{-1}) and C_f (mg.L^{-1}) represent metal concentration in the wastewater before and after sorption, respectively. Metal recovery (mg.g^{-1}) was calculated using the following expression:

$$Recovery = \frac{C_{eluent} V_{eluent}}{M} \qquad (24)$$

where C_{eluent} (mg.L^{-1}) and V_{eluent} (L) represent metal concentration in the spent eluent and eluent volume, respectively. M (g) is the dry mass of immobilized sorbet packed in the column.

References

Gusmao, K.A.G., Gurgel, L.V.A., Melo, T.M.S. & Gil, L.F., 2013. Adsorption studies of methylene blue and gentian violet on sugarcane bagasse modified with EDTA dianhydride (EDTAD) in aqueous solutions: Kinetic and equilibrium aspects. *J. Environ. Manage.*, 118, pp. 135–143.

Segal, L., Creely, J.J., Martin, A.E. & Conrad, C.M., 1959. An empirical method for estimating the degree of crystallinity of native cellulose using the X-Ray diffractometer. *Text. Res. J.*, 29(10), pp. 786–794.

CHAPTER 4

RESULTS AND DISCUSSION

4.1 Characterization of mango materials

To evaluate the removal of extractable lignocellulosic components together with the introduction of EDTA chains, the mango materials were characterized using elemental and FTIR analyses. Additionally, the effects of chemical modification on crystallinity and thermal degradation properties were characterized using XRD and thermogravimetric analysis, respectively.

4.1.1 Elemental analysis

Table 4.1 summarizes the composition of MSSP, ATMS and CFMS in terms of carbon, hydrogen, nitrogen and oxygen content.

Table 4.1: Elemental composition of MSSP, ATMS and CFMS.

Material	Composition (%)				C_{EDTA} introduced (mmol g^{-1})
	C	H	N	O*	
Mango seed shell powder (MSSP)	46.0 ± 0.0	5.5 ± 0.2	0.3 ± 0.0	48.2 ± 0.2	-
Alkali treated mango seed shell biomass (ATMS)	46.8 ± 0.0	6.8 ± 0.0	0.2 ± 0.0	46.2 ± 0.0	-
Carboxyl functionalized mango seed shell biomass (CFMS)	42.6 ± 0.1	5.1 ± 0.1	2.8 ± 0.0	49.4 ± 0.2	0.925

* Computed by difference

Conversion of MSSP to ATMS resulted in insignificant change in the proportion of nitrogen. Grafting of the nitrogen bearing ligand species onto the surfaces of the mango materials was clearly illustrated by the rise in nitrogen composition from 0.2% for ATMS to 2.8% for CFMS. The difference in nitrogen content of ATMS and CFMS was attributed to introduction of 0.925 mmol of EDTA per gram of CFMS.

4.1.2 FTIR spectrophotometric analysis

The FTIR spectra of MSSP and ATMS, which represent the mango material before and after alkali treatment are presented in Figure 4.1.

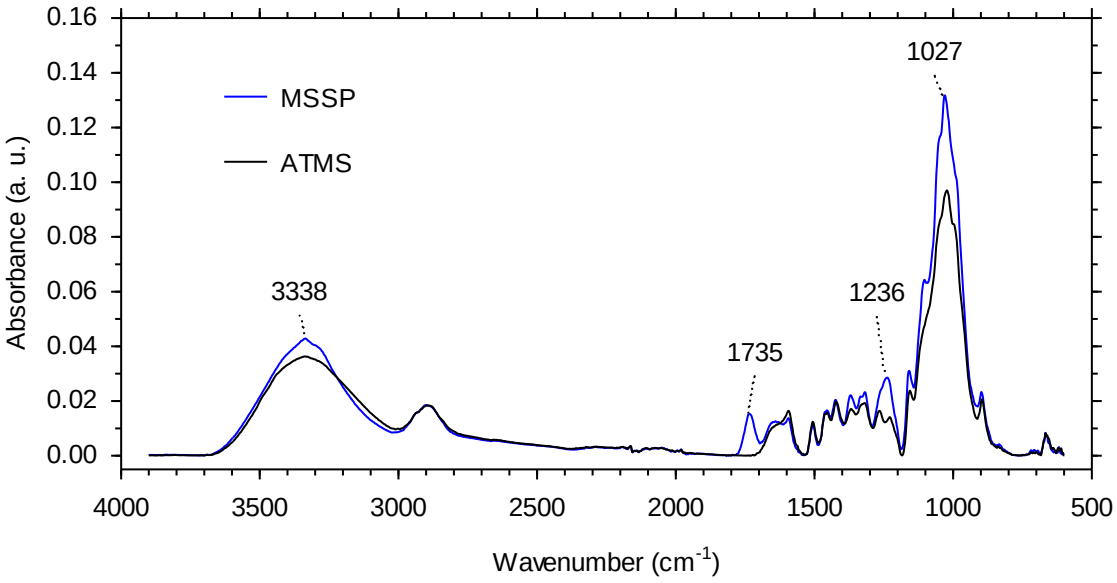

Figure 4.1: FTIR spectra of MSSP and ATMS depicting of alkali treatment.

The peaks at 1735 cm^{-1} and 1236 cm^{-1} in the MSSP spectrum assigned to stretch vibrations C=O and C–O of acetyl ester groups in hemicelluloses, respectively, disappeared after alkali treatment. This demonstrated the base catalyzed hydrolysis of ester linkages between lignin and hemicelluloses, where the latter dissolved in the alkali liquor. Similar observations were made by Feng *et al*. (2010) and Reddy *et al*. (2013) having treated orange peel and *Agave americana* biosorbents with 5% and 0.1 M sodium hydroxide solution, respectively. Jeffries (1994), Laine (2005) and Dutta *et al*. (2012) documented the abundance of primary alcohol groups in glucomannan type hemicelluloses while Li *et al*. (2015) observed strong FTIR bands at 1045 cm^{-1} for alkaline ethanol extracted hemicellulose fractions attributable to C–O stretching in these groups. Therefore, hemicellulose dissolution was confirmed by signal weakening of the peak at 3338 cm^{-1}. Moreover, reduction in the intensity of the alcoholic C–O stretch vibration peak at 1027 cm^{-1} was indicative of removal of hemicelluloses.

The effects of carboxyl functionalization are illustrated in Figure 4.2. Reappearance of the ester C=O stretch vibration peak at 1733 cm^{-1} on the CFMS spectrum signaled grafting through esterification similarly noted by Sun *et al*. (2014).

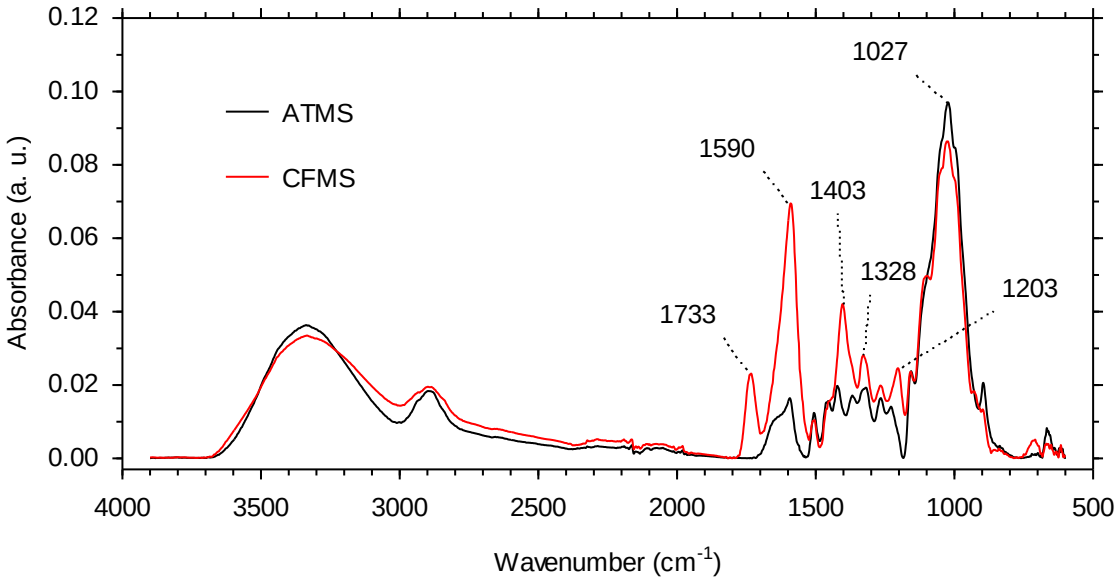

Figure 4.2: FTIR spectra of ATMS and CFMS depicting carboxyl functionalization.

Occurrence of the esterification reaction was corroborated by signal attenuation at 1027 cm^{-1} indicating conversion of primary alcoholic groups to ester links. In agreement with the results of Pereira *et al*. (2010) and Gusmao *et al*. (2013), EDTA ligand grafting was confirmed by signal strengthening at 1403 cm^{-1} and 1590 cm^{-1} attributed to carboxylate symmetric and asymmetric C–O stretching, respectively. The introduction of nitrogen, suggested earlier by the results of elemental analysis, was evidenced by the appearance of a peak at 1203 cm^{-1} assigned to C–N stretch vibrations of the tertiary amine groups of the grafted ligand. Amplification of the band at 1328 cm^{-1} attributable to CH_2 wagging supported grafting of EDTA substituents, each comprising six methylene groups.

The effect of lead(II) ion loading on the CFMS spectral bands is depicted in Figure 4.3. Major changes in the position and intensity of carboxyl C–O stretching peaks (1590 cm^{-1} and 1403 cm^{-1}) suggested strong binding on carboxylic acid groups of the grafted EDTA chains, which was corroborated by the weakening of the O–H stretch peak (3338 cm^{-1}). Additionally, attenuation of the C–H stretch peak (2902 cm^{-1}) as well as shifting and attenuation of the methylene CH_2 wagging peak (1328 cm^{-1}) were interpreted as a reflection of change in steric strain to accommodate lead(II) ions.

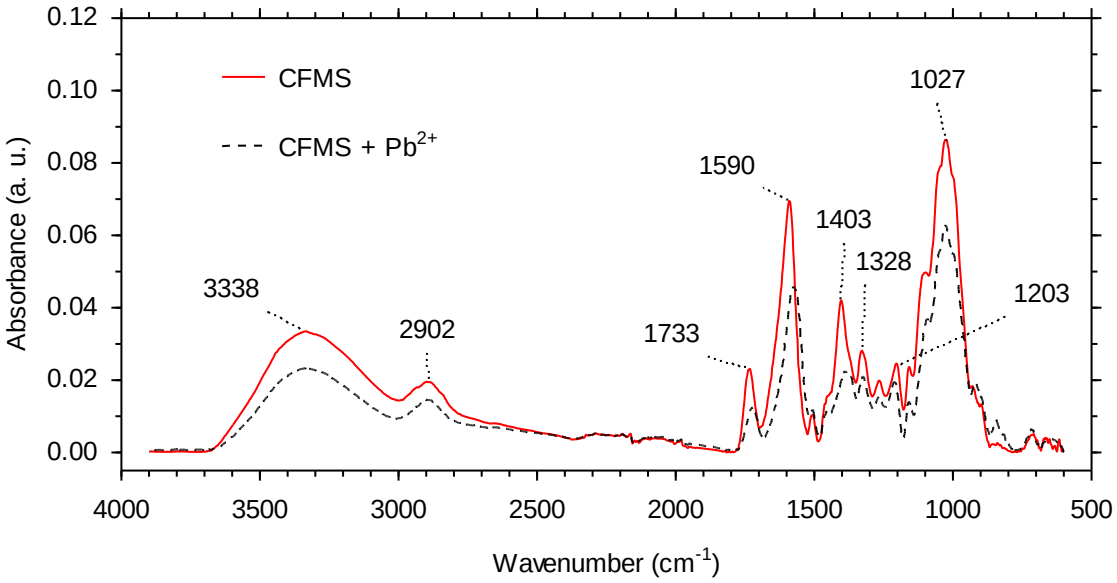

Figure 4.3: Effect of lead(II) ion loading on FTIR spectra CFMS.

Shifting and weakening for the C–N (1203 cm^{-1}) and C=O (1733 cm^{-1}) stretch vibration peaks also confirmed activity of the grafted EDTA. Signal weakening at 1027 cm^{-1} (alcoholic C–O stretching) demonstrated additional participation of cellulose hydroxyl groups in metal ion binding. Several researchers have proposed similar involvement of grated EDTA ligands groups in metal ion binding (Yu *et al*. 2008; Pereira *et al*. 2010; Xu *et al*. 2011; Yang *et al*. 2011; Sun *et al*. 2014).

Metal uptake had insignificant effect on the spectral bands of ATMS with respect to peak shifting (see Appendix I). However, slight signal weakening was noted at 3338 cm^{-1} (O–H stretch), 1593 cm^{-1} (carboxyl C–O stretch), 1505 cm^{-1} (aromatic C=C stretch), 1453 cm^{-1} (CH_2 bending at C-6 of cellulose), 1422 cm^{-1} (carboxyl C–O stretch) and 1265 cm^{-1} (aromatic C=C stretch). These changes illustrated the participation of cellulose hydroxyls, carboxyl, phenolic and lignin aromatic rings in lead(II) ion binding through physisorption.

4.1.3 XRD analysis

The X-ray diffraction patterns of MSSP, ATMS and CFMS are shown in Figure 4.4. The most intense peak in each pattern between 22° and 23° corresponded to the (0 0 2) lattice plane while the least intense peak occurring at 34.5°, corresponded to the (0 4 0) lattice plane. The broad peaks between 14° and 17° were mergers of two distinct peaks at approximately 15.2° and 16.5° corresponding to the (1 0 1) and (1 0 $\bar{1}$) lattice planes, respectively (El Oudiani *et al*. 2012; Sebe *et al*. 2012; Hajiha *et al*. 2014).

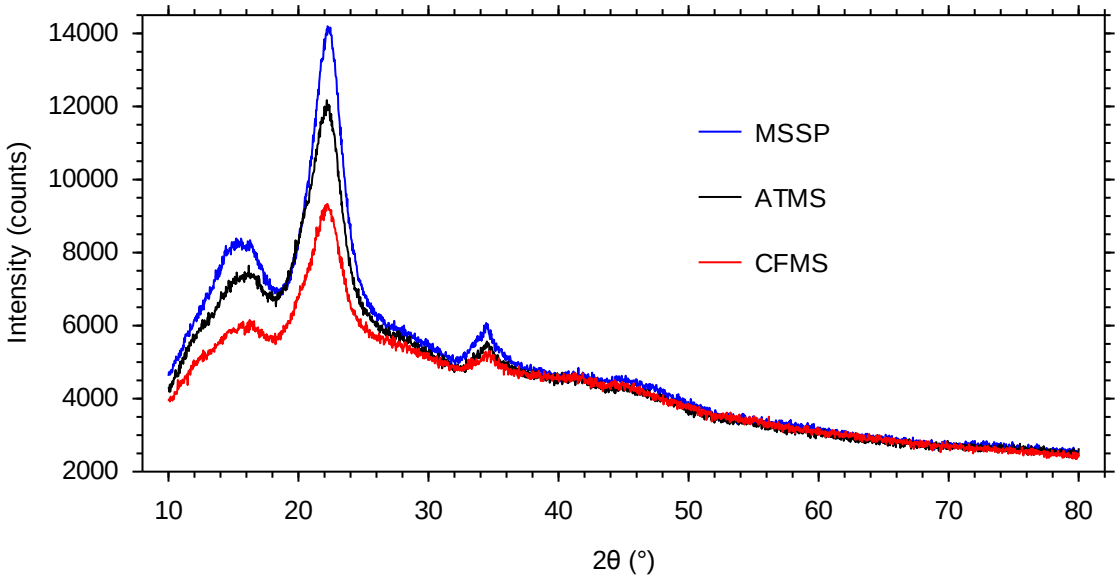

Figure 4.4: XRD patterns of MSSP, ATMS and CFMS.

Both alkali treatment and carboxyl functionalization resulted in attenuation of all the XRD peak intensities with the crystallinity index dropping from 51.6% for MSSP to 46.4% and 41.2% for ATMS and CFMS, respectively. This was due to conversion of the ordered crystal regions of cellulose into disoriented amorphous regions, which was accompanied by breakage of hydrogen bonds with subsequent formation of stronger ion-dipole bonds and ester bonds in alkali treatment and carboxyl functionalization, respectively. Under similar circumstances, Karnitz *et al*. (2009) as well as Singha and Guleria (2014) reported reduction in biomass crystallinity index owing to mercerization and grafting, respectively.

4.1.4 Thermogravimetric analysis

The thermogravimetric analysis (TGA) and derivative thermogravimetric (DTG) curves of MSSP, ATMS and CFMS are presented in Figure 4.5. The TGA curves of the parent materials, MSSP and ATMS, have some degree of resemblance. However, all three curves show an initial mass loss in the 40–150°C range corresponding to the loss of physically bound water accounting for 6.0%, 6.9% and 9.9% mass loss from MSSP, ATMS and CFMS, respectively. Higher moisture content in ATMS and CFMS was due to widespread hydrogen bonding between water molecules and more accessible hydroxyl groups in the amorphous cellulose regions that resulted from modification (Jiang *et al.* 2012). The water desorption stage was followed by a somewhat dormant stage that continued up to about 240°C for MSSP and ATMS, and up to 220°C for CFMS. Thereafter, in the 220–340°C range for CFMS and 240–400°C for MSSP and ATMS, mass loss was largely ascribed to thermolysis of cellulose and

hemicelluloses as well as, to a lesser extent, lignin (Roy *et al*. 2013; Hajiha *et al*. 2014). Above 400°C thermal degradation was characterized by sustained, less rapid thermolysis of lignin and residual tar.

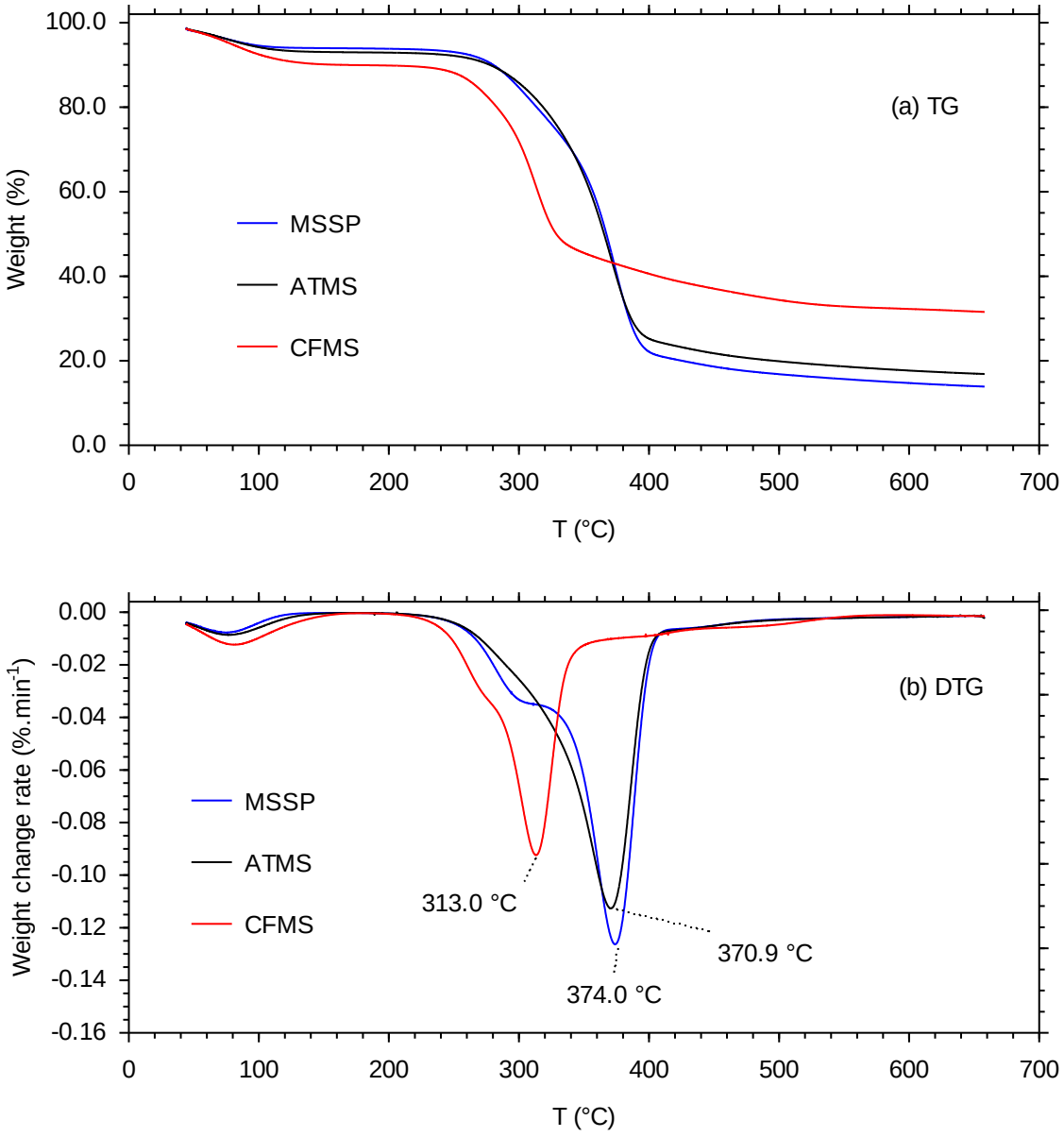

Figure 4.5: TGA and DTG curves of MSSP, ATMS and CFMS.

The greatest mass loss in the carbohydrate thermolysis stage was noted for MSSP (70.9%) followed by ATMS (66.9%) and CFMS (47.5%). The significant differences between CFMS mass loss and that of the parent biomaterials can be explained by the occurrence of competing dehydration and depolymerisation pathways of the mechanism of carbohydrate thermolysis. Dehydration involved cross-linking of the cellulose chains with together with evolution of water to form dehydrocellulose, which was then decomposed to char and volatile products. In the depolymerization pathway, cellulose chains were unzipped with scission of glucosidic bonds

to produce laevoglucosan (Scheme 1), which was further decomposed to volatile tars and gas (Beyler & Hirschler 2002; Ciolacu *et al*. 2011; Lomakin *et al*. 2011; Draman *et al.* 2014).

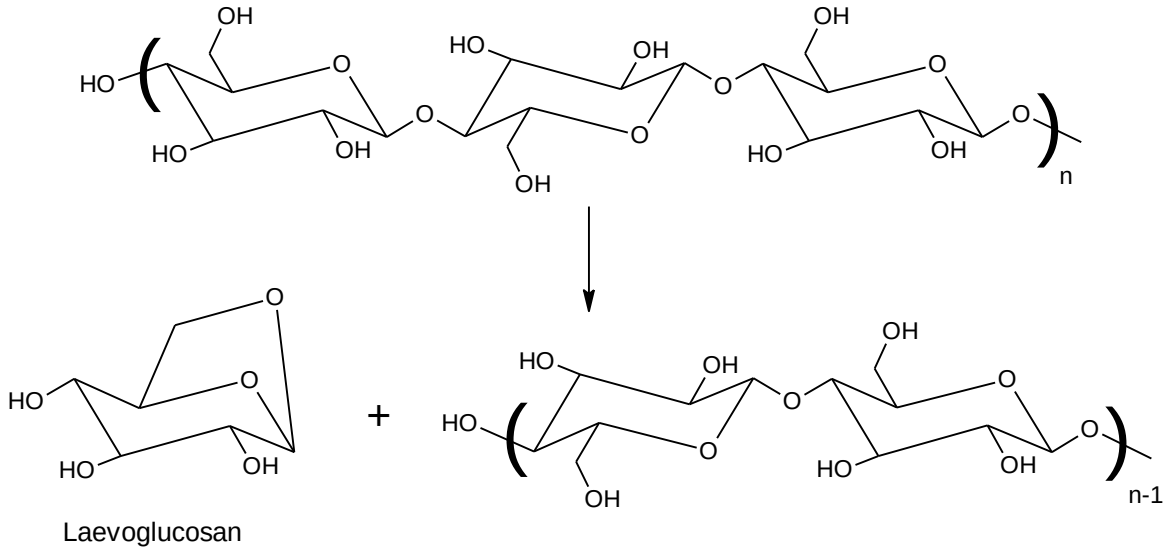

Scheme 1: Scission of cellulose in depolymerization pathway of thermal decomposition.

Larger weight losses recorded for MSSP and ATMS suggested that the carbohydrate decomposition stage was dominated by the depolymerisation pathway, which yielded a larger amount of volatile by-products. This has been corroborated by the lower residual masses of MSSP (14.73%) and ATMS (17.69%) at 600°C compared to that of CFMS (32.26%). Smaller weight loss at lower temperature for CFMS indicated the dominance of the dehydration pathway yielding large amounts of carbonaceous residue from which the high residual mass resulted. Suppression of depolymerization in CFMS thermolysis can be explained by the blockage of $–CH_2OH$ groups required for laevoglucosan formation through a reaction with the modifying agent, resulting in a stable network of amorphous crosslinked cellulose as illustrated in Scheme 2. Hindrance of depolymerization thus resulted in insignificant laevoglucosan formation, reduced volatilization and larger amounts of char (Medronho *et al*. 2013).

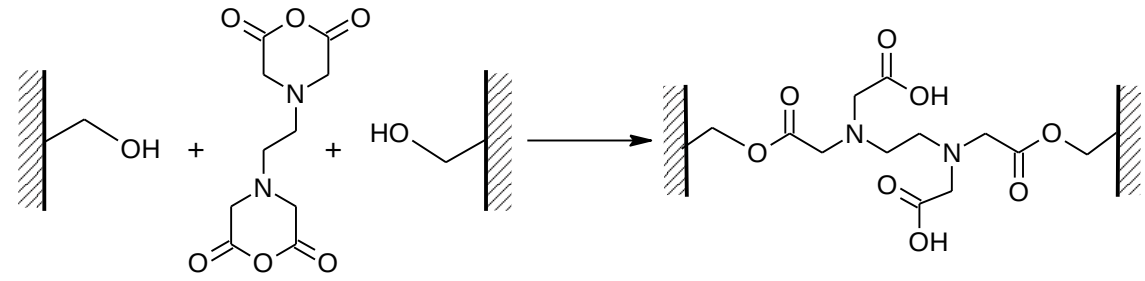

Scheme 2: Cellulose crosslinking by EDTA bisanhydride.

As shown by the DTG peak for the curves, the temperature at which CFMS decomposition rate reached maximum value, T_{max}, recorded as 313.0°C, was lower in comparison to 374.0°C and 370.9°C for MSSP and ATMS, respectively. This reaffirmed the significant dominance of the initial dehydration pathway in CFMS decomposition while higher T_{max} values for MSSP and ATMS confirmed the dominance of the delayed depolymerization pathway. In the case of MSSP, which contained more regions of organized crystalline cellulose with higher hydrogen bond intensity, the unzipping and scission reaction required more energy hence the slightly higher T_{max} for MSSP than ATMS.

The presence of a shoulder around 300 °C on the MSSP differential curve suggested a more rapid decomposition in the initial phase of the carbohydrate degradation stage (Moriana *et al.* 2014). This was a direct consequence of degradation of amorphous hemicelluloses with fewer organized hydrogen bonds amongst the polysaccharide chains. Removal of hemicellulose through alkali treatment led to the disappearance of the shoulder.

4.2 Batch sorption study

The performance of the carboxyl functionalized sorbent was evaluated in comparison to that of its parent alkali treated form. Based on documented studies of sorption by several biosorbents revealing that optimum pH for lead(II) ion uptake was within the 4.5 to 6.0 range (Martinez *et al*. 2006; Xuan *et al*. 2006; Cruz-Olivares *et al*. 2010; Tan *et al*. 2010; Bairagi *et al*. 2011; Salvado *et al*. 2012; Dong *et al*. 2013; Fadzil *et al*. 2016), thus a pH of 5.2 was selected. For kinetic studies, samples were drawn from each batch after 5, 10, 15, 20, 30, 40, 60, 80, 100, 120, 160 and 180 min of contact while for isotherm studies each batch, was allowed to run for 24 h to ensure the attainment of equilibrium (Olu-Owolabi *et al*. 2012).

4.2.1 Sorption kinetics

Graphical illustrations of sorption of lead(II) ions by ATMS and CFMS as functions of time are presented in Figure 4.6. The illustrations indicate that sorbent loading increased rapidly in the early stages of contact and slowed down as the sorption process progressed to equilibrium. The initial higher sorption rate can be attributed to a large number of unoccupied binding sites hence greater driving force. Thereafter, progressive decline in the number of vacant binding sites together with decrease in the concentration of lead(II) ions resulted in lowered sorption rates. Increasing the initial lead(II) ion concentration from 130 $mg.L^{-1}$ to 400 $mg.L^{-1}$ resulted similar trends with higher sorbent loading (see Appendix II).

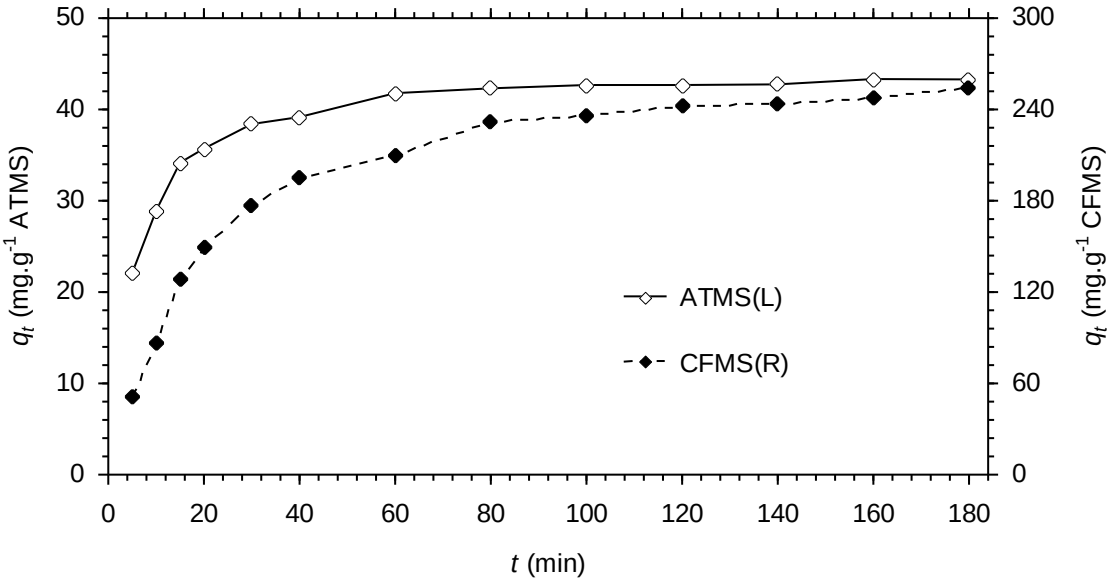

Figure 4.6: Effect of contact time on sorption of lead(II) ions by ATMS and CFMS.

[Room temperature, initial pH: 5.2, C_i: 250 mg.L^{-1}, ATMS dose: 1 g.L^{-1}, CFMS dose: 0.5 g.L^{-1}]

The increases in sorbent loading at higher lead(II) ion concentrations were also ascribed to higher driving force of concentration gradient (Anirudhan *et al*. 2012; Rout *et al*. 2014.

4.2.1.1 Reaction model simulation

Pseudo-first order, pseudo-second order, pseudo-nth order and Elovich model simulation plots for sorption by ATMS are depicted in Figure 4.7.

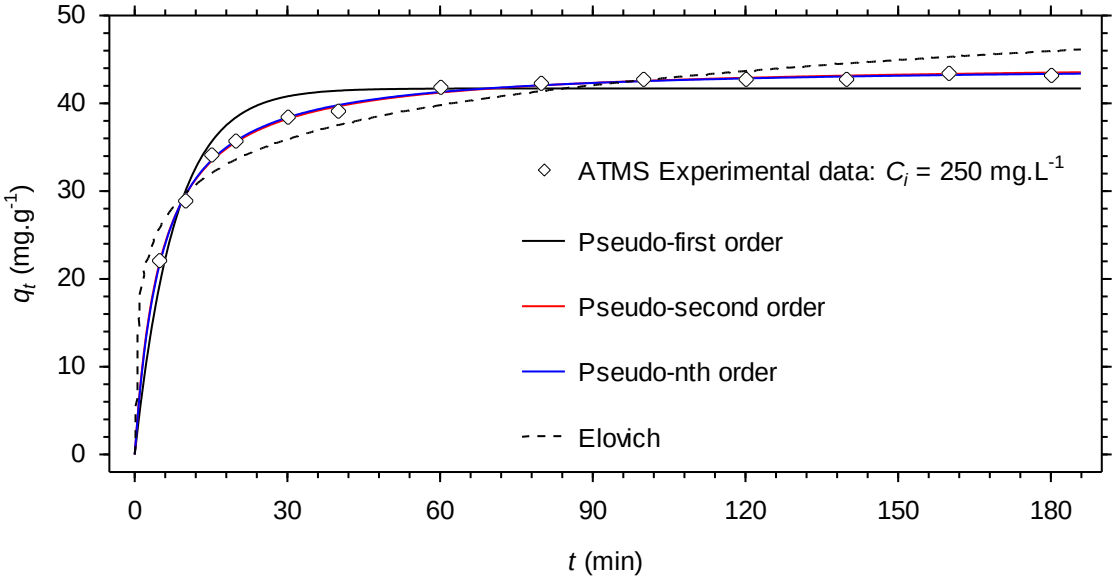

Figure 4.7: Reaction model simulation plots for sorption of lead(II) ions by ATMS.

[Room temperature, initial pH: 5.2, C_i: 250 mg.L^{-1}, Sorbent dose: 1 g.L^{-1}]

The pseudo-second order and pseudo-nth order models provided best fit for the kinetic data. However, the pseudo-nth order model had better simulation of the kinetic data as it yielded correlation coefficient (R^2) values greater than 0.98 in all instances (see Appendix III). This was attributed to the improved flexibility in the fitting procedure endowed by the additional parameter *n*. Similar simulation in which the pseudo-nth order and pseudo-second order models provided a good fit to the experimental data was noted for experiments using different initial lead(II) ion concentration (see Appendix IV). Analogous to ATMS, kinetics of the sorption by CFMS were well simulated by the pseudo-nth order and pseudo-second order models, the former providing better fit (see Appendix V). In the majority of cases, R^2 values related to pseudo-first order model fitting were lower than 0.98. Therefore, sorption by ATMS and CFMS did not follow pseudo-first order kinetics. The Elovich model accounted for the least values of R^2 together with the highest values of average relative error (ARE) indicating the inappropriateness of the model in interpreting the observed sorption kinetics. Since the Elovich model can be associated with heterogeneous sorbent surfaces (Plazinski *et al*. 2009), this was interpreted as implying homogeneity of the mango biosorbents, especially ATMS, which had $R^2 < 0.93$ in all instances. The pseudo-second order model facilitates the determination of half-life $t_{0.5}$ (min), the time required for completion of half the sorption process, expressed as:

$$t_{0.5} = \frac{1}{k_2 q_e} \tag{25}$$

Half-life can be used as a measure of the sorption rate (dq_t/dt) whereupon a smaller value implies a higher sorption rate (Dogan *et al*. 2009; Ofomaja & Naidoo 2011). The effect of initial lead(II) ion concentration on $t_{0.5}$ is illustrated in Figure 4.8.

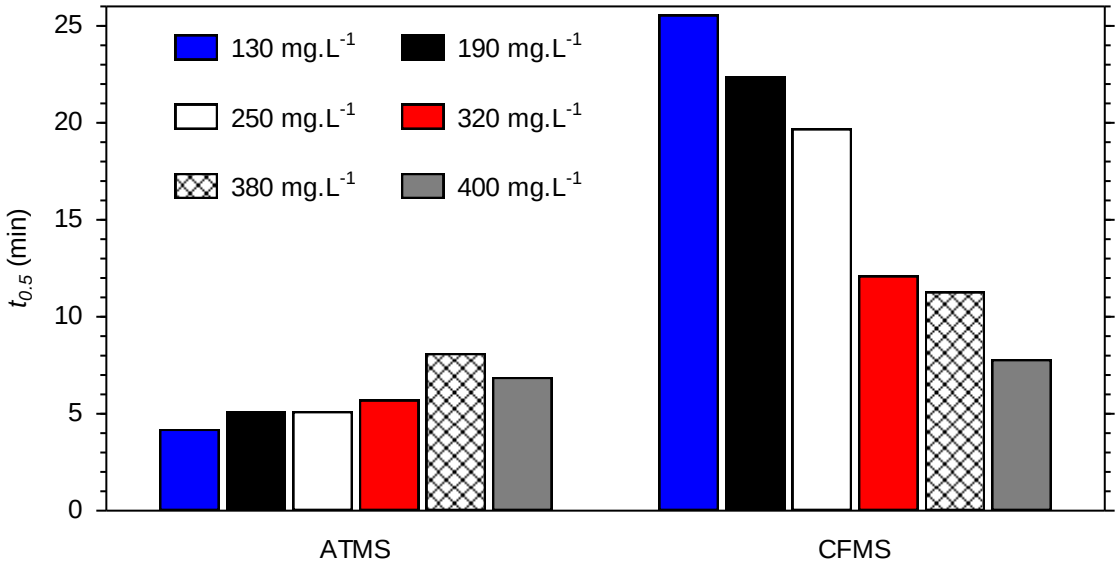

Figure 4.8: Effect of initial concentration on half-life of lead(II) ion sorption by ATMS and CFMS.

Half-life for sorption by ATMS and CFMS varied within the 4.21–8.12 min and 7.81–25.57 min range, respectively. The lower values associated with ATMS reflected higher rates of sorption than those observed for CFMS. This was explained by prevalence of binding on ATMS surfaces ascribed to rapid physisorption mechanisms (Bayramoglu *et al.* 2005). Conversely, slow sorption depicted by the highest half-life at lowest initial concentration for CFMS confirmed the occurrence of slower binding specifically onto carboxyl, amine and ester functional groups of the grafted species previously indicated by FTIR analysis.

A downward trend in the half-life of sorption by CFMS with increasing initial lead(II) ion concentration was noted. As initial concentration was increased, the driving force of concentration gradient also increased thereby increasing the rate of the sorption processes hence diminishing half-life. For ATMS, an upward trend in the half-life of sorption by ATMS was observed. This suggested that changes in driving force of concentration gradient had little effect on sorption rate and that the trend can be ascribed to increases in sorption capacity with increasing initial lead(II) ion concentration.

4.2.1.2 Diffusion model simulation

Simulation plots of Bangham's pore diffusion, the intra-particle diffusion and the double exponential models for sorption by CFMS are presented in Figure 4.9. The kinetic data conformed to the double exponential model, which yielded R^2 values greater than 0.99 in all experimental data sets (see Appendix VI).

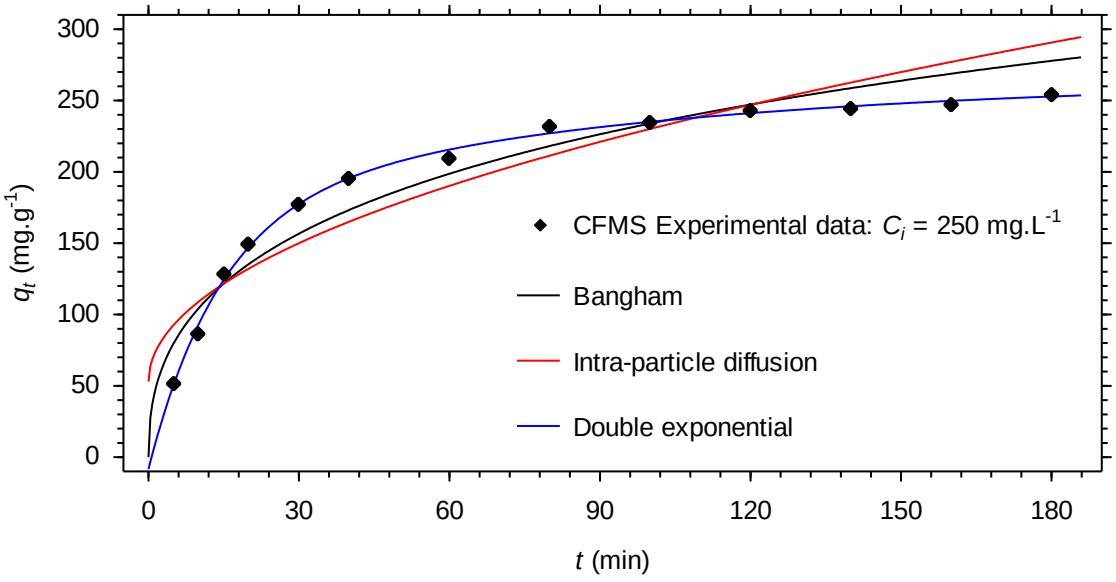

Figure 4.9: Diffusion model simulation plots for sorption of lead(II) ions by CFMS.

[Room temperature, pH: 5.2, C_i: 250 mg.L^{-1}, Sorbent dose: 0.5 g.L^{-1}]

The excellent fit was ascribed to possession of five adjustable parameters that endowed great flexibility in the fitting procedure. Nevertheless, the good simulation suggested occurrence of a two-phase sorption mechanism that proceeded through an initial rapid lead(II) ion uptake phase dominated by external and film diffusion followed by a slow phase in which intra-particle diffusion was most prominent (Blazquez *et al*. 2014). The intra-particle diffusion model, which yielded the lowest R^2 and highest ARE values, had the least appropriate fit to the kinetic data. Bangham's model also illustrated poor simulation of the kinetic data as signified by producing low R^2 values. Failure of Bangham's and the intra-particle diffusion models to fit the experiment data indicated that pore diffusion was not the sole rate-limiting step in the sorption processes (Ofomaja *et al*. 2010; Srivastava *et al*. 2015). Similar fitting was noted for experiments using various initial concentrations (see Appendix VIII) and for sorption by ATMS (see Appendix VII).

The probability of simultaneous sorption rate-control by film and intra-particle diffusion was tested using linearized plots of q_t versus $t^{0.5}$ depicted in Figure 4.10. None of the plots passed through the origin emphasizing that intra-particle diffusion was not the sole rate controlling step in the mechanism.

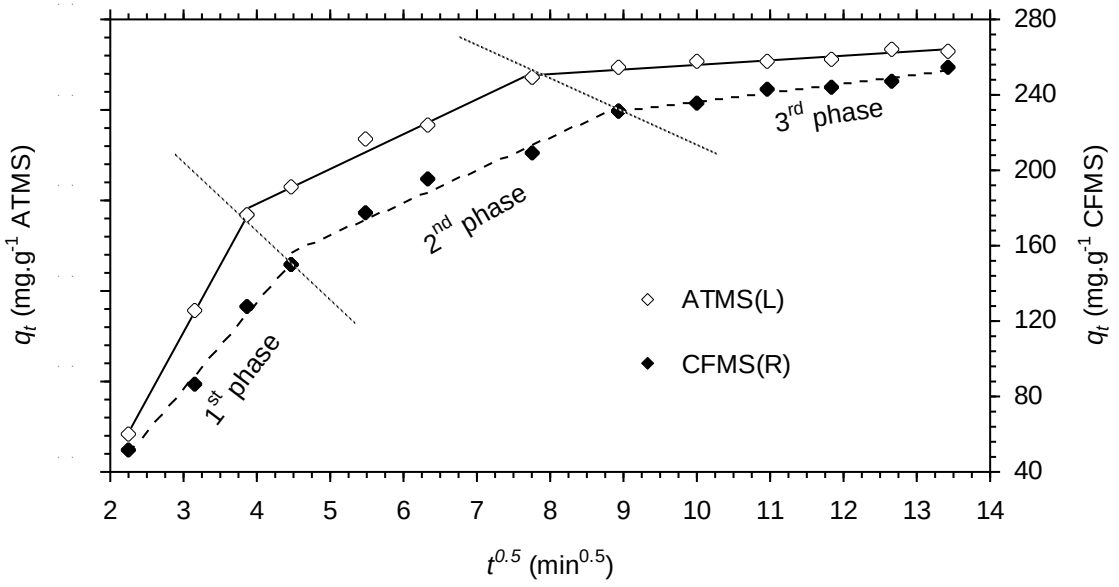

Figure 4.10: Intra-particle diffusion model plots for sorption of lead(II) ions by ATMS and CFMS.

[Room temperature, Initial pH: 5.2, C_i: 250 mg.L^{-1}, ATMS dose: 1 g.L^{-1}, CFMS dose: 0.5 g.L^{-1}]

All the kinetic data produced multi-linear plots indicating that two or more diffusion processes influenced the rate of lead(II) ion sorption by both CFMS and ATMS. The initial phases characterized by a higher slope corresponded to rapid sorption that was limited by a combination of film and intra-particle diffusion with the former being dominant. The second and third phases corresponded to slower sorption in the inner surfaces of the sorbents that featured rate control by intra-particle diffusion. Similar multi-linear plots were observed for

different initial solution concentrations (seeAppendix IX). Analogous results were reported by Saeid *et al*. (2012) for biosorption of Cr(III) ions by microalgae *Spirulina maxima* as well as Hu *et al*. (2015) for the uptake of copper ions by *Acidosasa edulis* shoot shell biosorbent.

4.2.2 Sorption isotherms

The isotherms obtained for lead(II) ion sorption by ATMS and CFMS together with simulation of the Langmuir, Freundlich, Dubinin-Radushkevich and Sips models are shown in Figure 4.11.

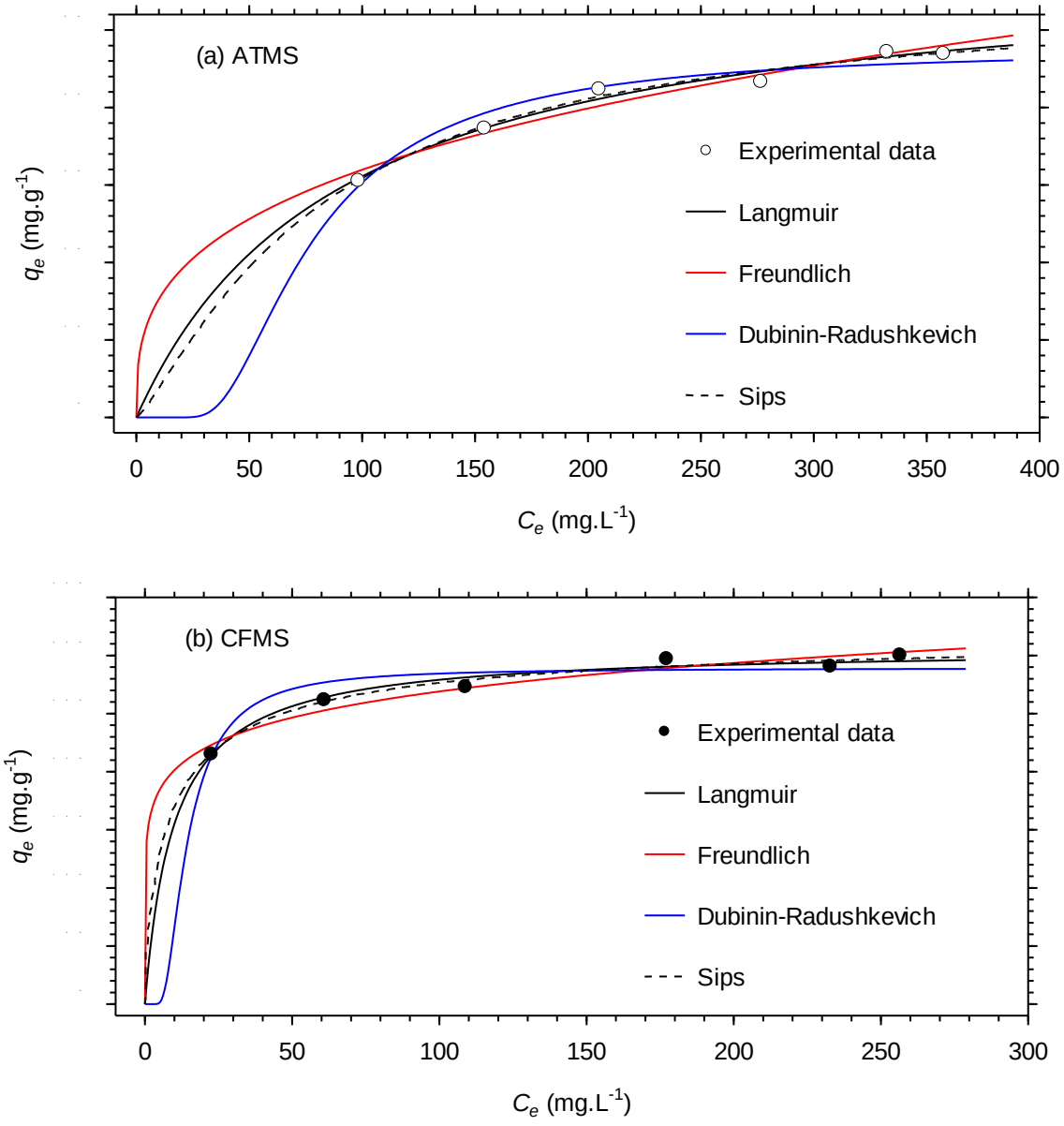

Figure 4.11: Sorption isotherms for lead(II) ion uptake by (a) ATMS and (b) CFMS.

[Room temperature, Initial pH: 5.2, Contact time: 24 h, ATMS dose: 1 g.L^{-1}, CFMS dose: 0.5 g.L^{-1}]

Table 4.2: Isotherm model parameters for lead(II) ion sorption by ATMS and CFMS.

	ATMS	CFMS		ATMS	CFMS
Langmuir			*Sips*		
q_{maxL} (mg.g^{-1})	59.25	306.33	q_{maxS} (mg.g^{-1})	54.49	321.34
K_L (L.mg^{-1})	0.011	0.103	K_S (L.mg^{-1})^n	0.004	0.202
χ^2	0.085	0.504	$1/n_s$	1.237	0.742
R^2	0.9823	0.9711	χ^2	0.075	0.394
ARE (%)	1.46	1.54	R^2	0.9839	0.9772
			ARE (%)	1.32	1.31
Freundlich			*Redlich-Peterson*		
K_F [(mg.g^{-1}) (L.mg^{-1})^n]	7.33	150.66	q_{maxRP} (mg.g^{-1})	69.16	267.94
$1/n_F$	0.320	0.126	K_{RP} (L.mg^{-1})	0.008	0.155
χ^2	0.212	1.167	β_{RP}	1.107	0.964
R^2	0.9590	0.9376	χ^2	0.076	0.389
ARE (%)	2.52	2.44	R^2	0.9836	0.9774
			ARE (%)	1.29	1.27
Dubinin-Radushkevich			*Toth*		
q_{maxDR} (mg.g^{-1})	47.49	289.06	q_{maxT} (mg.g^{-1})	53.72	322.69
K_{DR} (mol^2.kJ^{-2})	739.955	26.505	K_T (L.mg^{-1})	0.009	0.216
E (kJ.mol^{-1})	0.026	0.137	n_T	0.734	1.420
χ^2	0.247	2.007	χ^2	0.076	0.393
R^2	0.9498	0.8860	R^2	0.9838	0.9772
ARE (%)	2.89	3.05	ARE (%)	1.31	1.30

Amongst the two-parameter models, the Langmuir model simulation gave the highest R^2 as well as lowest ARE values and thus the best fit to the isotherms of both ATMS and CFMS. Accordingly, the sorption capacity of ATMS and CFMS was 59.25 mg.g^{-1} and 306.33 mg.g^{-1}, respectively. Enhanced sorption capacity reflected augmentation of metal ion sequestering groups through carboxyl functionalization. The value of the affinity related constant K_L increased significantly from 0.011 to 0.103 L.mg^{-1}. This was because the carboxyl functionalized sorbent had higher affinity for lead(II) ions endowed by the grafted EDTA groups.

Table 4.3: Comparison of sorption capacities of various biomass for divalent metal ions with the mango seed shell biomass of the present study.

Biomass	Modifying Agent	Metal ion	Sorption capacity ($mg.g^{-1}$)		Reference
			Unmodified	Modified	
Baker's yeast	EDTA dianhydride	Pb^{2+}	20.00	192.30	Yu *et al*. (2008)
		Cu^{2+}	4.50	65.00	
Soybean straw	Citric acid	Cu^{2+}	42.97	48.80	Zhu *et al*. (2008)
Baker's yeast	EDTA dianhydride	Pb^{2+}	13.53	66.89	Xu *et al*. (2011)
		Cd^{2+}	8.24	38.66	
		Ca^{2+}	4.41	25.38	
Brewer's yeast	EDTA dianhydride	Pb^{2+}	21.78	89.21	Zhang *et al*. (2011)
		Cd^{2+}	13.02	41.00	
Apple pomace	Succinic anhydride	Cd^{2+}	4.45	91.75	Chand *et al*. (2014)
Mango seed shell	EDTA dianhydride	Pb^{2+}	59.25	306.33	This study

To determine favorability of the sorbents and the sorption processes, values of the dimensionless separation factor R_L proposed by Hall *et al*. (1966) were also calculated using the following expression that makes use of the Langmuir constant K_L:

$$R_L = \frac{1}{1 + K_L C_i} \tag{26}$$

The variation of R_L during the course of the sorption experiments is depicted in Figure 4.12.

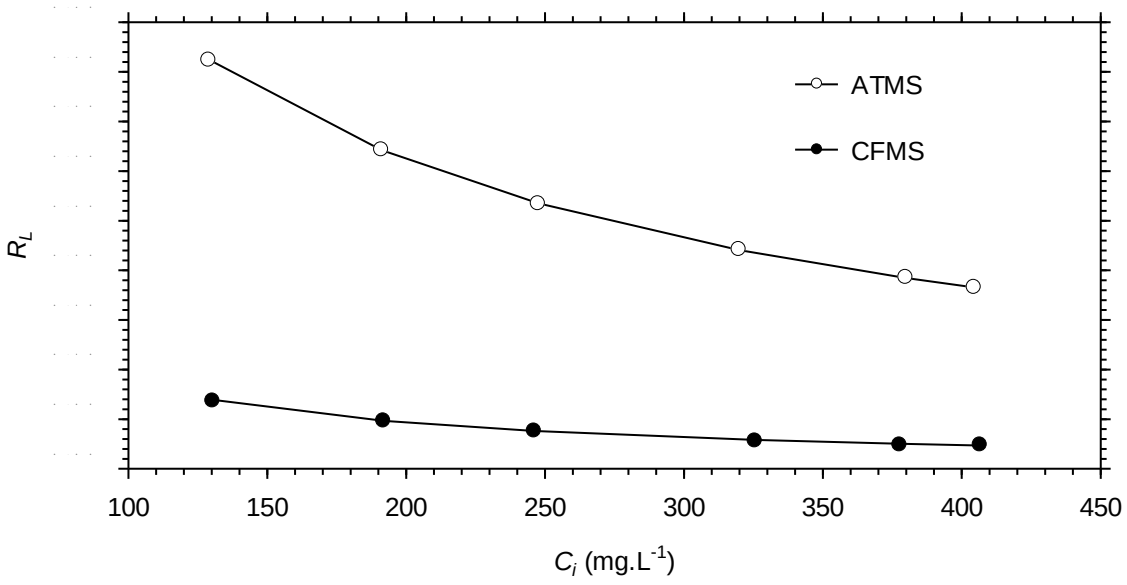

Figure 4.12: Variation of R_L for sorption of lead(II) ions by ATMS and CFMS.

For sorption by both ATMS and CFMS, the values of R_L varied between 0 and 1 indicating favorability of the sorption processes (Mohan *et al.* 2006; Gok *et al.* 2013; Won *et al.* 2013).

The Langmuir constant has been used to calculate the free energy change of sorption using the following formula (Aryal & Ziagova 2011; Karmacharya *et al.* 2016):

$$\Delta G = -RT \ln K_L \quad (27)$$

where R is the universal gas constant (8.314×10^{-3} KJ.mol^{-1}.K^{-1}), T is the temperature (K). However, to accurately apply this formula, the Langmuir constant should be expressed as a dimensionless term by multiplication with the density of the lead(II) solution ρ ($\rho = 10^6$ mg.L^{-1}) (Milonjic 2007) so that, equation (27) becomes:

$$\Delta G = -RT \ln(\rho K_L) \quad (28)$$

The free energy change of sorption calculated thus was –23.07 kJ.mol^{-1} and –28.59 kJ.mol^{-1} for ATMS and CFMS, respectively, indicating that sorption of lead(II) ions by both sorbents was spontaneous.

The Freundlich and Dubinin-Radushkevich produced higher ARE and lower R^2 values than the Langmuir model indicating less appropriate fit to the experimental data. Nonetheless, according to the application of the Dubinin-Radushkevich model, mean free energy values of 0.026 kJ.mol^{-1} and 0.137 kJ.mol^{-1} for ATMS and CFMS, respectively, demonstrated that binding occurred through physisorption.

Application of the three parameter models yielded higher R^2 and lower ARE values for sorption by both ATMS and CFMS relative to simulation by the two-parameter models. This was primarily due to availability of an additional parameter that endowed some degree of flexibility in simulating the isotherm data. For both ATMS and CFMS isotherms the values of the simulation error statistic, particularly R^2, corresponding to the Langmuir model were similar to those the Sips, Redlich-Peterson and Toth models (Table 4.2). This was shown by the high degree of overlap amongst the simulations (see Appendix X). The values of the three-parameter models' exponents, which varied between 0.73 and 1.43, were close to unity, in which case the respective model would reduce to the Langmuir form. Therefore, the Sips, Redlich-Peterson and Toth models had more Langmuir than Freundlich features. Similarity of Langmuir, Sips and Toth model simulation was reported for the uptake of lead, copper and cadmium by *Caulerpa lentillifera* biomass (Apiratikul & Pavasant 2008), and the removal of Ni(II) ions by *Litchi chinensis* seed biosorbent (Flores-Garnica *et al*. 2013).

Appropriateness of the Langmuir, Sips, Redlich-Peterson and Toth models in describing the observed isotherms against a background of unsuitable simulation by the Freundlich and Dubinin-Radushkevich models implied monolayer coverage of the mango biomass by lead(II) ions together with equivalence of binding sites. Such equivalence of CFMS binding sites could be interpreted as domination of grafted EDTA carboxyl functional groups in the sequestration of lead(II) ions.

4.3 Column sorption: Application testing on electroplating wastewater

The performance of the calcium alginate immobilized biosorbent was assessed by experimental treatment of electroplating wastewater samples. The wastewater had a characteristic pH of 3.4 and total dissolved copper, chromium, nickel and iron content of 890 $mg.L^{-1}$, 690 $mg.L^{-1}$, 5405 $mg.L^{-1}$ and 580 $mg.L^{-1}$, respectively. In one set of experiments the wastewater was used in its natural state while in another the wastewater was acidified to a pH of 1.8 using concentrated sulfuric acid in order to improve the uptake of chromium on the basis of several reports in the literature that indicated that acidic conditions are suitable for removal of anionic chromium species (Baral *et al.* 2006; Kiran & Kaushik 2008; Anandkumar & Mandal 2011; Saha & Saha 2014; Kumari & Sobha 2016). After acidification, total copper, chromium, nickel and iron content was 915 $mg.L^{-1}$, 770 $mg.L^{-1}$, 5325 $mg.L^{-1}$ and 755 $mg.L^{-1}$, respectively.

4.3.1 Sorption from non-acidified wastewater

Figure 4.13 illustrates total copper, chromium, nickel and iron removal from non-acidified electroplating wastewater with an initial pH of 3.4. For copper, chromium and iron the highest removal, noted as 12.3%, 14.8% and 13.8%, respectively, occurred in the first experimental run. Thereafter, there was progressive decrease in removal, which was ascribed to a decrease in the number of unoccupied irreversible binding sites (Morton *et al.* 2001). The low metal removals that were observed in the fourth experimental run were attributed to binding on reversible binding sites, which, throughout all the desorption components of the experiments, were amenable to regeneration by hydrochloric acid scrubbing (Zhou & Kiff 1991). The percentage removal values corresponding to nickel removal were lower in comparison to those of the three other metals largely due to significantly higher initial concentration in the wastewater.

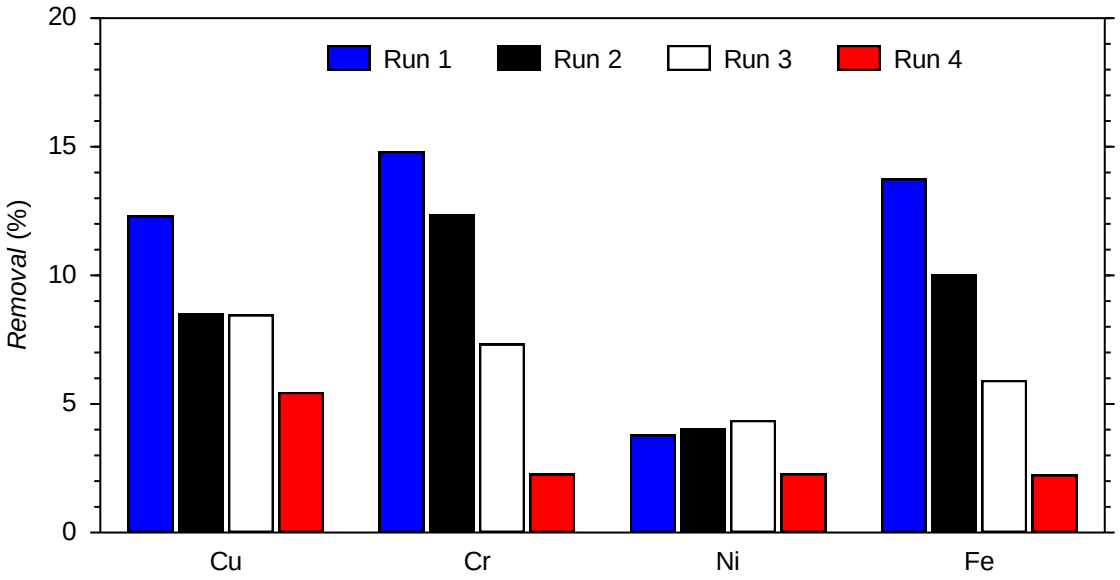

Figure 4.13: Copper, chromium, nickel and iron removal from non-acidified electroplating wastewater. [Room temperature, Bed mass: 4.0 g, Flow rate: 30 mL.min^{-1}, Initial pH: 3.4, Contact time: 24 h, Initial concentration: Cu 890 mg.L^{-1}; Cr 690 mg.L^{-1}; Ni 5405 mg.L^{-1}; Fe 580 mg.L^{-1}]

Figure 4.14 presents the amounts of metal recovered from the loaded non-acidified wastewater treatment column though desorption with dilute hydrochloric acid.

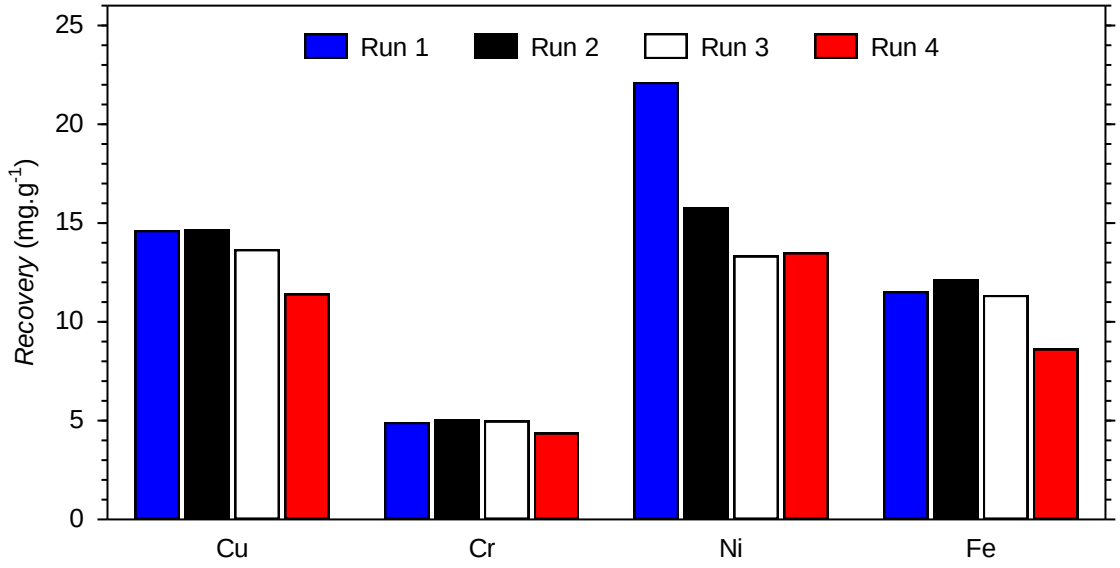

Figure 4.14: Copper, chromium, nickel and iron recovery from the non-acidified wastewater treatment column.

The amount of desorbed copper, chromium and iron varied slightly in the first three experimental runs. These results reflected the fraction metallic species bound reversibly on the sorbent surface, which were amenable to elution by dilute hydrochloric acid. Reduction in recovery observed in run 4 therefore confirmed conversion of reversibly binding secondary

hydroxyls to irreversibly binding carboxyl groups by oxidation. Nickel recovery, however, progressively decreased from run 1 to run 3 suggesting progressive increase in the proportion for irreversible binding sites, which was attributed to the oxidation of hydroxyl groups to ketone and carboxyl groups with the oxidation products having the ability to form stronger interactions with metal cations. Mild oxidation was facilitated by prevailing slightly acidic conditions at an initial pH of 3.4 (see Section 4.3.2). This downward trend in recovery was only noticeable with nickel primarily because of its high initial concentration, which, owing to much higher driving force for sorption, resulted in preferential binding by freshly produced carboxyl groups. Insignificant change in nickel recovery was noted in run 4, which indicated the cessation of the oxidation process.

4.3.2 Sorption from acidified wastewater

Figure 4.15 shows variation of copper, chromium, nickel and iron removal from acidified wastewater adjusted to a pH of 1.8. Apart from the temporary decrease in the removal of copper observed between experimental runs 1 and 2, the removal of all four metals increased progressively throughout the four experimental runs. This was attributed to widespread oxidation of hydroxyl to carboxyl groups with improved metals ion sequestration capabilities.

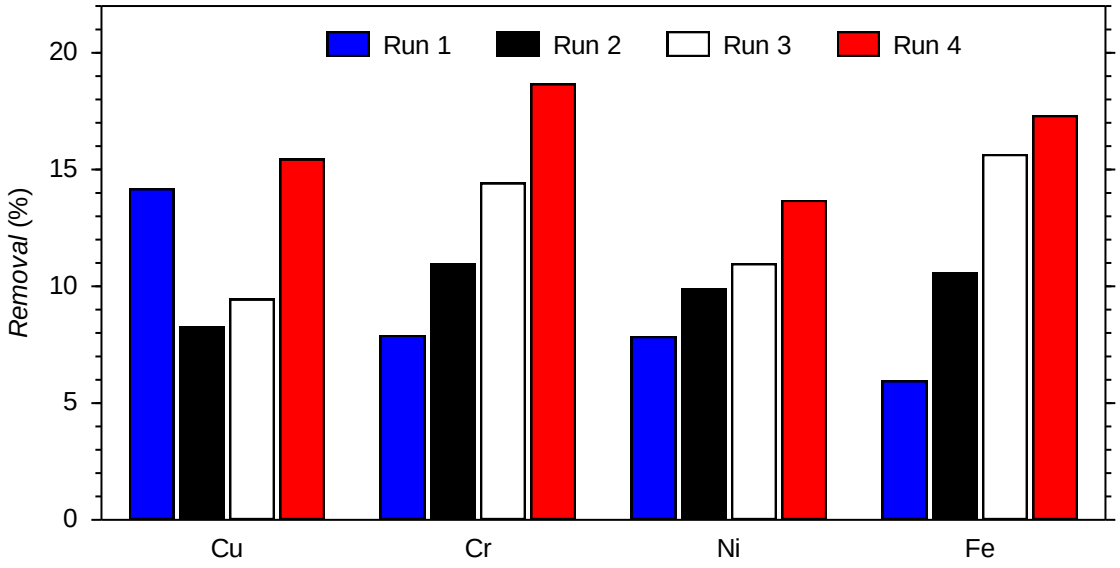

Figure 4.15: Copper, chromium, nickel and iron removal from acidified electroplating wastewater. [Room temperature, Bed mass: 4.0 g, Flow rate: 30 mL.min^{-1}, Initial pH: 1.8, Contact time: 24 h, Initial concentration: Cu 915 mg.L^{-1}; Cr 770 mg.L^{-1}; Ni 5325 mg.L^{-1}; Fe 755 mg.L^{-1}]

Under the conditions that prevailed at an initial pH of 1.8, it can be envisaged that binding of cationic metallic species would be greatly suppressed by competing H^+ ions, which would

protonate the surface functional groups and reduce surface negative charge. However, peak copper, chromium, nickel and iron removal levels noted in run 4 as 15.5%, 18.7%, 13.7% and 17.3%, respectively, were higher than those observed for sorption from raw wastewater indicating a lack of adverse effects of the high initial H^+ concentration on metal removal. This can be explained by consumption of a large quantity of H^+ ions during the hydroxyl groups as summarized in Scheme 3.

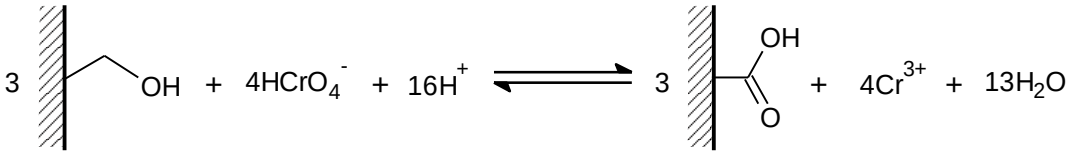

Scheme 3: Overall reaction for secondary hydroxyl oxidation and Cr(VI) reduction.

Most of the H^+ ions in the acidified solution were used in the protonation of $HCrO_4^-$ and $H_2Cr_2O_7^{2-}$ to form chromic and dichromic acid, respectively. Thereafter, as exemplified by reaction I in Scheme 4, chromate esters were formed on both alginate and CFMS surfaces richly endowed with hydroxyl groups.

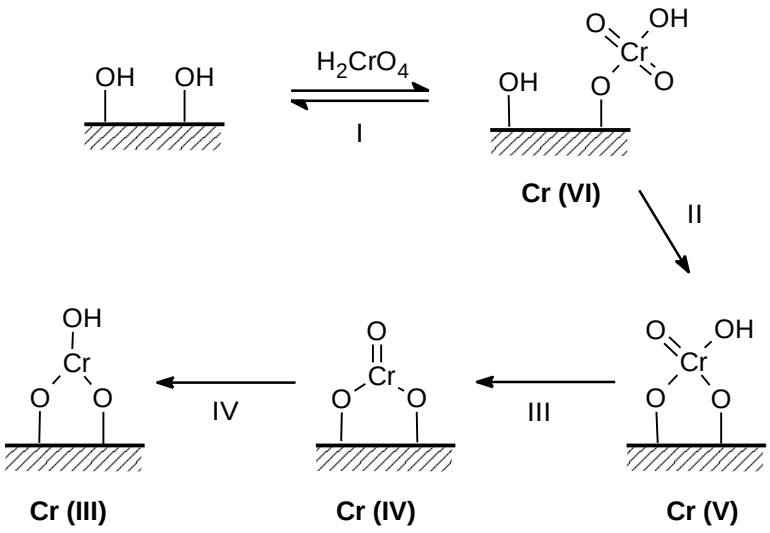

Scheme 4: Chromate ester formation and chromium reduction pathway.

Initial esterification was followed by reduction of Cr(VI) to Cr(V) with subsequent esterification of the product with a vicinal hydroxyl (reaction II). Thereafter, the bound chromium was reduced to the +4 and +3 oxidation states as depicted by reactions III and IV, respectively. Occurring simultaneously with reactions II, III and IV was the oxidation of primary and secondary hydroxyls to carboxyl and keto groups, respectively (Nakano *et al*. 2001; Solomon *et al.* 2014). Higher affinity of carboxyl and ketone groups in comparison to their parent hydroxyl groups therefore accounted for enhanced successive irreversible binding capabilities

of the calcium alginate immobilized CFMS sorbent. Recovery from the acidified wastewater treatment column is presented in Figure 4.16 that follows:

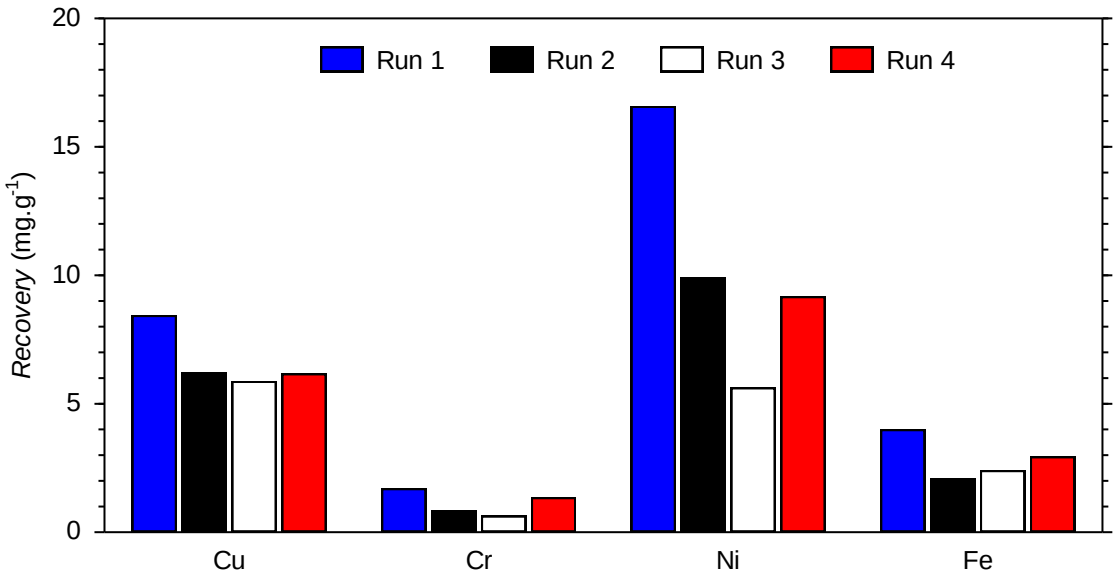

Figure 4.16: Copper, chromium, nickel and iron recovery from the acidified wastewater treatment column.

Progressing from run 1 to run 2 in all instances, the amount of desorbed metal was reduced thereby confirming conversion of reversibly binding hydroxyls to irreversibly binding carboxyl groups. Continued decrease in amount of recovered nickel once again indicated preferential irreversible binding on newly formed carboxyl groups. Comparatively, recovery from the acidified wastewater treatment column was lower than that from the raw wastewater treatment column (see Appendix XI) due to more extensive oxidation in the acidified wastewater treatment batches.

References

Anandkumar, J. & Mandal, B., 2011. Adsorption of chromium(VI) and Rhodamine B by surface modified tannery waste: Kinetic, mechanistic and thermodynamic studies. *J. Hazard. Mater.*, 186(2-3), pp. 1088–1096.

Anirudhan, T.S., Fernandez, N.B. & Mullassery, M.D., 2012. Adsorptive removal of As(III) and As(V) from water and wastewaters using an anion exchanger derived from polymer-grafted banana stem. *Toxicol. Environ. Chem.*, 99(4), pp. 37–41.

Apiratikul, R. & Pavasant, P., 2008. Batch and column studies of biosorption of heavy metals by *Caulerpa lentillifera*. *Bioresour. Technol.*, 99(8), pp. 2766–2777.

Aryal, M. & Ziagova, M., 2011. Comparison of Cr(VI) and As(V) removal in single and binary mixtures with Fe(III)-treated *Staphylococcus xylosus* biomass: Thermodynamic studies. *Chem. Eng. J.*, 169(1-3), pp. 100–106.

Bairagi, H., Khan, M.M.R., Ray, L. & Guha, A.K., 2011. Adsorption profile of lead on *Aspergillus versicolor*: a mechanistic probing. *J. Hazard. Mater.*, 186(1), pp. 756–64.

Baral, S.S., Das, S.N. & Rath, P., 2006. Hexavalent chromium removal from aqueous solution by adsorption on treated sawdust. *Biochem. Eng. J.*, 31(3), pp. 216–222.

Bayramoglu, G., Celik, G., Yalcin, E., Yilmaz, M. & Arica, M.Y., 2005. Modification of surface properties of *Lentinus sajor-caju* mycelia by physical and chemical methods: evaluation of their Cr^{6+} removal efficiencies from aqueous medium. *J. Hazard. Mater.*, 119(1-3), pp. 219–229.

Beyler, C.L. & Hirschler, M.M., 2002. Thermal decomposition of polymers. In P. J. Dinenno et al., eds. *SFPE Handbook of Fire Protection Engineering*. Quincy, Massachusetts: National Fire Protection Association, pp. 110–131.

Blazquez, G., Calero, M., Ronda, A., Tenorio, G. & Martin-Lara, M.A., 2014. Study of kinetics in the biosorption of lead onto native and chemically treated olive stone. *J. Ind. Eng. Chem.*, 20(5), pp. 2754–2760.

Ciolacu, D., Ciolacu, F. & Popa, V.I., 2011. Amorphous cellulose - structure and characterization. *Cellul. Chem. Technol.*, 45(1-2), pp. 13–21.

Chand, P., Shil, A.K., Sharma, M. & Pakade, Y.B., 2014. Improved adsorption of cadmium ions from aqueous solution using chemically modified apple pomace: Mechanism,

kinetics, and thermodynamics. *Int. Biodeterior. Biodegradation*, 90, pp. 8–16.

Cruz-Olivares, J., Perez-Alonso, C., Barrera-Diaz, C., Lopez, G. & Balderas-Hernandez, P., 2010. Inside the removal of lead(II) from aqueous solutions by De-Oiled Allspice Husk in batch and continuous processes. *J. Hazard. Mater.*, 181(1-3), pp. 1095–1101.

Dogan, M., Abak, H. & Alkan, M., 2009. Adsorption of methylene blue onto hazelnut shell: Kinetics, mechanism and activation parameters. *J. Hazard. Mater.*, 164(1), pp. 172–181.

Dong, C., Zhang, H., Pang, Z., Liu, Y. & Zhang, F., 2013. Sulfonated modification of cotton linter and its application as adsorbent for high-efficiency removal of lead(II) in effluent. *Bioresour. Technol.*, 146, pp. 512–518.

Dutta, S., De, S., Saha, B. & Alam, M.I., 2012. Advances in conversion of hemicellulosic biomass to furfural and upgrading to biofuels. *Catal. Sci. Technol.*, 2(10), pp. 2025–2036.

Draman, S.F.S., Daik, R., Latif, F.A. & El-Sheikh, S.M., 2014. Characterization and thermal decomposition kinetics of kapok (*Ceiba pentandra L.*)-based cellulose. *BioResources*, 9(1), pp. 8–23.

El Oudiani, A., Chaabouni, Y., Msahli, S. & Sakli, F., 2012. Mercerization of *Agave americana L*. fibers. *J. Text. Inst.*, 103(5), pp. 565–574.

Fadzil, F., Ibrahim, S. & Hanafiah, M.A.K.M., 2016. Adsorption of lead(II) onto organic acid modified rubber leaf powder: Batch and column studies. *Process Saf. Environ. Prot.*, 100, pp. 1–8.

Feng, N.-C., Guo, X.-Y. & Liang, S., 2010. Enhanced Cu(II) adsorption by orange peel modified with sodium hydroxide. *Trans. Nonferrous Met. Soc. China*, 20, pp. s146–s152.

Flores-Garnica, J.G., Morales-Barrera, L., Pineda-Camacho, G. & Cristiani-Urbina, E., 2013. Biosorption of Ni(II) from aqueous solutions by *Litchi chinensis* seeds. *Bioresour. Technol.*, 136, pp. 635–643.

Gok, C., Gerstmann, U. & Aytas, S., 2013. Biosorption of radiostrontium by alginate beads: Application of isotherm models and thermodynamic studies. *J. Radioanal. Nucl. Chem.*, 295(1), pp. 777–788.

Gusmao, K.A.G., Gurgel, L.V.A., Melo, T.M.S. & Gil, L.F., 2013. Adsorption studies of methylene blue and gentian violet on sugarcane bagasse modified with EDTA dianhydride (EDTAD) in aqueous solutions: Kinetic and equilibrium aspects. *J. Environ.*

Manage., 118, pp. 135–143.

Hajiha, H., Sain, M. & Mei, L.H., 2014. Modification and characterization of hemp and sisal fibers. *J. Nat. Fibers*, 11(2), pp. 144–168.

Hall, K.R., Eagleton, L.C., Acrivos, A. & Vermeulen, T., 1966. Pore- and solid-diffusion kinetics in fixed-bed adsorption under constant-pattern conditions. *Ind. Eng. Chem. Fundam.*, 5(2), pp. 212–223.

Hu, H., Zhang, J., Lu, K. & Tian, Y., 2015. Characterization of *Acidosasa edulis* shoot shell and its biosorption of copper ions from aqueous solution. *J. Environ. Chem. Eng.*, 3(1), pp. 357–364.

Jeffries, T.W., 1994. Biodegradation of lignin and hemicelluloses. In C. Ratledge, ed. *Biochemistry of Microbial Degradation*. Dordrecht, Netherlands: Springer Netherlands, pp. 233–277.

Jiang, G.-B., Lin, Z.-T., Huang, X.-Y., Zheng, Y.-Q., Ren, C.-C., Huang, C.-K. & Huang, Z.-J., 2012. Potential biosorbent based on sugarcane bagasse modified with tetraethylenepentamine for removal of eosin Y. *Int. J. Biol. Macromol.*, 50(3), pp. 707–712.

Karmacharya, M.S., Kumar, V., Tyagi, I., Agarwal, S. & Jha, V.K., 2016. Removal of As(III) and As(V) using rubber tire derived activated carbon modified with alumina composite. *J. Mol. Liq.*, 216, pp. 836–844.

Karnitz, O., Gurgel, L.V.A., De Freitas, R.P. & Gil, L.F., 2009. Adsorption of Cu(II), Cd(II), and Pb(II) from aqueous single metal solutions by mercerized cellulose and mercerized sugarcane bagasse chemically modified with EDTA dianhydride (EDTAD). *Carbohydr. Polym.*, 77(3), pp. 643–650.

Kiran, B. & Kaushik, A., 2008. Chromium binding capacity of *Lyngbya putealis* exopolysaccharides. *Biochem. Eng. J.*, 38(1), pp. 47–54.

Kumari, A.R. & Sobha, K., 2016. Removal of lead by adsorption with the renewable biopolymer composite of feather (*Dromaius novaehollandiae*) and chitosan (*Agaricus bisporus*). *Environ. Technol. Innov.*, 6, pp. 11–26.

Laine, C., 2005. *Structures of hemicelluloses and pectins in wood and pulp*. Doctoral Thesis. Helsinki University of Technology. Espoo, Finland.

Li, H.-Y., Sun, S.-N., Zhou, X., Peng, F. & Sun, R.-C., 2015. Structural characterization of hemicelluloses and topochemical changes in Eucalyptus cell wall during alkali ethanol treatment. *Carbohydr. Polym.*, 123, pp. 17–26.

Limousin, G., Gaudet, J.-P., Charlet, L., Szenknect, S., Barthes, V. & Krimissa, M., 2007. Sorption isotherms: A review on physical bases, modeling and measurement. *Appl. Geochemistry*, 22(2), pp. 249–275.

Lomakin, S.M., Rogovina, S.Z., Grachev, A.V., Prut, E.V. & Alexanyan, C.V., 2011. Thermal degradation of biodegradable blends of polyethylene with cellulose and ethylcellulose. *Thermochim. Acta*, 521(1-2), pp. 66–73.

Martinez, M., Miralles, N., Hidalgo, S., Fiol, N., Villaescusa, I. & Poch, J., 2006. Removal of lead(II) and cadmium(II) from aqueous solutions using grape stalk waste. *J. Hazard. Mater.*, 133(1-3), pp. 203–211.

Medronho, B., Andrade, R., Vivod, V., Ostlund, A., Miguel, M.G., Lindman, B., Voncina, B. & Valente, A.J.M., 2013. Cyclodextrin-grafted cellulose: Physico-chemical characterization. *Carbohydr. Polym.*, 93(1), pp. 324–330.

Milonjic, S., 2007. A consideration of the correct calculation of thermodynamic parameters of adsorption. *J. Serbian Chem. Soc.*, 72(12), pp. 1363–1367.

Mohan, D., Singh, K.P. & Singh, V.K., 2006. Trivalent chromium removal from wastewater using low cost activated carbon derived from agricultural waste material and activated carbon fabric cloth. *J. Hazard. Mater.*, 135(1-3), pp. 280–295.

Moriana, R., Vilaplana, F., Karlsson, S. & Ribes, A., 2014. Correlation of chemical, structural and thermal properties of natural fibres for their sustainable exploitation. *Carbohydr. Polym.*, 112, pp. 422–431.

Morton, J.D., Semrau, J.D. & Hayes, K.F., 2001. An X-ray absorption spectroscopy study of the structure and reversibility of copper adsorbed to montmorillonite clay. *Geochim. Cosmochim. Acta*, 65(16), pp. 2709–2722.

Nakano, Y., Takeshita, K. & Tsutsumi, T., 2001. Adsorption mechanism of hexavalent chromium by redox within condensed-tannin gel. *Water Res.*, 35(2), pp. 496–500.

Ofomaja, A.E. & Naidoo, E.B., 2011. Biosorption of copper from aqueous solution by chemically activated pine cone: A kinetic study. *Chem. Eng. J.*, 175, pp. 260–270.

Ofomaja, A.E., Naidoo, E.B. & Modise, S.J., 2010. Kinetic and pseudo-second-order modeling of lead biosorption onto pine cone powder. *Ind. Eng. Chem. Res.*, 49(6), pp. 2562–2572.

Olu-Owolabi, B.I., Oputu, O.U., Adebowale, K.O., Ogonsolu, O. & Olujimi, O.O., 2012. Biosorption of Cd^{2+} and Pb^{2+} ions onto mango stone and cocoa pod waste: Kinetic and equilibrium studies. *Sci. Res. Essays*, 7(15), pp. 1614–1629.

Pereira, F. V, Gurgel, L.V.A. & Gil, L.F., 2010. Removal of Zn^{2+} from aqueous single metal solutions and electroplating wastewater with wood sawdust and sugarcane bagasse modified with EDTA dianhydride (EDTAD). *J. Hazard. Mater.*, 176(1-3), pp. 856–863.

Plazinski, W., Rudzinski, W. & Plazinska, A., 2009. Theoretical models of sorption kinetics including a surface reaction mechanism: A review. *Adv. Colloid Interface Sci.*, 152(1-2), pp. 2–13.

Reddy, K.O., Reddy, K.R.N., Zhang, J., Zhang, J. & Rajulu, A. V, 2013. Effect of alkali treatment on the properties of century fiber. *J. Nat. Fibers*, 10(3), pp. 282–296.

Rout, P.R., Bhunia, P. & Dash, R.R., 2014. Modeling isotherms, kinetics and understanding the mechanism of phosphate adsorption onto a solid waste: Ground burnt patties. *J. Environ. Chem. Eng.*, 2(3), pp. 1331–1342.

Roy, A., Chakraborty, S., Kundu, S.P., Majumder, S.B. & Adhikari, B., 2013. Surface grafting of *Corchorus olitorius* fibre: A green approach for the development of activated bioadsorbent. *Carbohydr. Polym.*, 92(2), pp. 2118–2127.

Saeid, A., Chojnacka, K. & Balkowski, G., 2012. Two-phase exponential model for describing kinetics of biosorption of Cr(III) ions by microalgae *Spirulina maxima*. *Chem. Eng. J.*, 197, pp. 49–55.

Saha, R. & Saha, B., 2014. Removal of hexavalent chromium from contaminated water by adsorption using mango leaves (*Mangifera indica*). *Desalin. Water Treat.*, 52(10-12), pp. 1928–1936.

Salvado, A.P.A., Campanholi, L.B., Fonseca, J.M., Tarley, C.R.T., Caetano, J. & Dragunski, D.C., 2012. Lead(II) adsorption by peach palm waste. *Desalin. Water Treat.*, 48(1-3), pp. 335–343.

Sebe, G., Ham-Pichavant, F., Ibarboure, E., Koffi, A.L.C. & Tingaut, P., 2012. Supramolecular structure characterization of cellulose II nanowhiskers produced by acid hydrolysis of cellulose I substrates. *Biomacromolecules*, 13(2), pp. 570–578.

Singha, A.S. & Guleria, A., 2014. Chemical modification of cellulosic biopolymer and its use in removal of heavy metal ions from wastewater. *Int. J. Biol. Macromol.*, 67, pp. 409–417.

Solomon, G.T.W., Fryhle, C.B. & Snyder, S.A., 2014. *Organic chemistry*, Eleventh edition, Hoboken, New Jersey: John Wiley & Sons.

Srivastava, S., Agrawal, S.B. & Mondal, M.K., 2015. Biosorption isotherms and kinetics on removal of Cr(VI) using native and chemically modified *Lagerstroemia speciosa* bark. *Ecol. Eng.*, 85, pp. 56–66.

Sun, Z., Liu, Y., Huang, Y., Tan, X., Zeng, G., Hu, X. & Yang, Z., 2014. Fast adsorption of Cd^{2+} and Pb^{2+} by EGTA dianhydride (EGTAD) modified ramie fiber. *J. Colloid Interface Sci.*, 434, pp. 152–158.

Tan, G., Yuan, H., Liu, Y. & Xiao, D., 2010. Removal of lead from aqueous solution with native and chemically modified corncobs. *J. Hazard. Mater.*, 174(1-3), pp. 740–745.

Won, S.W., Kim, S., Kotte, P., Lim, A. & Yun, Y.-S., 2013. Cationic polymer-immobilized polysulfone-based fibers as high performance sorbents for Pt(IV) recovery from acidic solutions. *J. Hazard. Mater.*, 263, pp. 391–397.

Xu, M., Zhang, Y., Zhang, Z., Shen, Y., Zhao, M. & Pan, G., 2011. Study on the adsorption of Ca^{2+}, Cd^{2+} and Pb^{2+} by magnetic Fe_3O_4 yeast treated with EDTA dianhydride. *Chem. Eng. J.*, 168(2), pp. 737–745.

Xuan, Z., Tang, Y., Li, X., Liu, Y. & Luo, F., 2006. Study on the equilibrium, kinetics and isotherm of biosorption of lead ions onto pretreated chemically modified orange peel. *Biochem. Eng. J.*, 31(2), pp. 160–164.

Yang, L., Li, Y., Jin, X., Ye, Z., Ma, X., Wang, L. & Liu, Y., 2011. Synthesis and characterization of a series of chelating resins containing amino/imino-carboxyl groups and their adsorption behavior for lead in aqueous phase. *Chem. Eng. J.*, 168, pp. 115–124.

Yu, J., Tong, M., Sun, X. & Li, B., 2008. Enhanced and selective adsorption of Pb^{2+} and Cu^{2+} by EDTAD-modified biomass of baker's yeast. *Bioresour. Technol.*, 99(7), pp. 2588–2593.

Zhang, Y., Liu, W., Zhang, L., Wang, M. & Zhao, M., 2011. Application of bifunctional Saccharomyces cerevisiae to remove lead(II) and cadmium(II) in aqueous solution. *Appl. Surf. Sci.*, 257(23), pp. 9809–9816.

Zhou, J.L. & Kiff, R.J., 1991. The uptake of copper from aqueous solution by immobilized fungal biomass. *J. Chem. Technol. Biotechnol.*, 52(3), pp. 317–330.

Zhu, B., Fan, T. & Zhang, D., 2008. Adsorption of copper ions from aqueous solution by citric acid modified soybean straw. *J. Hazard. Mater.*, 153(1–2), pp. 300–308.

CHAPTER 5

CONCLUSIONS AND RECOMMENDATIONS

5.1 Conclusions

In this work, carboxyl functionalized mango seed shell biomass (CFMS) was prepared by an esterification reaction with dehydrated EDTA salt. En route to CFMS synthesis raw mango seed shells were initially treated with alkali solution to produce alkali treated mango seed shell biomass (ATMS). The chemically modified mango seed shell biomaterials were initially tested for removal of lead(II) ions from synthetic aqueous solutions. CFMS was immobilized in calcium alginate and the granular sorbents were tested for nickel, chromium and nickel removal from electroplating wastewater. The following are major conclusions drawn from the work:

(i) Based on XRD, both alkali treatment and carboxyl functionalization showed significant reduction in cellulose crystallinity through disruption of hydrogen bonding.

(ii) FTIR demonstrated removal of hemicelluloses through alkali treatment and, together with elemental analysis confirmed inclusion of EDTA groups on the CFMS surfaces. Additionally, FTIR spectral band shifting and signal alteration confirmed participation of carboxyl, ester and amine functions in lead(II) ion binding.

(iii) Kinetic studies revealed that sorption of lead(II) ions by ATMS was rapid and equilibrium was established within 1 h of contact. For CFMS, equilibrium was established after 3 h and consequently the approach the equilibrium was less rapid.

(iv) The kinetics of lead(II) ion sorption were best simulated by the pseudo-n^{th} order reaction kinetic model and the double exponential diffusion model. Multi-linearity of intra-particle diffusion model plots showed that sorption rates were controlled by both film and intra-particle diffusion.

(v) Sorption of lead(II) ions by both ATMS and CFMS were represented by the Langmuir model better than the Freundlich model. Application of the three-parameter Redlich-Peterson, Sips and Toth models revealed their approximation to the Langmuir model. Maximum sorption capacities of ATMS and CFMS were 59.25 $mg.g^{-1}$ and 306.33 $mg.g^{-1}$, respectively.

(vi) Sorption from acidified electroplating wastewater resulted in oxidation of hydroxyl to carboxyl groups. This enhanced removal efficiency and lowered recovery efficiency in subsequent sorption-desorption experiments.

5.2 Recommendations for further work

More conclusive research is required prior to proposal of the immobilized sorbents for use in wastewater treatment. Accordingly, for additional work, it is recommended to:

(i) Test the granular sorbents on more dilute solutions such as water from supernatants obtained from precipitation steps in electroplating wastewater treatment as opposed the concentrated spent electrolyte used in this study;

(ii) Analyze the influence of additional operating conditions such as agitation, ionic strength, sorbent dose, sorbent particle size and temperature on equilibrium and kinetic aspects of sorbent performance;

(iii) Characterize the granular sorbent before and after chromium uptake using X-ray photoelectron spectroscopy to ascertain the oxidation state of bound chromium and thus confirm occurrence of Cr(VI) reduction to Cr(III);

(iv) Design and carry out column sorption experiments that allow application of kinetic models for breakthrough curve analysis;

(v) Study sorption of individual metal solutions to facilitate comparison of the biosorbents' performance with other biomass documented in the literature as well as two allow speciation; and

(vi) Replicate the sorption experiments in order to assess reproducibility.

APPENDICIES

List of appendices

Appendix I: Effect of lead(II) ion loading on FTIR spectra ATMS.

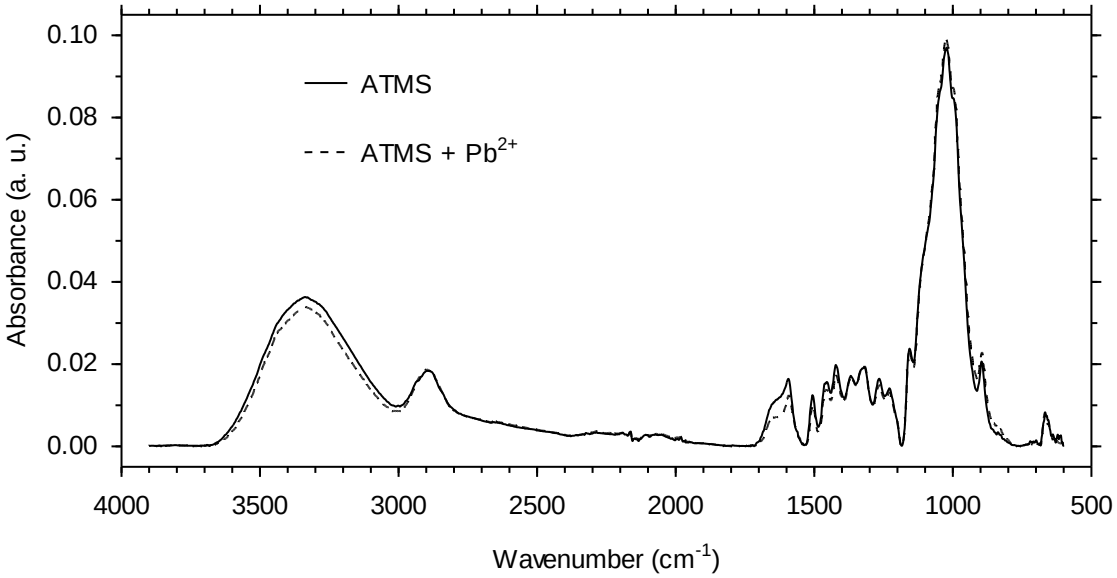

Appendix II: Effect of contact time on lead(II) ion sorption by ATMS and CFMS.

[Room temperature, pH: 5.2, ATMS dose: 1 g.L^{-1}, CFMS dose: 0.5 g.L^{-1}]

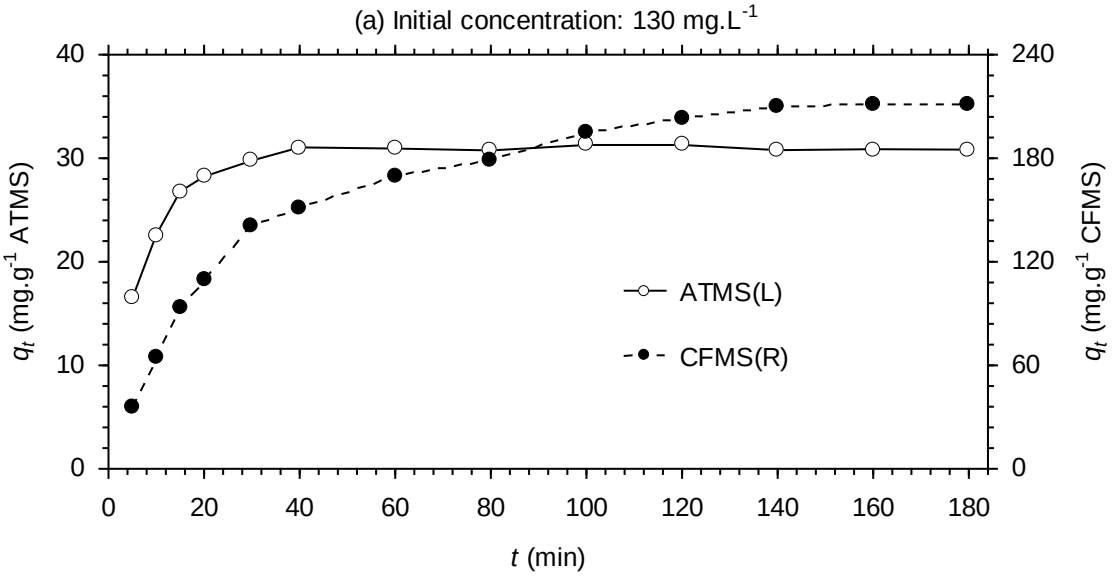

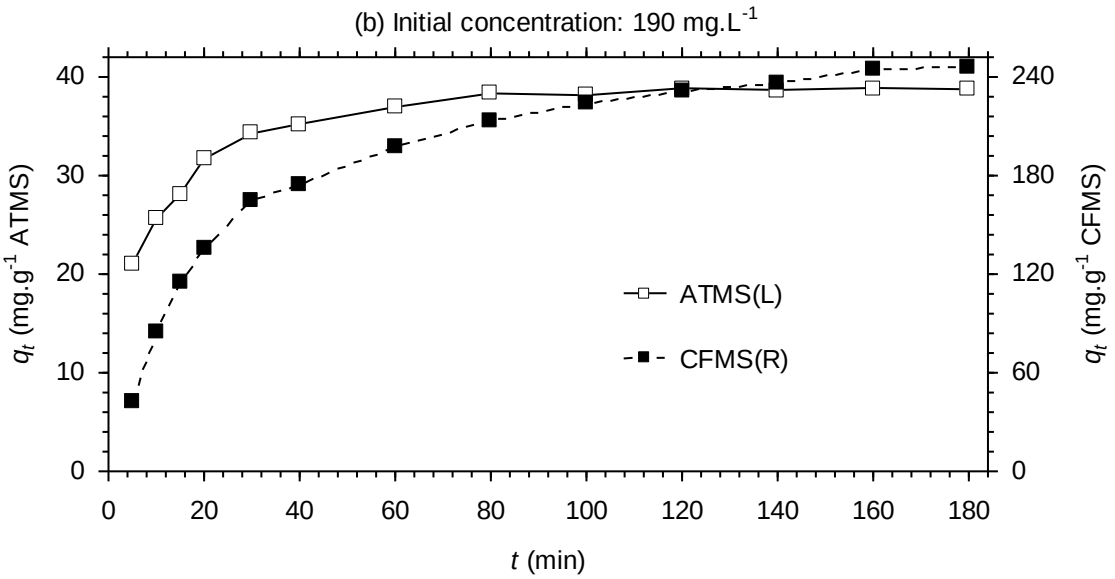

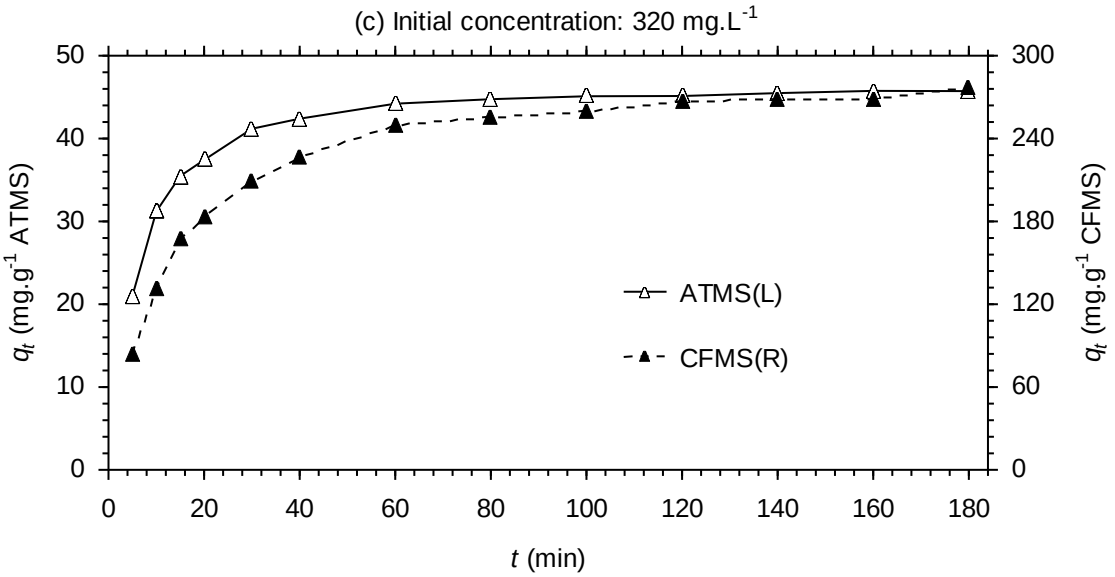

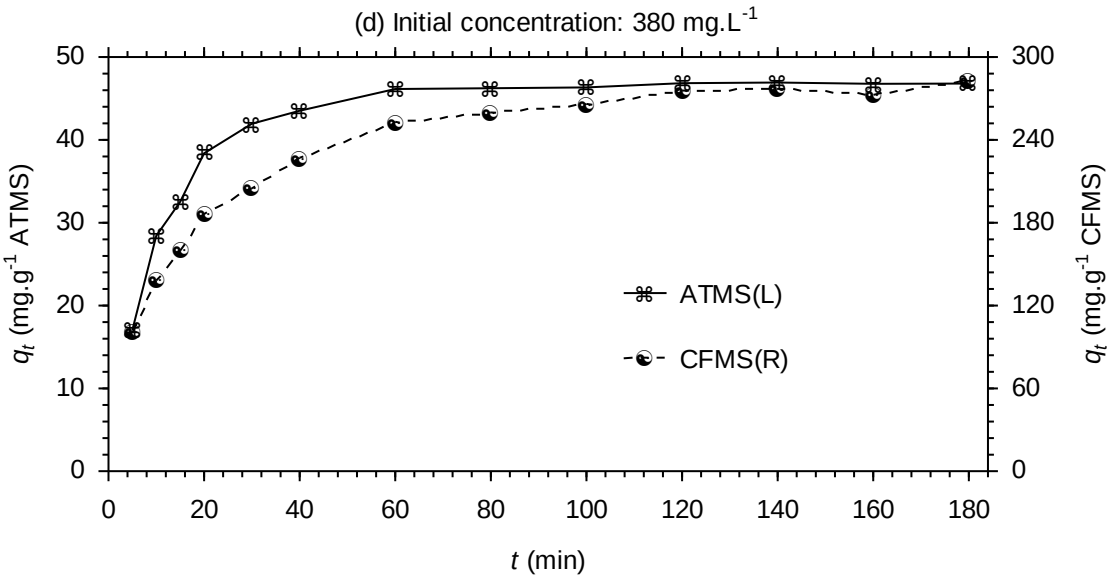
(d) Initial concentration: 380 mg.L-1
qt (mg.g-1 ATMS)
qt (mg.g-1 CFMS)
t (min)
ATMS(L)
CFMS(R)
0
10
20
30
40
50
60
120
180
240
300
0
20
40
60
80
100
120
140
160
180

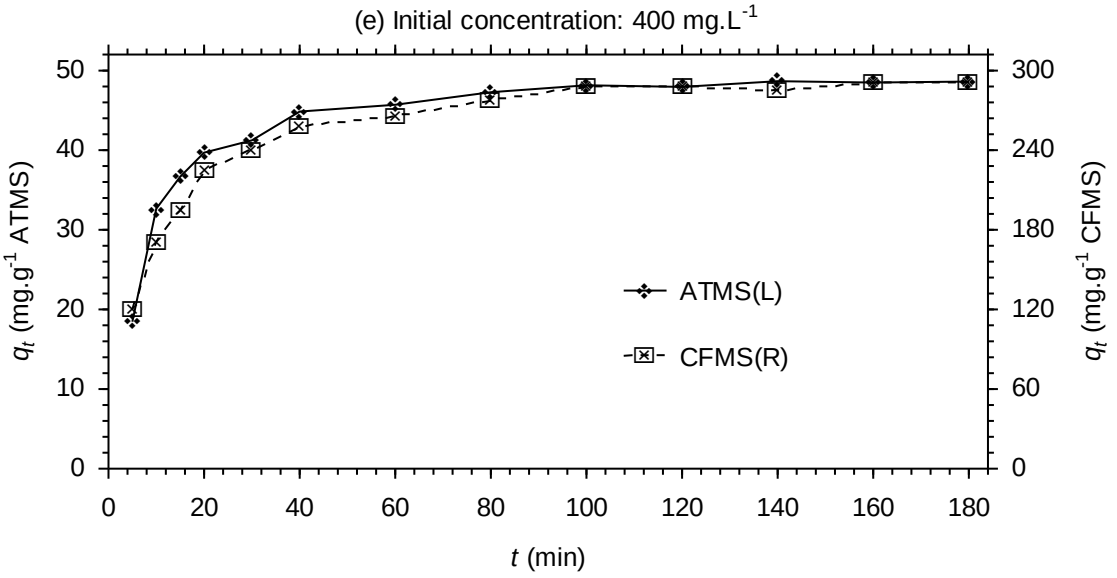
(e) Initial concentration: 400 mg.L-1
qt (mg.g-1 ATMS)
qt (mg.g-1 CFMS)
t (min)
ATMS(L)
CFMS(R)
0
10
20
30
40
50
60
120
180
240
300
0
20
40
60
80
100
120
140
160
180

Appendix III: Reaction model parameters for sorption of lead(II) ions by ATMS and CFMS.

	ATMS						CFMS					
C_i (mg.L^{-1})	130	190	250	320	380	400	130	190	250	320	380	400
Pseudo first order												
$q_{e,expt}$ (mg.g^{-1})	30.56	37.24	42.42	43.43	47.12	46.99	215.74	262.48	273.63	296.97	290.00	299.83
q_e (mg.g^{-1})	30.80	37.28	41.70	44.45	46.28	47.21	203.60	232.65	241.74	261.48	264.80	278.63
k_1 (min^{-1})	0.142	0.129	0.128	0.116	0.089	0.102	0.038	0.042	0.046	0.066	0.070	0.093
χ^2	0.122	1.888	1.058	0.599	0.235	0.819	3.618	5.597	3.402	6.177	16.207	8.976
R^2	0.9876	0.8700	0.9298	0.9654	0.9917	0.9635	0.9847	0.9792	0.9868	0.9723	0.9358	0.9459
ARE (%)	1.50	5.88	4.22	3.06	1.75	3.21	3.63	4.40	3.25	4.25	6.65	4.90
Pseudo second order												
$q_{e,expt}$ (mg.g^{-1})	30.56	37.24	42.42	43.43	47.12	46.99	215.74	262.48	273.63	296.97	290.00	299.83
q_e (mg.g^{-1})	32.72	40.01	44.74	47.90	50.73	51.37	245.15	276.12	283.43	293.96	295.84	304.89
k_2 (10^{-3} g.mg^{-1}.min^{-1})	7.258	4.875	4.366	3.650	2.428	2.827	0.160	0.162	0.179	0.281	0.299	0.420
χ^2	0.441	0.231	0.059	0.182	0.772	0.809	1.579	2.221	2.635	0.420	2.418	0.573
R^2	0.9496	0.9852	0.9959	0.9913	0.9748	0.9758	**0.9958**	**0.9961**	0.9937	0.9981	0.9912	**0.9962**
ARE (%)	3.13	1.65	0.86	1.66	3.49	3.19	2.79	**3.00**	3.45	0.98	2.45	**1.07**
Pseudo-n^{th} order												
$q_{e,expt}$ (mg.g^{-1})	30.56	37.24	42.42	43.43	47.12	46.99	215.74	262.48	273.63	296.97	290.00	299.83
q_e (mg.g^{-1})	31.07	42.29	44.28	45.93	46.84	48.37	225.04	259.77	255.38	282.07	318.59	296.96
k_{nth} [10^{-3} min^{-1}(mg.g^{-1})$^{1-n}$]	73.787	0.705	6.412	18.281	42.254	26.029	1.651	0.977	4.858	1.369	0.016	1.325
n	1.23	2.54	1.89	1.55	1.22	1.39	1.59	1.69	1.42	1.72	2.50	1.80
χ^2	0.042	0.158	0.054	0.039	0.106	0.477	1.287	2.028	1.535	0.347	1.485	0.731
R^2	**0.9951**	**0.9884**	**0.9963**	**0.9981**	**0.9967**	**0.9839**	0.9958	0.9956	**0.9956**	**0.9983**	**0.9940**	0.9953
ARE (%)	**0.93**	**1.65**	**0.82**	**0.65**	**1.11**	**2.35**	**2.41**	3.10	**2.26**	**0.94**	**1.88**	1.30
Elovich												
α (mg.g^{-1}.min^{-1})	302.48	88.63	111.82	82.63	28.07	46.61	14.04	19.22	23.96	59.10	67.76	174.09
β (g.mg^{-1})	0.289	0.195	0.178	0.158	0.125	0.134	0.017	0.015	0.016	0.018	0.018	0.021
χ^2	2.433	0.885	1.561	2.544	4.441	3.884	7.847	9.735	13.836	10.947	5.062	10.528
R^2	0.7327	0.9294	0.8961	0.8666	0.8499	0.8611	0.9779	0.9778	0.9604	0.9534	0.9731	0.9342
ARE (%)	7.16	4.01	5.17	6.28	8.42	7.80	6.43	6.95	8.12	6.15	3.73	5.12

Lowest ARE and highest R^2 values per column are in bold.

Appendix IV: Pseudo-first order, pseudo-second order, pseudo-nth order and Elovich model plots for sorption of lead(II) ions by ATMS. [Room temperature, pH: 5.2, Sorbent dose: 1 g.L^{-1}]

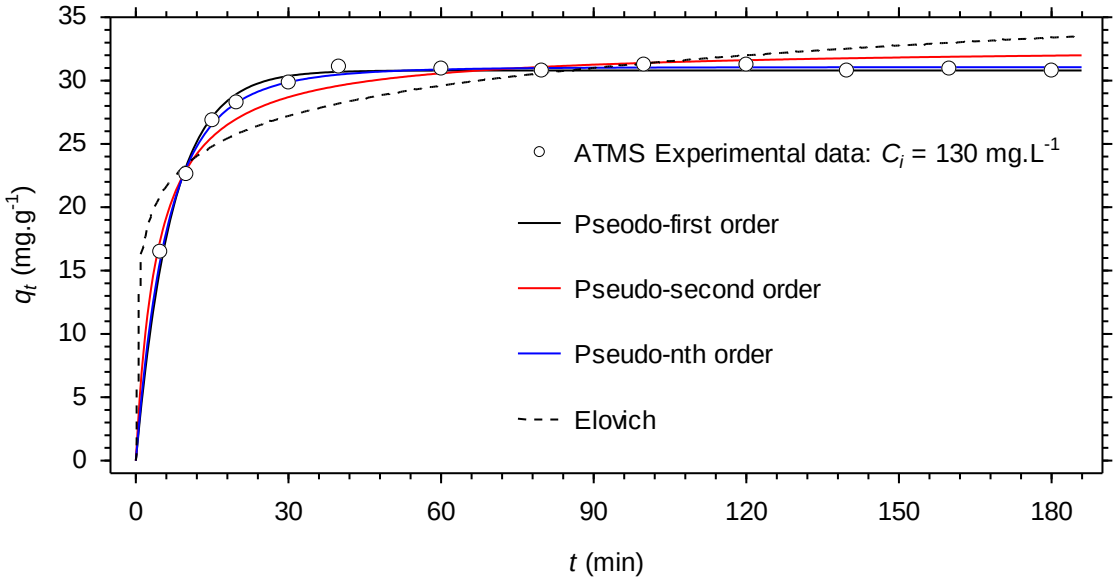

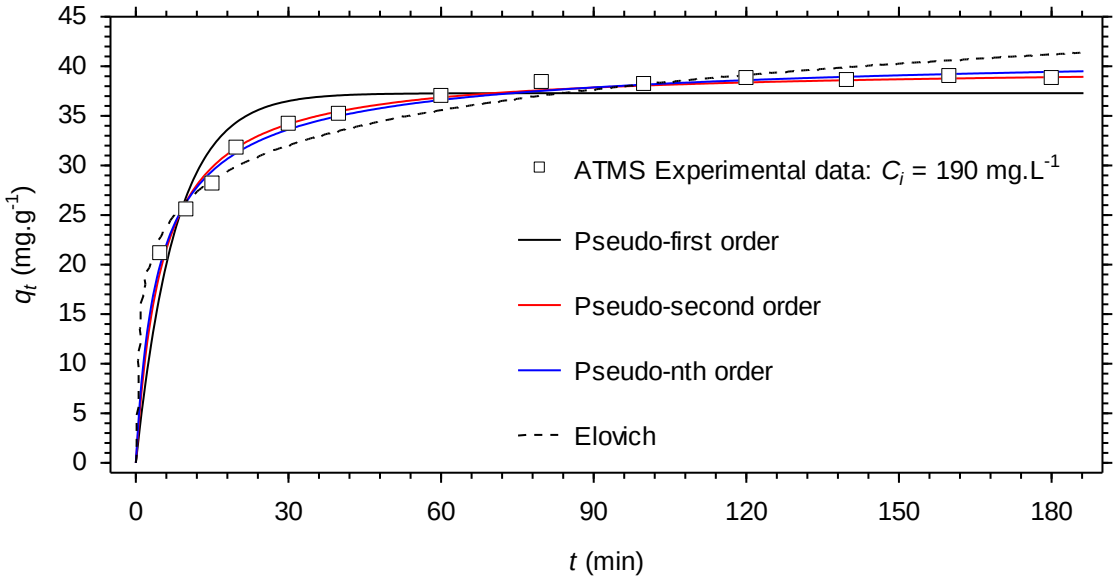

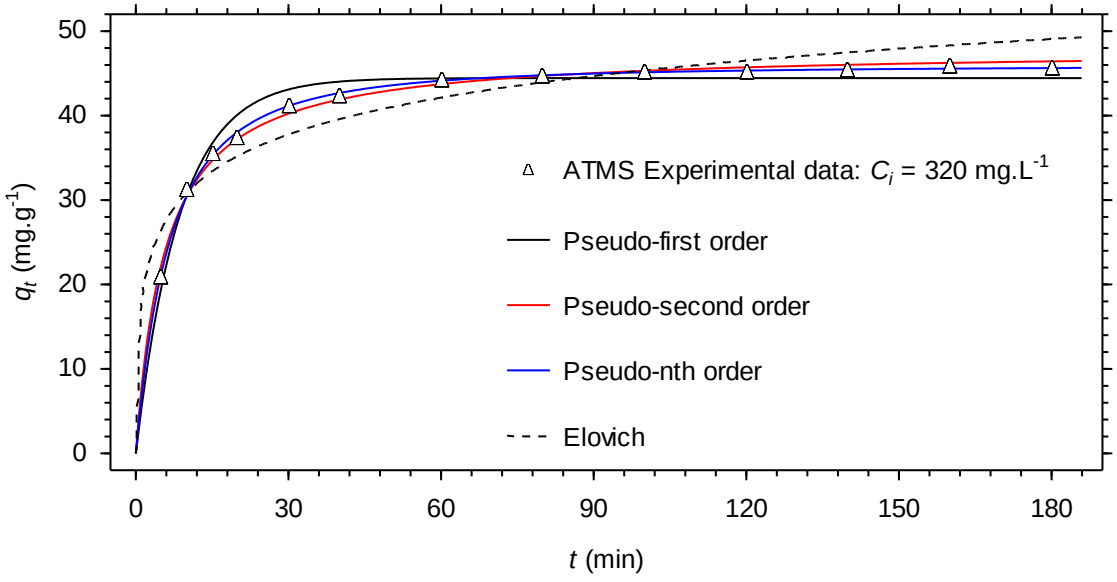

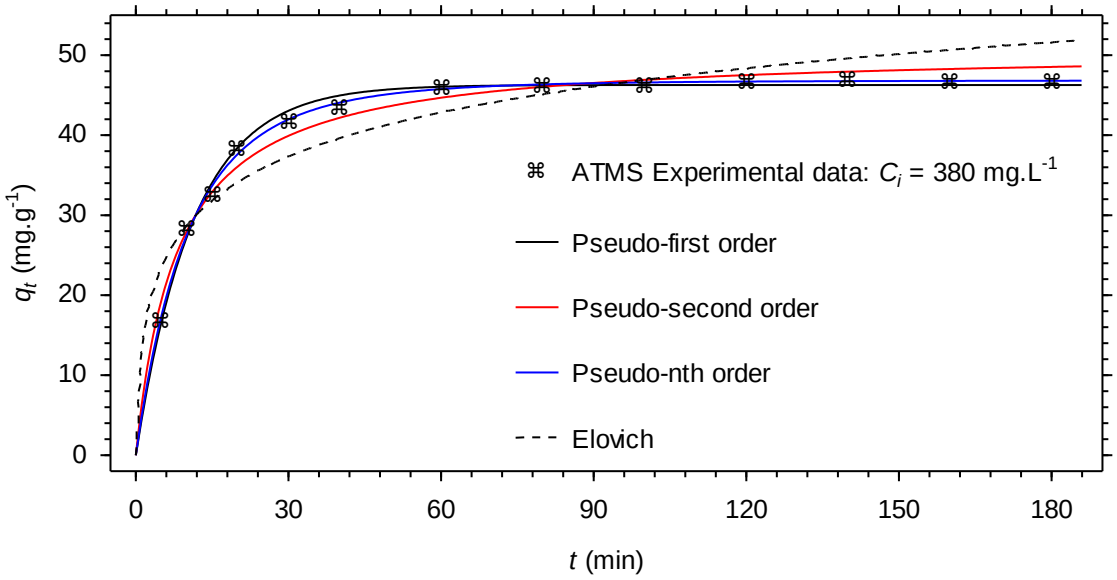
50
40
30
20
10
0
q_t (mg.g^{-1})
0
30
60
90
120
150
180
t (min)
ATMS Experimental data: C_i = 380 mg.L^{-1}
Pseudo-first order
Pseudo-second order
Pseudo-nth order
Elovich

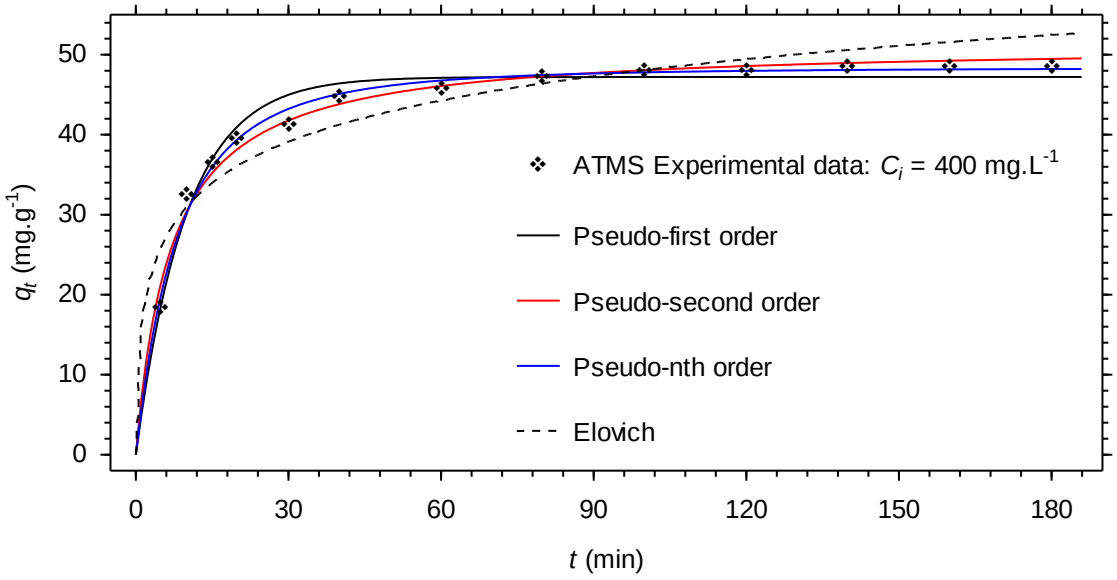
50
40
30
20
10
0
q_t (mg.g^{-1})
0
30
60
90
120
150
180
t (min)
ATMS Experimental data: C_i = 400 mg.L^{-1}
Pseudo-first order
Pseudo-second order
Pseudo-nth order
Elovich

Appendix V: Pseudo-first order, pseudo-second order, pseudo-nth order and Elovich model plots for sorption of lead(II) ions by CFMS. [Room temperature, pH: 5.2, Sorbent dose: 0.5 g.L^{-1}]

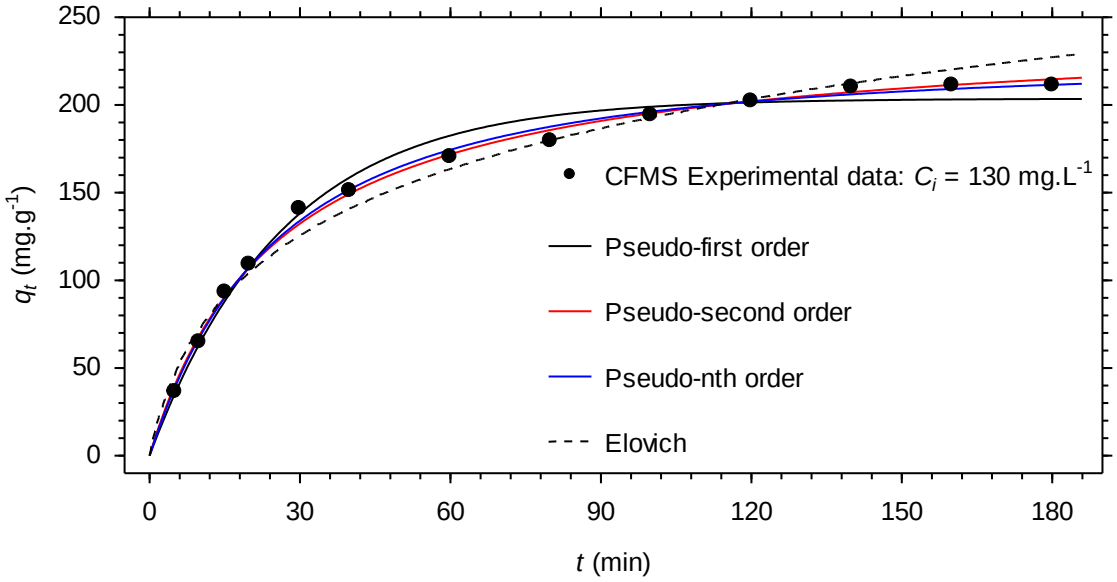

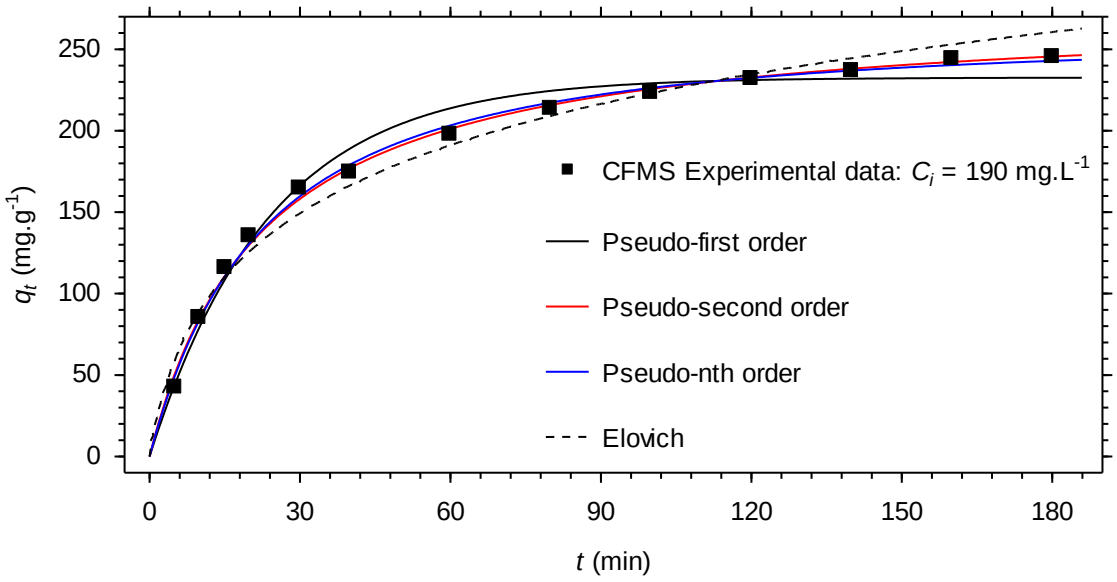

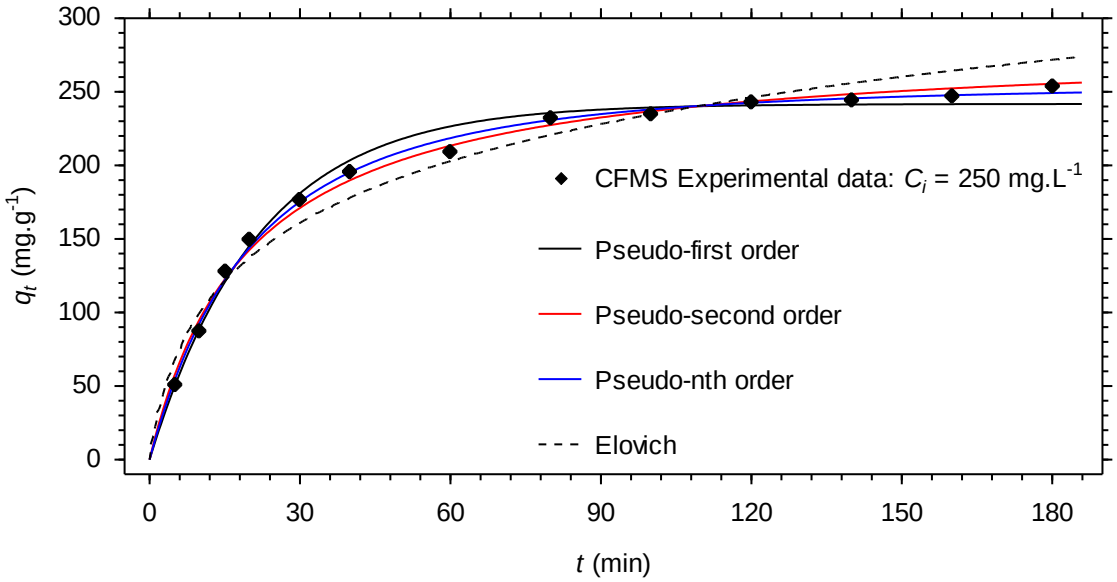

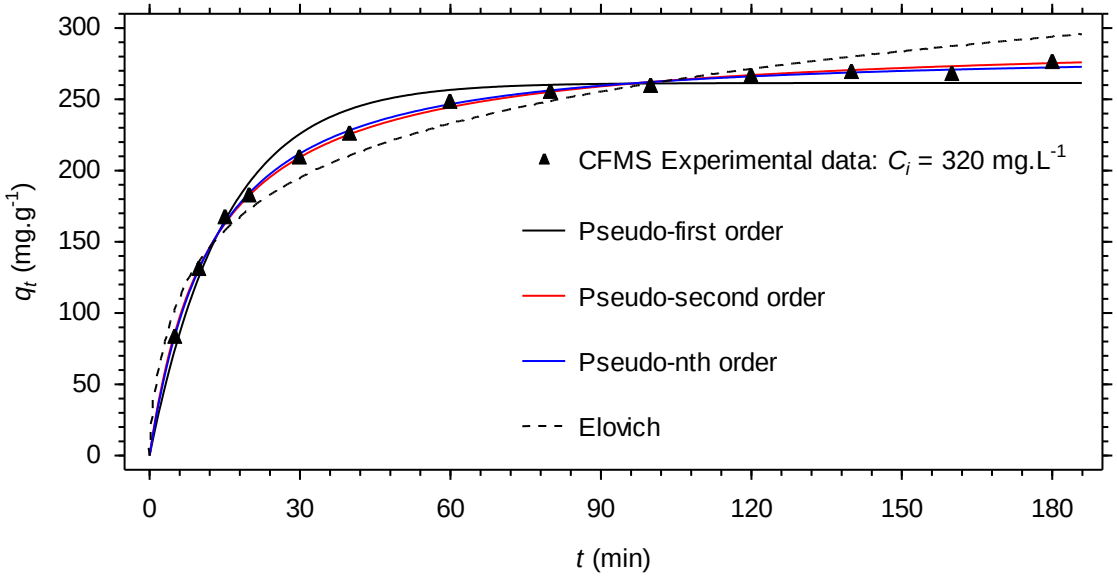
300
250
200
150
100
50
0
q_t (mg.g^{-1})
0
30
60
90
120
150
180
t (min)
CFMS Experimental data: C_i = 320 mg.L^{-1}
Pseudo-first order
Pseudo-second order
Pseudo-nth order
Elovich

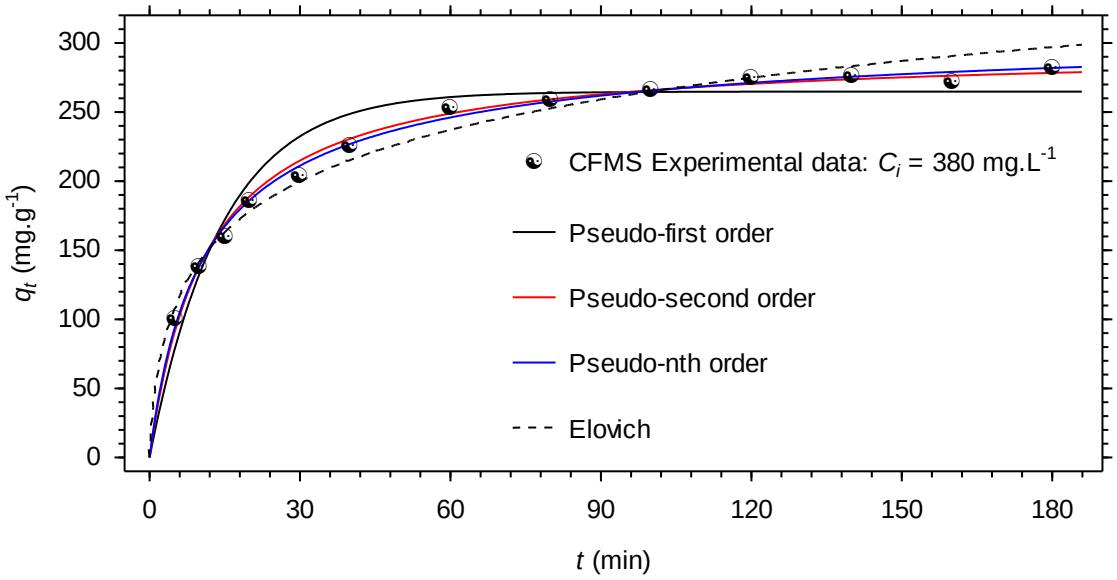
300
250
200
150
100
50
0
q_t (mg.g^{-1})
0
30
60
90
120
150
180
t (min)
CFMS Experimental data: C_i = 380 mg.L^{-1}
Pseudo-first order
Pseudo-second order
Pseudo-nth order
Elovich

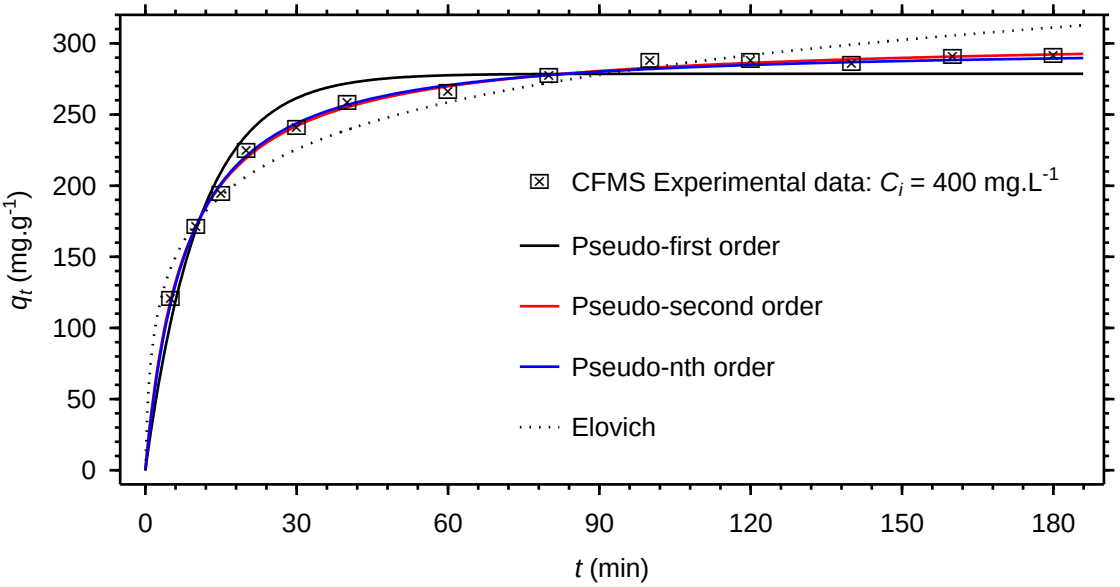
300
250
200
150
100
50
0
q_t (mg.g^{-1})
0
30
60
90
120
150
180
t (min)
CFMS Experimental data: C_i = 400 mg.L^{-1}
Pseudo-first order
Pseudo-second order
Pseudo-nth order
Elovich

Appendix VI: Diffusion model parameters for sorption of lead(II) ions by ATMS and CFMS.

	ATMS						CFMS					
C_i (mg.L^{-1})	130	190	250	320	380	400	130	190	250	320	380	400
Bangham												
K_B (L.g^{-1})	0.114	0.077	0.068	0.054	0.039	0.041	0.111	0.129	0.132	0.177	0.160	0.215
α	0.131	0.166	0.158	0.163	0.200	0.181	0.639	0.503	0.432	0.317	0.302	0.236
χ^2	2.835	1.359	2.202	3.485	6.362	5.293	9.297	18.064	26.169	20.780	11.868	17.172
R^2	0.6916	0.8960	0.8567	0.8202	0.7921	0.8099	0.9746	0.9583	0.9282	0.9167	0.9437	0.8976
ARE (%)	7.71	4.98	6.12	7.15	10.14	8.88	7.41	9.78	11.47	8.50	5.91	6.64
Intra-particle diffusion												
k_{id} (mg.g^{-1}.min$^{-0.5}$)	0.858	1.436	1.527	1.683	2.110	1.984	16.279	17.815	17.715	15.728	15.920	13.404
c (mg.g^{-1})	22.09	23.14	26.54	27.51	24.58	27.06	26.74	40.87	52.98	98.32	100.74	142.89
χ^2	4.265	2.905	4.068	5.822	9.809	8.133	33.332	39.694	48.842	41.468	28.168	34.530
R^2	0.5258	0.7797	0.7293	0.6890	0.6688	0.6897	0.9008	0.8954	0.8573	0.8282	0.8684	0.7899
ARE (%)	9.50	7.29	8.30	9.43	13.03	11.21	14.44	15.22	16.00	12.20	9.29	9.61
Double exponential												
$q_{e,expt}$ (mg.g^{-1})	30.56	37.24	42.42	43.43	47.12	46.99	215.74	262.48	273.63	296.97	290.00	299.83
q_e (mg.g^{-1})	30.99	39.00	43.25	45.47	46.47	48.58	231.67	260.12	264.74	274.34	279.97	292.89
D_1 (mg.L^{-1})	20.29	18.20	24.69	38.52	43.31	71.74	67.29	76.48	90.67	75.11	76.46	84.00
K_{D1} (min^{-1})	0.125	0.076	0.146	0.285	0.081	0.317	0.066	0.097	0.070	0.114	0.027	0.110
D_2 (mg.L^{-1})	5.79	6.21	10.78	19.18	0.34	18.27	52.26	65.99	45.87	59.44	40.26	42.32
K_{D2} (min^{-1})	0.091	0.023	0.029	0.046	0.263	0.034	0.010	0.013	0.011	0.024	0.114	0.022
χ^2	0.027	0.043	0.043	0.016	0.169	0.053	0.634	0.162	0.920	0.336	0.524	0.500
R^2	**0.9966**	**0.9966**	**0.9970**	**0.9990**	**0.9970**	**0.9975**	**0.9978**	**0.9994**	**0.9975**	**0.9983**	**0.9973**	**0.9966**
ARE (%)	**0.74**	**0.79**	**0.73**	**0.43**	**1.51**	**0.72**	**1.64**	**0.60**	**1.72**	**0.89**	**1.16**	**1.00**

Lowest ARE and highest R^2 values per column are in bold.

Appendix VII: Bangham's, double exponential and intra-particle diffusion model simulation plots for sorption of lead(II) ions by ATMS. [Room temperature, pH: 5.2, Sorbent dose: 1 g.L^{-1}]

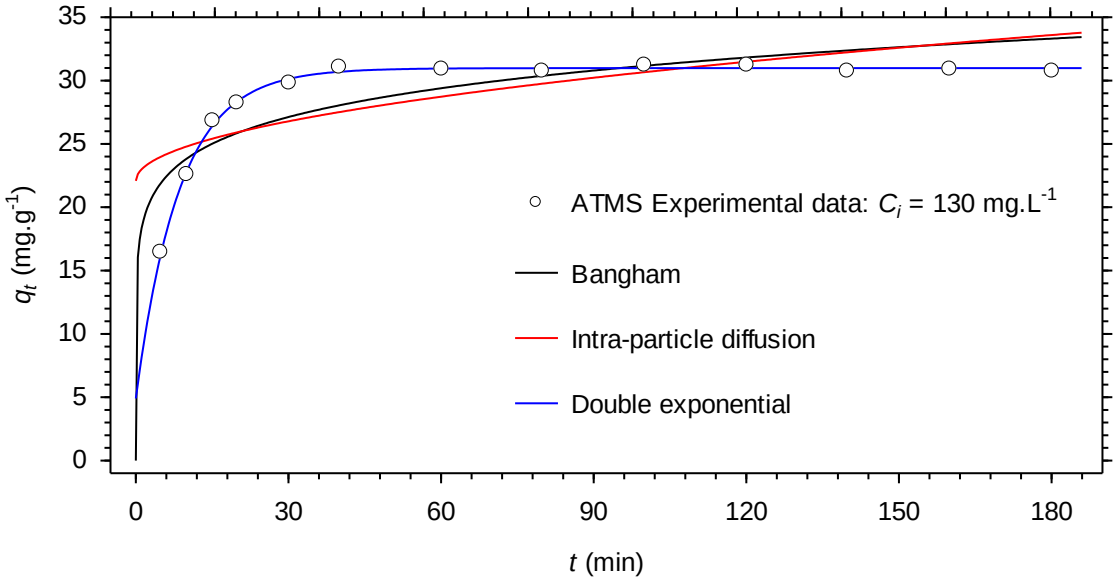

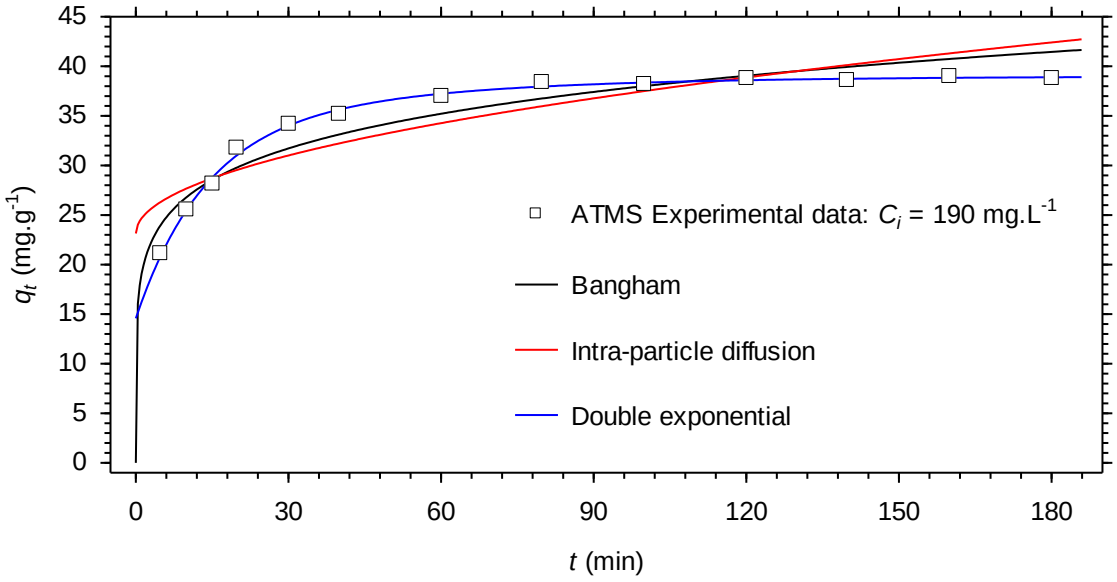

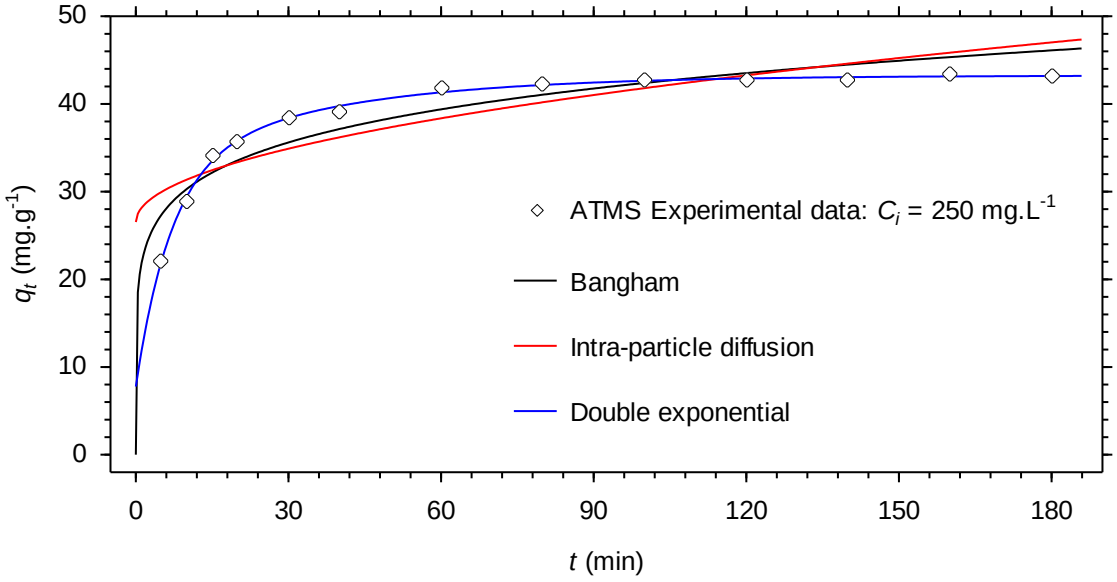

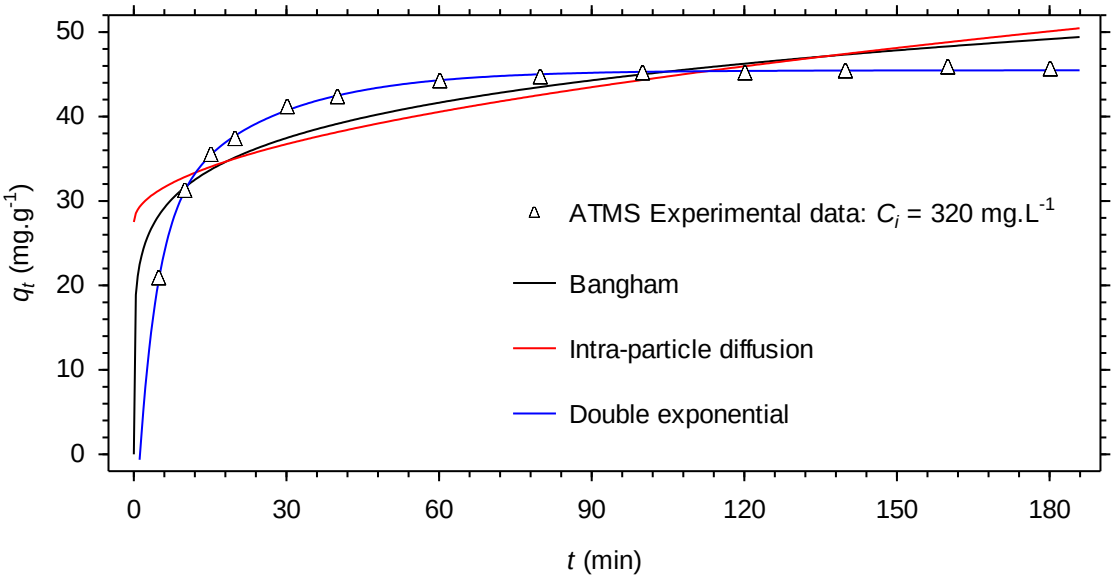
ATMS Experimental data: C_i = 320 mg.L^{-1}
Bangham
Intra-particle diffusion
Double exponential
q_t (mg.g^{-1})
t (min)
0
10
20
30
40
50
0
30
60
90
120
150
180

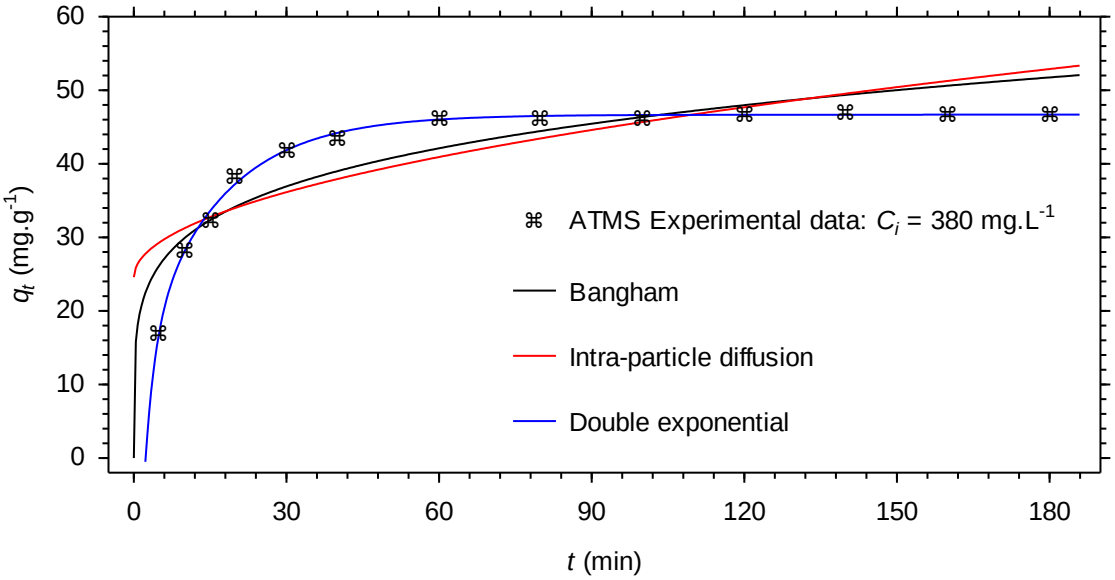
ATMS Experimental data: C_i = 380 mg.L^{-1}
Bangham
Intra-particle diffusion
Double exponential
q_t (mg.g^{-1})
t (min)
0
10
20
30
40
50
60
0
30
60
90
120
150
180

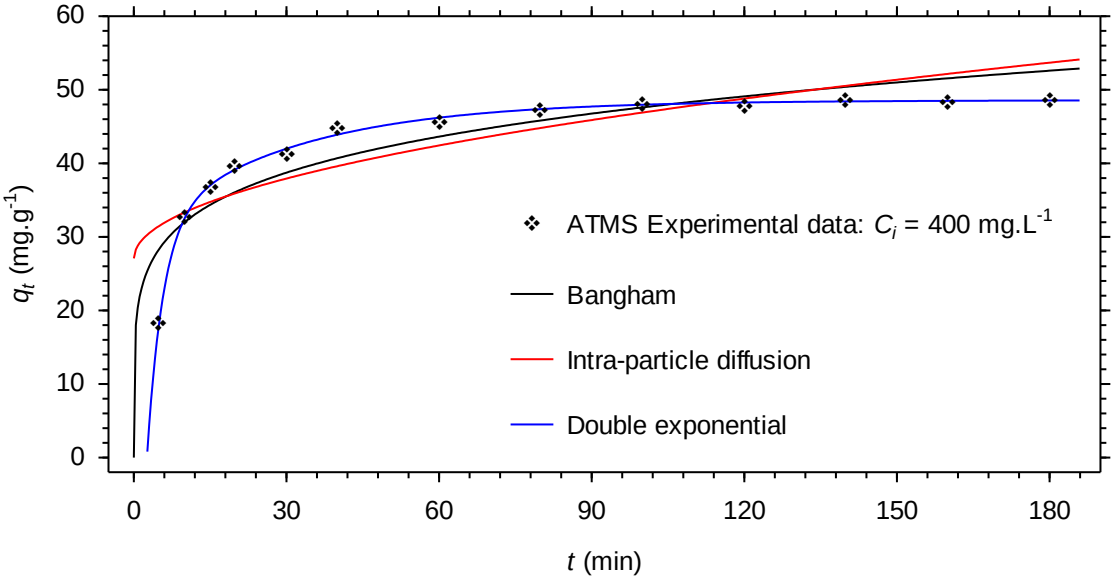
ATMS Experimental data: C_i = 400 mg.L^{-1}
Bangham
Intra-particle diffusion
Double exponential
q_t (mg.g^{-1})
t (min)
0
10
20
30
40
50
60
0
30
60
90
120
150
180

Appendix VIII: Bangham's, double exponential and intra-particle diffusion model simulation plots for sorption of lead(II) ions by CFMS. [Room temperature, pH: 5.2, Sorbent dose: 0.5 g.L^{-1}]

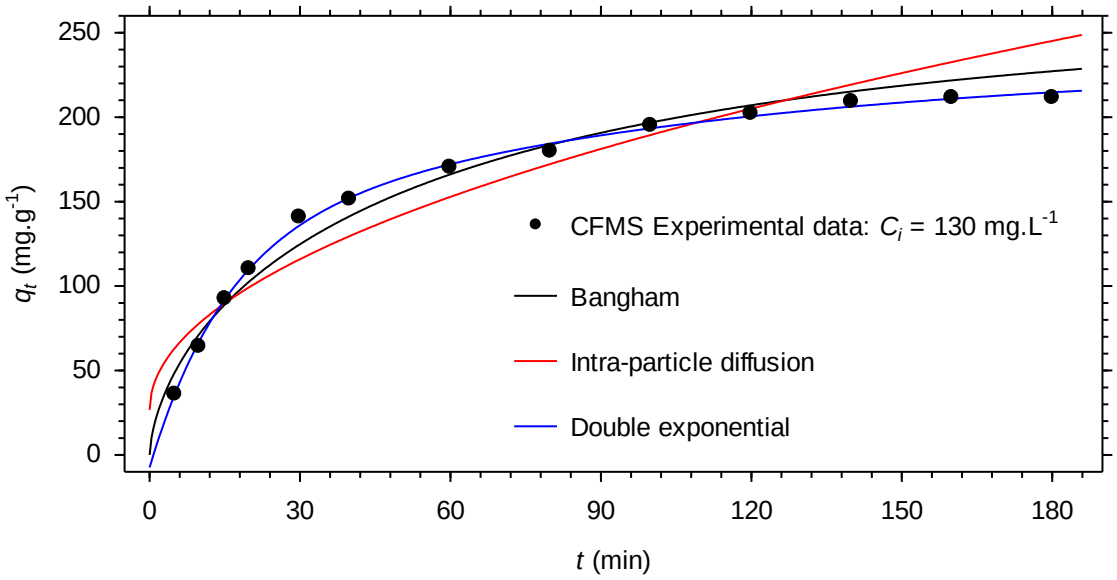

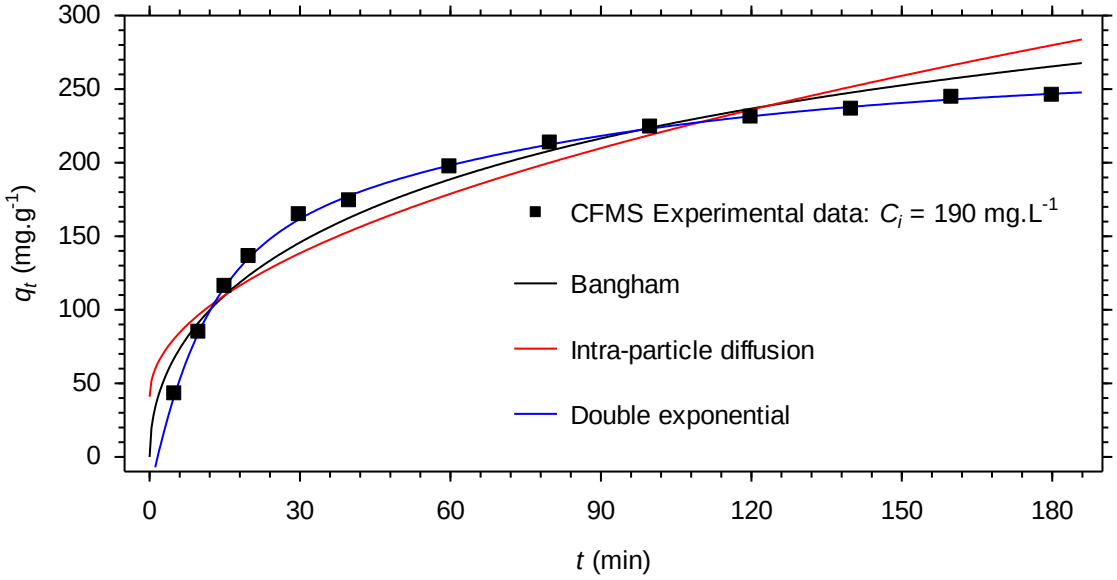

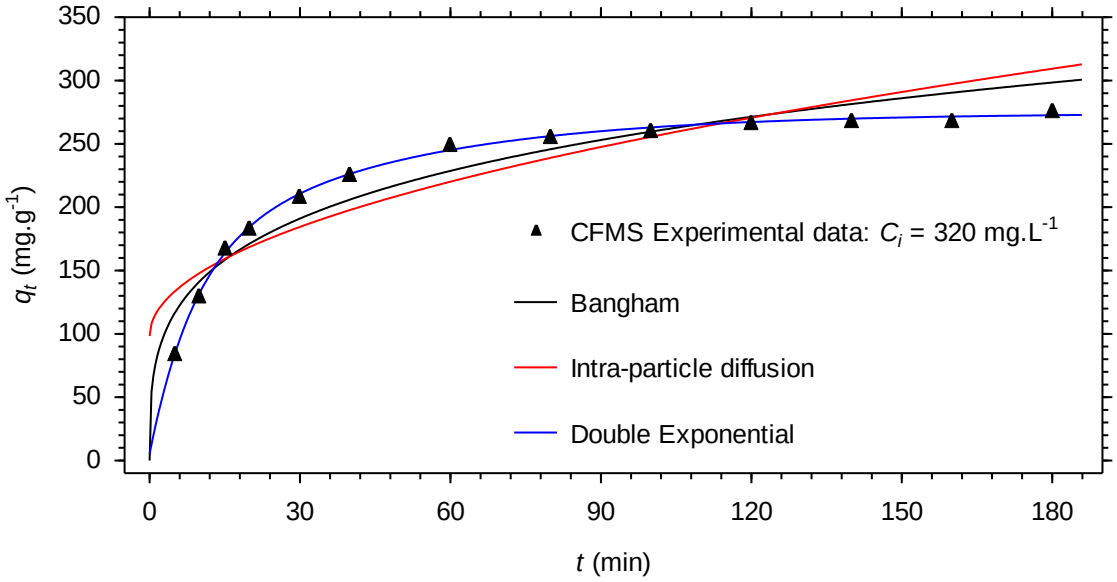
350
300
250
200
150
100
50
0
q_t (mg.g^{-1})
0
30
60
90
120
150
180
t (min)
CFMS Experimental data: C_i = 320 mg.L^{-1}
Bangham
Intra-particle diffusion
Double Exponential

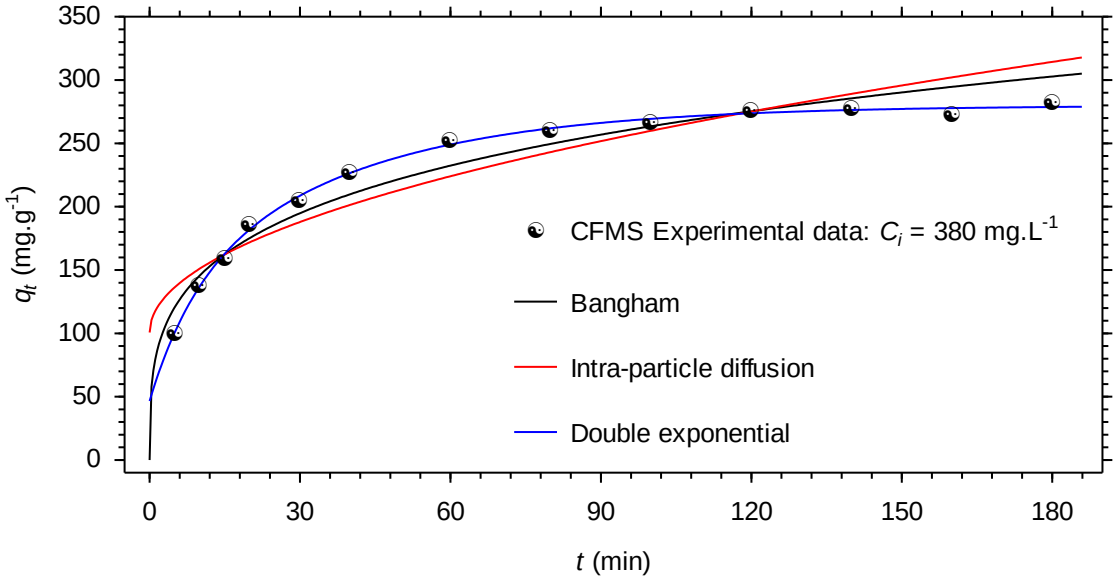
350
300
250
200
150
100
50
0
q_t (mg.g^{-1})
0
30
60
90
120
150
180
t (min)
CFMS Experimental data: C_i = 380 mg.L^{-1}
Bangham
Intra-particle diffusion
Double exponential

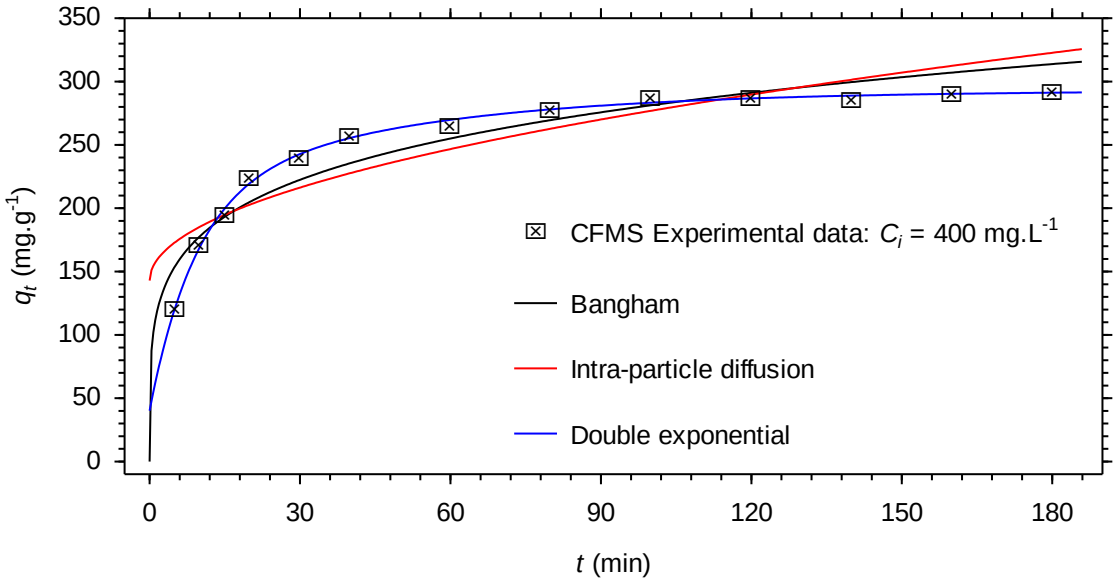
350
300
250
200
150
100
50
0
q_t (mg.g^{-1})
0
30
60
90
120
150
180
t (min)
CFMS Experimental data: C_i = 400 mg.L^{-1}
Bangham
Intra-particle diffusion
Double exponential

Appendix IX: Intra-particle diffusion model simulation plots for sorption of lead(II) ions by ATMS and CFMS. [Room temperature, pH: 5.2, ATMS dose: 1 g.L^{-1}, CFMS dose: 1 g.L^{-1}]

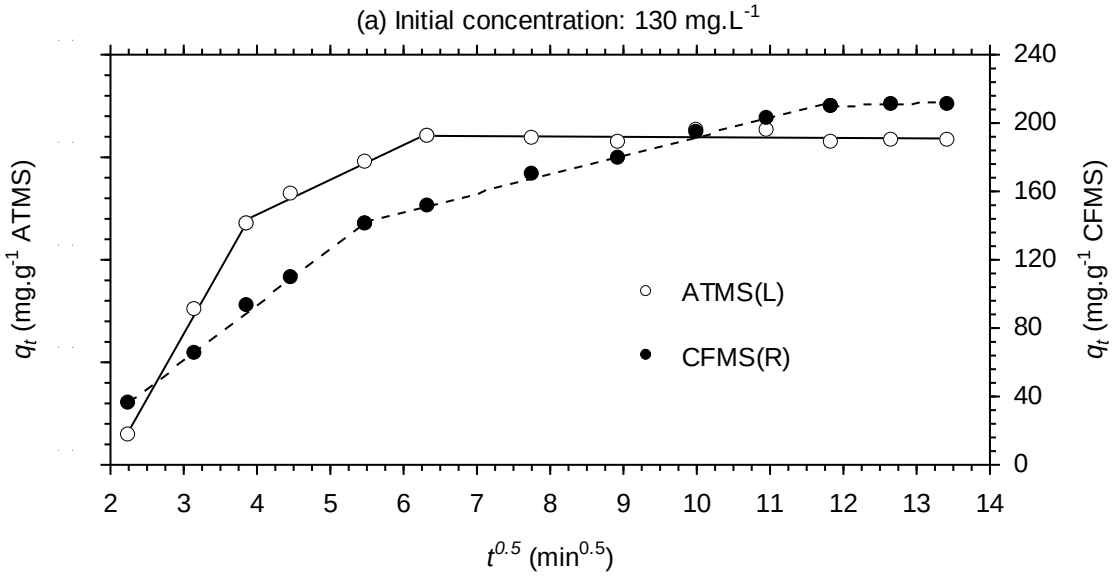

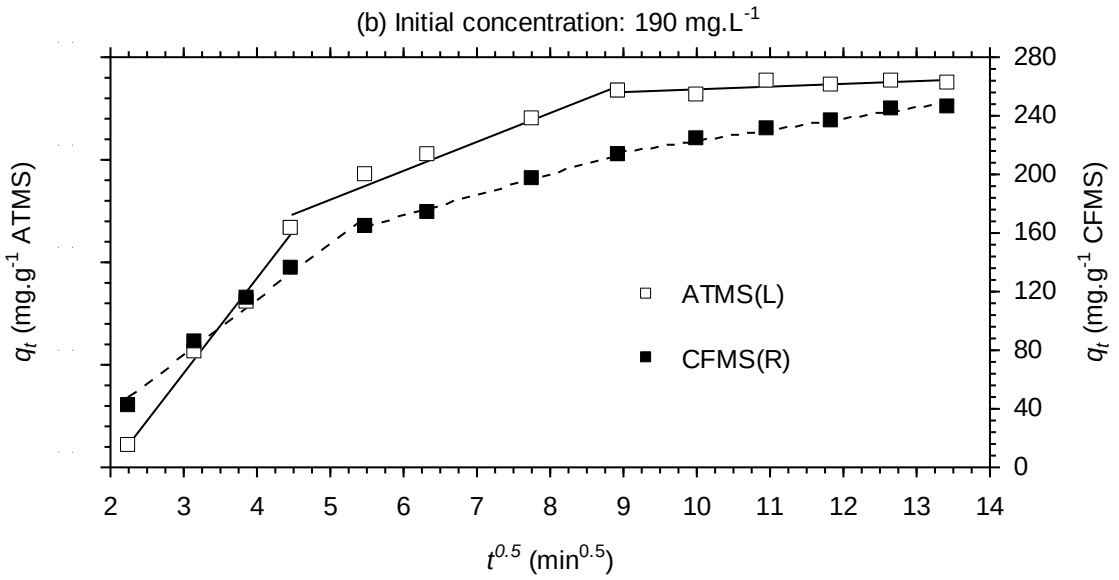

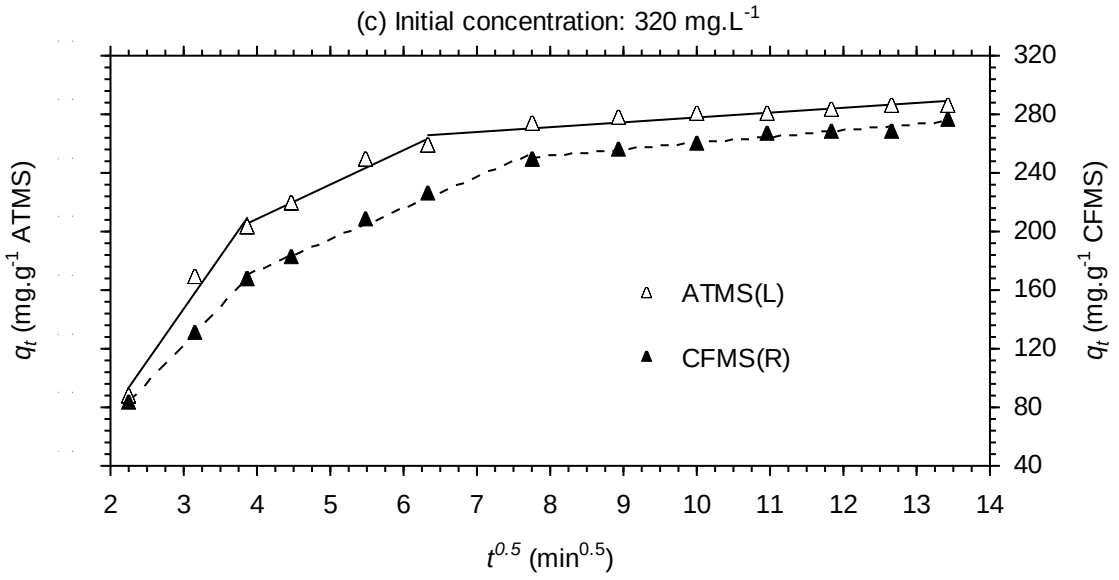

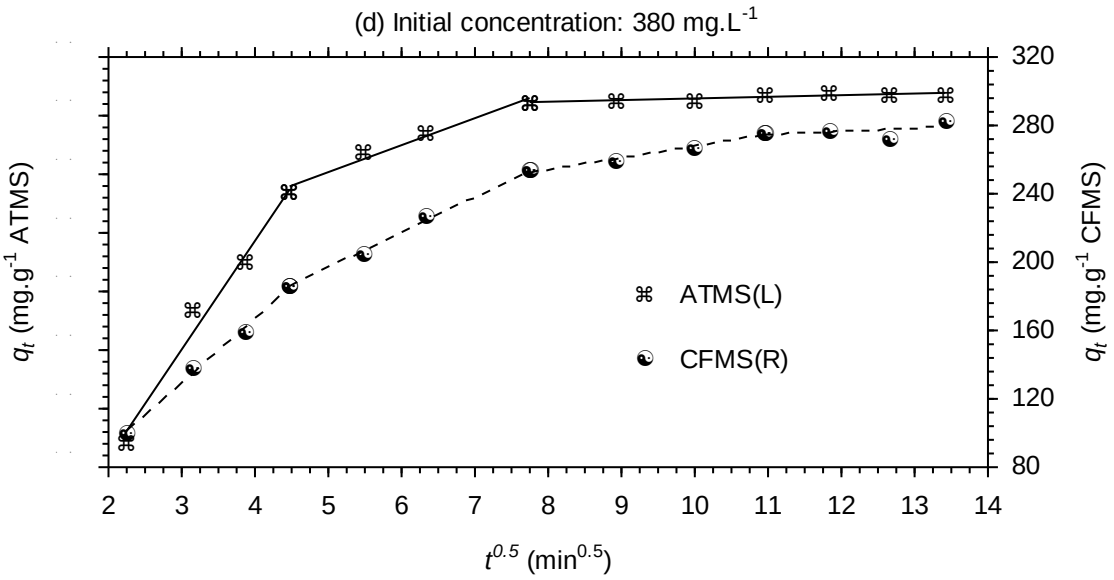
(d) Initial concentration: 380 mg.L-1
qt (mg.g-1 ATMS)
qt (mg.g-1 CFMS)
ATMS(L)
CFMS(R)
t0.5 (min0.5)
2
3
4
5
6
7
8
9
10
11
12
13
14
80
120
160
200
240
280
320

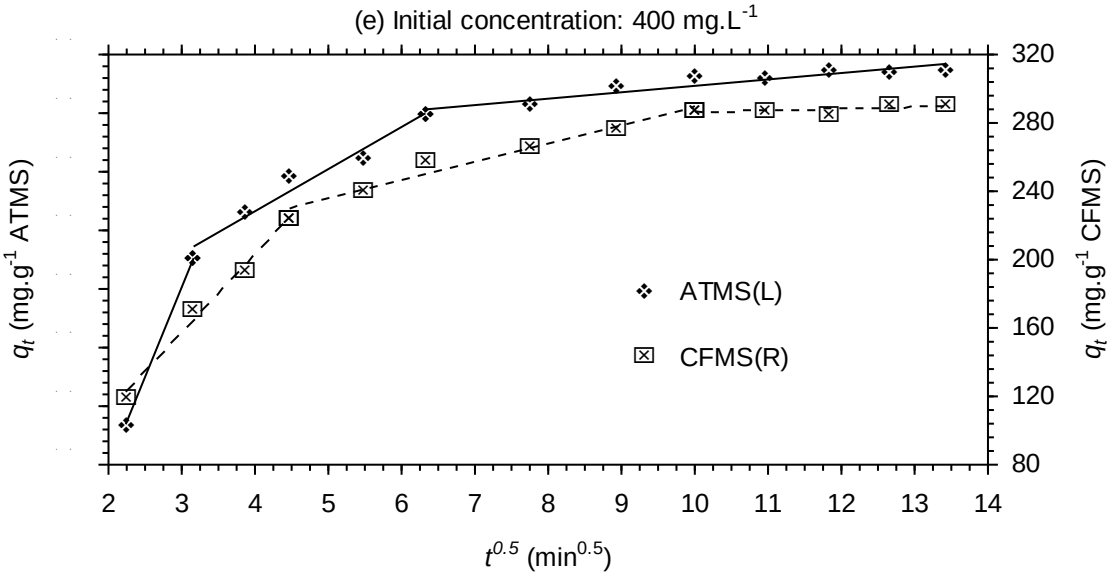
(e) Initial concentration: 400 mg.L-1
qt (mg.g-1 ATMS)
qt (mg.g-1 CFMS)
ATMS(L)
CFMS(R)
t0.5 (min0.5)
2
3
4
5
6
7
8
9
10
11
12
13
14
80
120
160
200
240
280
320

Appendix X: Langmuir, Sips, Toth and Redlich-Peterson isotherm model simulation plots for sorption of lead(II) ions by ATMS and CFMS. [Room temperature, Initial pH: 5.2, Contact time: 24 h, ATMS dose: 1 $g.L^{-1}$, CFMS dose: 0.5 $g.L^{-1}$]

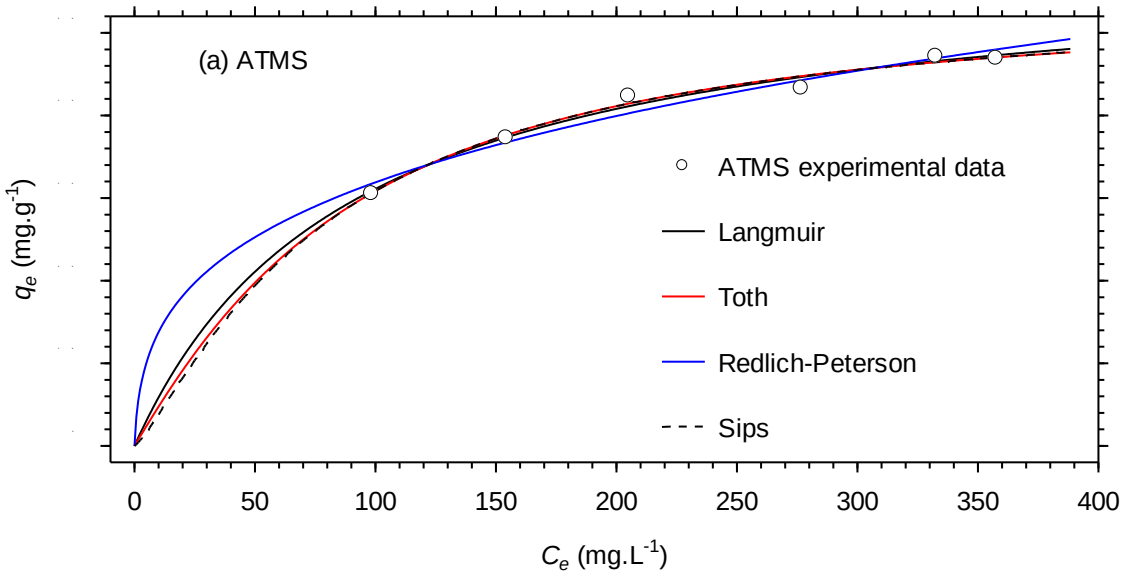

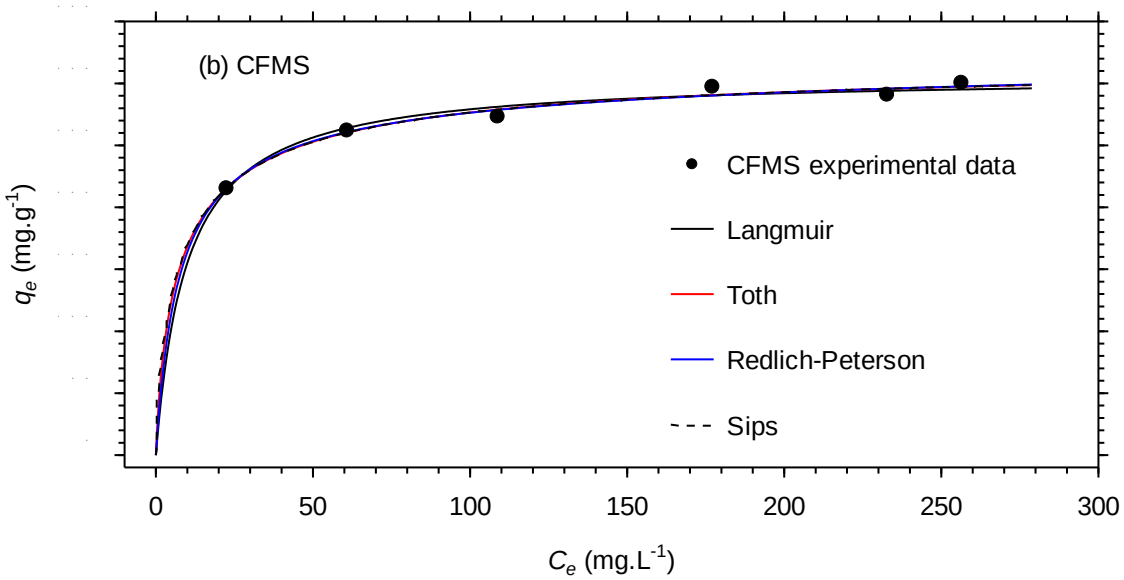

Appendix XI: Effect of initial solution pH on metal recovery from raw (pH 3.4) and acidified (pH1.8) electroplating wastewater treatment columns.

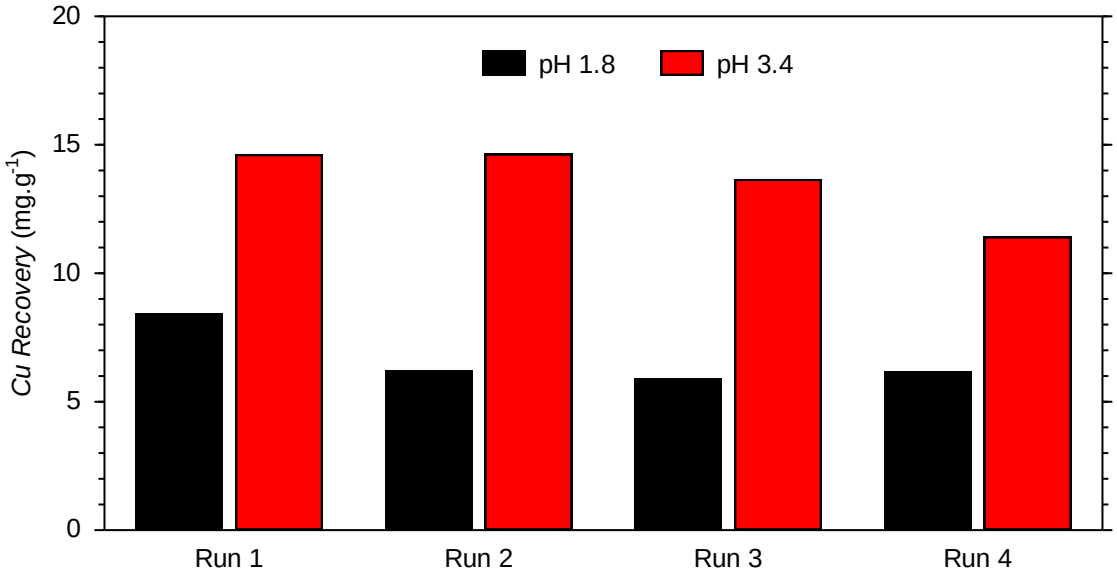

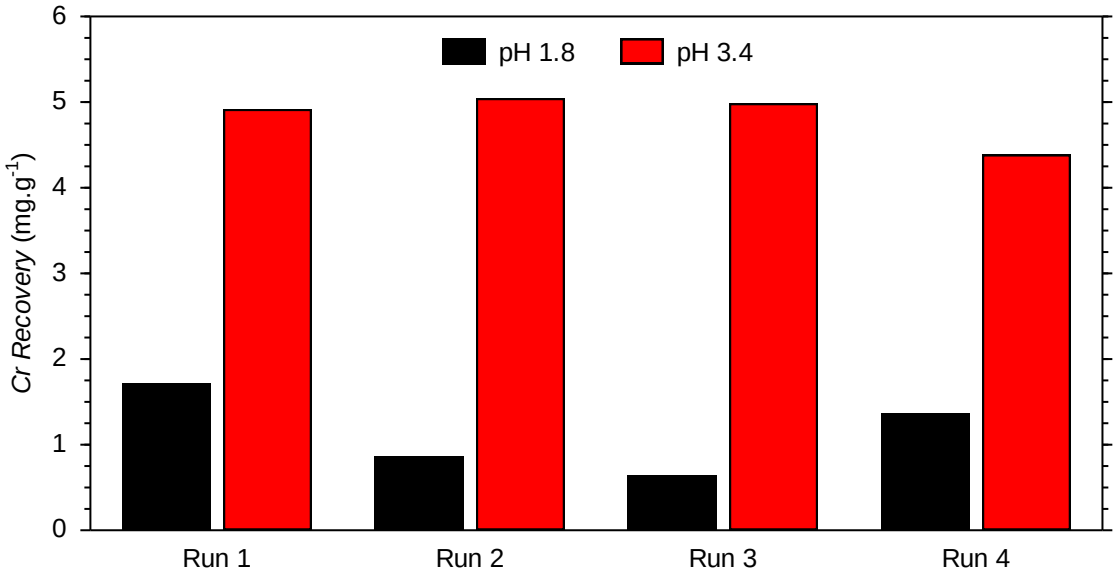

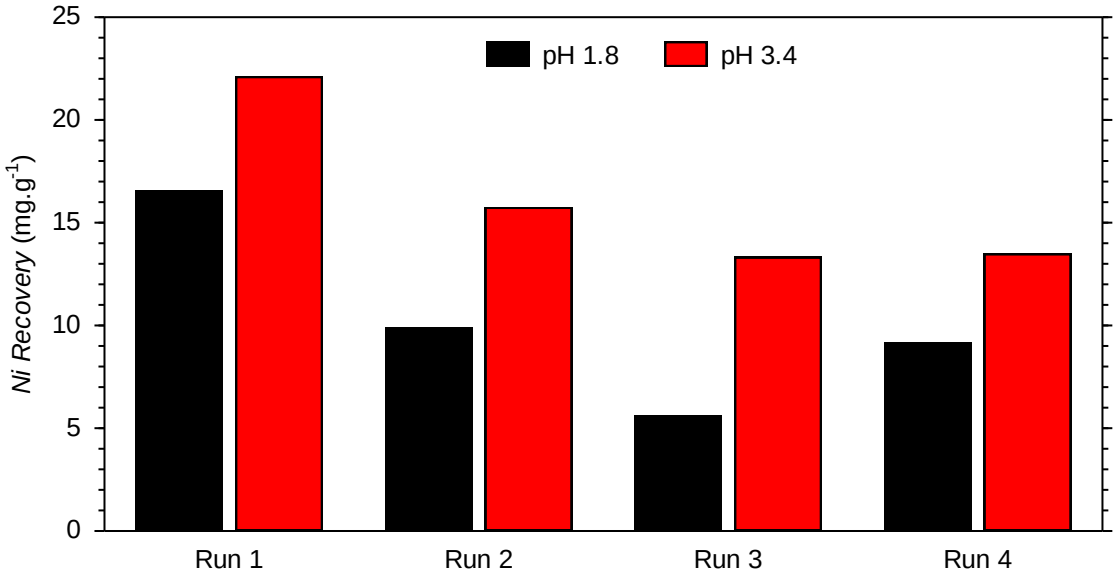
25
20
15
10
5
0
Ni Recovery (mg.g-1)
pH 1.8
pH 3.4
Run 1
Run 2
Run 3
Run 4

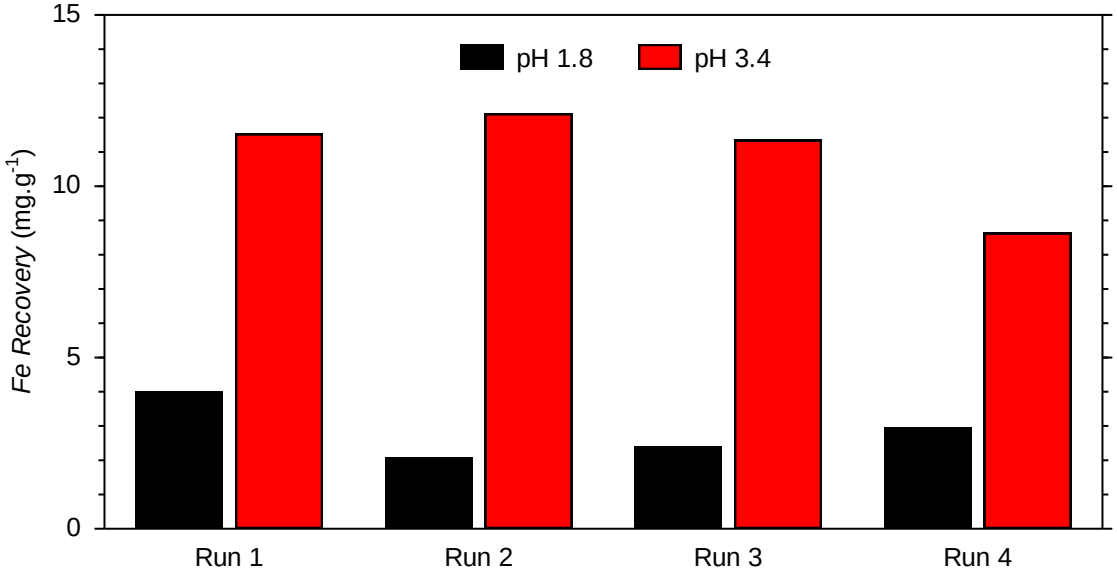
15
10
5
0
Fe Recovery (mg.g-1)
pH 1.8
pH 3.4
Run 1
Run 2
Run 3
Run 4